Journal of Thermal Analysis and Calorimetry (2025) 150:18917–18965
https://doi.org/10.1007/s10973-025-14631-9

# Cutting-edge dielectric nanofluids: a review of factors influencing stability and thermo-dielectric properties

**Rizwan A. Farade[1] · Noor Izzri Abdul Wahab[1] · Muhammad Rafiq[2,3] · Nehad Ali Shah[4] · T. M. Yunus Khan[5] · Syed Waheedullah Ghori[5]**

Received: 24 April 2025 / Accepted: 22 July 2025 / Published online: 6 September 2025


## Abstract

Dielectric nanofluids (DNFs) exhibit extraordinary potential in sustainability efforts, as they pave the way for the advancement of compact transformers and heat transfer equipment. This is primarily attributed to their remarkable capacity to augment the thermo-dielectric performance. Numerous factors exert a profound influence on the performance of dielectric nanofluids. Hence, these factors hold paramount significance. Many existing review articles lacking in comprehensive, multifactor perspective. This leads to fragmented insights and difficulty in comparing studies. Existing studies lack real-world relevance, and there is a disconnect between experimental results and industrial settings. This article critically analyzes multiple factors in a single, unified article. Offers deeper insights into the underlying surface mechanisms by empirical support. Provides a comprehensive analysis of the practical implications, challenges in practical applications, and future research directions. In this context, extensively incorporated cutting-edge literature encompasses both commercial and noncommercial grade transformer fluids and heat transfer oils, as well as single-constituent, hybrid, composite, and doped nanoparticles. The encompassed studies indicate that these factors significantly influence the stability and thermo-dielectric properties of dielectric nanofluids. The average AC breakdown voltage (BDV) enhancement was approximately 35%, thermal conductivity improved by around 26%, and tan δ was reduced by about 33%. This article serves as a valuable resource to address challenges and optimize the performance of DNFs focused on energy-efficient transformers and heat transfer equipment, bridges experimental findings with industrial applications, and highlights future research directions.

**Keywords** Dielectric nanofluids · Nanoparticles · Dielectric properties · Thermal conductivity · Dispersion stability · Sustainability

## Abbreviations

| | |
|---|---|
| $A$ | Coulomb constant [$Nm^2C^{-2}$] |
| AGQD | Amine-treated graphene quantum dots |
| APTES | γ-Amino-propyl triethoxysilane |
| BDV | Breakdown voltage [kV] |
| BF | Base fluid |
| $C_i$ | Specific heat of mode i [$JK^{-1}kg^{-1}$] |
| CNO | Canola oil |
| CTAB | Cetyl trimethyl ammonium bromide |
| CSO | Cottonseed oil |
| COO | Coconut oil |
| $C_V$ | Specific heat [$JK^{-1}kg^{-1}$] |
| $d$ | Size of nanoparticle [nm] |
| DFT | Density functional theory |
| DNF | Dielectric nanofluid |
| $D_{np}$ | Nanoparticle diameter [nm] |
| $E_0$ | External electric field strength [$Vm^{-1}$] |
| $E_{g2}$ | Bandgap energy of nanoparticles [eV] |
| $F_a$ | Adhesive force [N] |

✉ Rizwan A. Farade
rizwan.projects@gmail.com; rijavan@upm.edu.my

[1] Department of Electrical and Electronics Engineering, Advanced Lightning, Power and Energy Research (ALPER), Faculty of Engineering, University Putra Malaysia, 43400 Serdang, Malaysia

[2] Department of Electrical Engineering, University of Engineering & Technology, Taxila 47050, Pakistan

[3] Institute for Energy and High Voltage Technology, FHWS University of Applied Sciences Würzburg-Schweinfurt, Schweinfurt, Germany

[4] Department of Mechanical Engineering, Sejong University, Seoul 05006, South Korea

[5] Department of Mechanical Engineering, College of Engineering, King Khalid University, 61421 Abha, Saudi Arabia

| | |
|---|---|
| $Fc$ | Basic fluid's drag force [N] |
| $F_e$ | Dielectrophoretic forces [N] |
| $F_g$ | Gravity force [N] |
| $F_N$ | Adjacent nanoparticles' supportive force [N] |
| FCHT | Forced convective heat transfer |
| HCT | Heat transfer coefficient [$Wm^{-2}K^{-1}$] |
| $i$ | Branch index |
| $I_c$ | Charging current [A] |
| $I_l$ | Effective current [A] |
| $k$ | Thermal conductivity [$Wm^{-1}K^{-1}$] |
| $k_1$, $k_2$ | Proportionality constants |
| $K_B$ | Boltzmann constant [$JK^{-1}$] |
| LI | Lightning impulse |
| $L_{np}$ | Nanoparticles' mean free path [nm] |
| $L_{oil}$ | Mean free path of oil molecules [nm] |
| MO | Mineral oil |
| M-M | Masroom-Mashroom |
| $M_{np}$ | Nanoparticle mass [fg] |
| $n$ | Phonon polarization branch count |
| $N$ | Nanoparticle concentration |
| $N_1$ | Base fluid molecule counts in free space |
| $N_2$ | Number of nanoparticles molecules |
| $N_3$ | Number of liquid-medium molecules at nanoparticle-medium contact |
| NCHT | Natural convective heat transfer |
| NE | Natural ester liquid |
| PAO | Palm oil |
| PKEO | Palm kernel ester oil |
| PKOME | Palm kernel oil methyl ester |
| Prep. | Preparation |
| $q$ | Nanoparticle' surface charge [C] |
| R/r | Radius of nanoparticles [m] |
| RBD | Refined, bleached, and deodorized |
| SE | Synthetic ester oil |
| SO | Soybean oil |
| RT | Room temperature [K] |
| $T$ | Temperature [K] |
| TO | Transformer oil |
| $v_i$ | Phonon group velocity [$ms^{-1}$ |

**Greek symbols**

| | |
|---|---|
| $\varepsilon' / \mathcal{E}r$ | Dielectric constant |
| $\tau_{NF}$ | Nanofluids' dielectric relaxation time [s] |
| $\varepsilon_0$ | Permittivity of free space [$Fm^{-1}$] |
| $\mathcal{E}_1$ & $\mathcal{E}_2$ | Base fluid and nanoparticle relative permittivity |
| $\mathcal{E}_{NF}$ | Dielectric constant of nanofluid |
| $\alpha_1$ | Base fluid polarizability [$m^2V^{-1}$] |
| $\alpha_2$ | Inner nanoparticle polarizability [$m^2V^{-1}$] |
| $\alpha_3$ | Orientation-based polarizability of charged particles [$m^2V^{-1}$] |
| $\delta$ | Phase angle between the $I_l$ and $I_c$, [rad] |
| $\varepsilon''$ | Loss factor |
| $\varepsilon_{oil}$ | Dielectric constant of oil |
| $\mu$ | Viscosity [$Nsm^{-2}$] |
| $\rho$ | Resistivity [Ωm] |
| $\sigma_1$ | Conductivity of base oil [$Sm^{-1}$] |
| $\sigma_2$ | Conductivity of nanoparticles [$Sm^{-1}$] |
| $\sigma_{ac}$ | AC conductivity [$Sm^{-1}$] |
| $\tau_i$ | Phonon relaxation time [s] |
| $\varphi$ | Volume fraction of nanoparticles |
| $\omega$ | Angular frequency [$rads^{-1}$] |
| $\zeta$ | Nanoparticle surface zeta potential [mV] |

## Introduction

The utilization of dielectric nanofluids (DNFs) holds immense promise in bolstering sustainability efforts through the facilitation of compact transformers and heat transfer apparatus [1]. DNFs possess immense potential in advancing this objective through their ability to enhance dielectric strength and heat transfer capabilities of liquid dielectrics. This, in turn, leads to a reduction in the size and mass of transformers, decreased operating temperatures, enhanced transformer performance in challenging conditions, and prolonged service life of transformers [2–4]. DNFs exhibit immense promise for application in electrical apparatus such as transformers, circuit breakers, tap changers, cables, and capacitors. The utilization of DNFs in these applications serves a dual purpose, acting as both liquid dielectrics and cooling agents [5, 6].

Mineral oil (MO), silicone oil, synthetic ester oil, and natural ester liquids are the primary base oils employed in DNFs [7–9]. However, the utilization of infused nanoparticles encompasses insulating, semiconductive, and conductive nanoparticles for the purpose of preparing nanofluids [10–12]. The stability, electrical, thermal, physical, and chemical properties of DNFs were examined through experimental analysis. The effectiveness of nanofluids is contingent upon their stability [13]. The researchers employed both qualitative and quantitative methodologies in order to assess the stability of DNFs [14]. The electrical characteristics of DNFs primarily include dielectric breakdown voltages (BDVs) subjected to alternating current, direct current, and impulse voltages [15]; in addition to loss tangent; dielectric constant; and volume resistivity [16, 17]. These properties are essential for achieving effective electrical insulation [18]. The thermal properties of DNFs include measurements of thermal conductivity and specific heat capacity [19, 20]. The physical properties of DNFs include color, flash point, fire point, pour point, density, viscosity, and biodegradation [21]. Chemical properties of DNFs include corrosive sulfur, water content, acid number, PCB content, and oxidation stability [22, 23].

Research on DNFs has significantly evolved over the past two decades [24]. This is due to an increasing demand for high-performance insulating and cooling fluids in power apparatus. The initial studies primarily focused on enhancing the dielectric BDV through the utilization of individual nanoparticles in MOs. Subsequently, research expanded to encompass bending of various types of nanoparticles and their efficacy with diverse base fluids (BFs) [25, 26], such as natural and synthetic ester liquids, silicone oils. Advancements in nanotechnology, characterization tools, and preparation methods have facilitated a deeper understanding of interfacial phenomena and charge transport mechanisms [27, 28]. Despite these advancements, the field remains fragmented, and limited reviews on the optimal methods for producing stable and efficient DNFs. This underscores the need for a thorough review of the diverse factors influencing their performance.

Research studies in the literature have demonstrated that several factors influence the performance of DNFs for use in transformers. Due to the high repulsive force between nanoparticles, highly electronegative or electropositive materials exhibit greater dispersion stability [29]. The phenomenon underlying the increase in their dielectric breakdown strength can be attributed to the capacity of nanoparticles to capture charges, a process reliant upon the dielectric relaxation time [30]. Conductive, semiconductive, and insulating nanoparticles are capable of improving the BDV, dielectric constant, dissipation factor, and volume resistivity of a dielectric BFs [10–12]. Nanoparticles with a higher thermal conductivity will contribute more to the thermal conductivity of nanofluids [31]. Phase, bandgap reduction, and shape of nanoparticles also play a significant role in enhancing the heat transfer and dielectric properties of nanofluids [32–34]. Numerous researchers employed single-unit nanoparticles to enhance the basal dielectric fluid's properties. Alternatively, blended (mixture of multiple nanoparticle types), composite (combining or arranging various materials within a single particle), and doped (introducing minute amounts of a dopant substance into a host nanomaterial) nanoparticles demonstrated more superior dielectric and thermal properties [35–37]. The size, concentration, and surfactant treatment of nanoparticles have an impact on the stability, dielectric, and thermal performance of nanofluids. The observed phenomenon can be clearly ascribed to a remarkable augmentation in the overall surface area, an increase in the number of nanoparticles at a given concentration, charge trapping, EDL-induced phonon transport, Brownian motion and interaction between particles, rigid interfacial zone, and screening effect [38–41].

Furthermore, the common impurity found within transformer oil is none other than moisture. The breakdown strength of nanofluids is contingent upon the phenomenon of moisture binding [42, 43]. Dry nanofluids consist of nanoparticles that effectively bind individual water molecules or dimers, thereby enhancing the BDV at both low and high nanoparticle concentrations. The premature breakdown at lower nanoparticle concentrations in wet nanofluids can be attributed to the bridging of aligned water molecules, dimers, or water clusters. At elevated concentrations, nanoparticles exhibit the ability to adsorb water onto their surface, thereby impeding the formation of aligned water bridges and resulting in enhanced BDV. The performance of DNFs is also influenced by temperature variation and thermal aging [44–47]. The observed phenomenon can be ascribed to the presence of emulsified dissolved water, degradation process, thermal activation of charge carriers, trapping and de-trapping mechanisms, phonon transport, and Brownian motion [48–50]. The thermo-dielectric properties of DNFs are subject to influence from forced circulation and external magnetic field [51, 52]. This can be attributed to the dispersion of nanoparticles, the trapping of charges, and the convective heat transfer [53, 54]. The application of an external electrical field induces a force that leads to the resuspension of nanoparticles, thereby enhancing thermal performance [55].

DNFs are a promising solution to the limited dielectric strength and heat transfer efficiency of dielectric BFs [56, 57]. However, maintaining uniform nanoparticle dispersion, preventing agglomeration, and achieving long-term stability remain significant challenges. DNFs show great potential in the field of sustainability since they provide a means for the development of compact transformers and heat transfer devices [1]. However, understanding the key factors affecting the thermo-dielectric properties of DNFs holds significant relevance. Although the scientific community has paid great attention to the reported development in DNFs [17], yet there are several knowledge gaps particularly related to stability, dielectric, and thermal properties. There is currently no comprehensive review article that focuses solely on the factors influencing the performance of DNFs, resulting in fragmented insights and difficult comparisons. A deeper understanding of the significance and underlying mechanisms by which various factors affect the thermo-dielectric performance of DNFs is essential. Existing studies lack real-world relevance, and there is a disconnect between experimental results and their application in industrial settings.

This review article addresses this gap by integrating and critically analyzing multiple factors in a single, unified article. The influential factors under examination encompass the nanoparticle bandgap, nanoparticle size variation and ultrasonic cavitation, phase and shape of nanoparticles, blending and nano-structuring of nanoparticles, nanoparticle concentration, surfactant treatment, moisture content, temperature variation, thermal aging, forced circulation, and external magnetic and electrical fields. This article offers deeper insights into the underlying mechanisms by which various factors influence the thermo-dielectric performance of DNFs by empirical support. Provides a comprehensive analysis of the practical implications, challenges in practical applications, and future research directions to bridge the gap between experimental studies and industrial settings. The article is structured as follows: Sect. "Overview of the research" presents an overview of the research, Sect. "Influential factors affecting properties of dielectric nanofluids" discusses influential factors affecting DNFs, Sect. "Practical implications" explores their practical implications, Sect. "Challenges in practical applications" outlines challenges in practical applications, and Sect. "Future research directions" suggests future research directions.

## Overview of the research

DNF research overview and applications are depicted in Fig. 1. Preparation of nanofluids for experimentation requires mixing of nanoparticles and base dielectric fluid. Nanoparticles of metal oxides, metal carbides, nitrides, and nonmetals (with/without surfactants) can be dispersed in BFs (mineral, vegetable, synthetic, etc.) [58–60]. Nanofluids are prepared using one-step or two-step methods [20, 61, 62]. Nanofluids require stable and uniform nanoparticle suspension on BF, low nanoparticle agglomeration, and minimal chemical variation [63].

The one-step method involves production and dispersion of nanoparticles simultaneously in the BF [64]. One-step methods have certain potential aids, few researchers reported one-step method for the preparation of insulating and heat transfer nanofluids. Apparently, transformer oil-based $WO_3$-Ag hybrid nanofluid was prepared by electrical explosion of wire [36]. Heat transfer oil T66-based $TiO_2$ nanofluids were prepared through hydrothermal approach [32]. MO-based $Fe_3O_4$ nanoparticles decorated MWCNTs nanocomposite nanofluid was prepared by chemical co-precipitation technique [65]. Transformer oil (TO)-based monodispersed oleic acid-capped ceria nanoparticles dispersed nanofluids were prepared by thermal decomposition [66]. One-step method has few limitations; not often suited

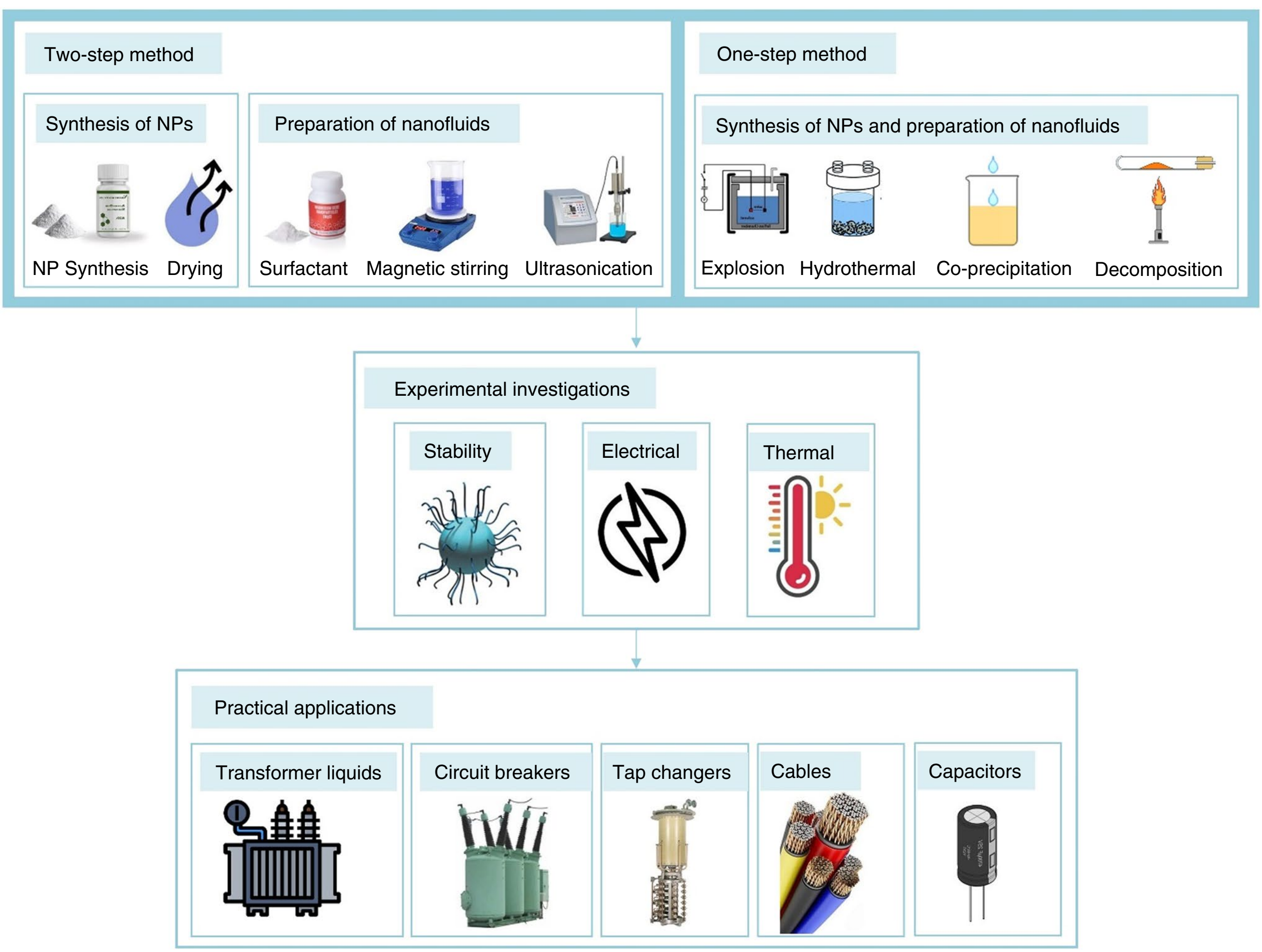


**Fig. 1** A concise overview of research and practical applications of dielectric nanofluids

for large-scale manufacture and require precise nanoparticle properties for stability. Therefore, the two-step nanofluid preparation method is most prevalent in DNFs. First, chemical or physical methods prepare nanomaterial; second, combination magnetic stirring, ultrasonic agitation, homogenizing disperse nanomaterial into a BF [67, 68]. Since nanopowder production has been industrialized, the two-step process is the cheapest option to make large-scale nanofluids [69]. Nanoparticles agglomerate because of their large surface area and surface activity; surfactants and ultrasonic agitation are essential for DNF dispersion stability.

Visual inspection [61], UV–Vis spectroscopy [70], transmission electron microscopy (TEM) [5], dynamic light scattering (DLS) [47], zeta potential method [71], and sedimentation analysis by photograph capturing are the methods [72] and are the primary methods adopted by researchers to evaluate the dispersion stability of DNFs. Visual inspection remains the simplest method for identifying nanoparticle sedimentation, though it is limited by subjectivity and lack of quantification [61]. Quantitative techniques, such as UV–Vis spectroscopy, enable time-dependent absorbance measurements that correlate with nanoparticle concentration and stability [70]. More advanced techniques, including transmission electron microscopy (TEM), provide detailed imaging of nanoparticle distribution and agglomeration, albeit only in the dried state [5]. Dynamic light scattering (DLS) is used to monitor changes in nanoparticle size over time, particularly during thermal aging, offering insights into agglomeration behavior [47]. Zeta potential analysis serves as a direct measure of colloidal stability, with values above $\pm 30$ mV indicating good dispersion and above $\pm 60$ mV indicating excellent stability [71]. Additionally, sedimentation analysis through photographic capture allows visual tracking of nanoparticle settling, validating the impact of surfactant usage, sonication time, and dispersion methods [72]. These combined methods offer a comprehensive and reliable framework for evaluating nanofluid stability, which is essential for ensuring consistent dielectric and thermal performance in power transformer applications.

DNFs were tested for stability, electrical, thermal, physical, and chemical properties by experimentation. Nanofluids' effectiveness depends on their stability. Both qualitative and quantitative methods were adopted to determine DNF stability [62, 72–76]. DNFs' electrical properties mainly include dielectric BDVs in the presence of AC, DC, and impulse, loss tangent, relative permittivity, and volume resistivity [16, 17]. These properties are necessary for their electrical insulation [18]. Thermal conductivity and specific heat capacity measurements are the thermal properties of DNFs [19, 20]. They are useful for heat transfer and thermal management applications [77]. Color, flash point, fire point, pour point, density, viscosity, and biodegradation are physical properties of DNFs [21]. Corrosive sulfur, water content, acid number, PCB content, and oxidation stability are chemical properties of DNFs [22, 23]. The potential applications of DNFs include various electrical components like transformers, circuit breakers, tap changers, cables, and capacitors [22, 78–80]. These applications utilize DNFs for cooling purposes or as a dielectric medium, or sometimes both. Liquid dielectrics are favored in these applications for their superior cooling capabilities and reduced risk of insulation breakdown. Nanoparticles have a considerable impact on the thermo-dielectric properties of transformer oil. The subsequent section delves into the impact of various factors on the dielectric and thermal performance of DNFs.

## Influential factors affecting properties of dielectric nanofluids

Nanoscale particles in a dielectric fluid medium form DNFs. DNF properties are affected by various factors [61, 81]. Table 1 summarizes the reviewed literature on DNFs to explore influential factors. Nanofluid dielectric and thermal properties percentage enhancement over BF are also listed, positive and negative numbers indicate increment and decrement, respectively. BFs considered are commercial and non-commercial grade transformer fluids and heat transfer oils. Nanoparticles considered are single constituents, composites/hybrid, doped, functionalized/non-functionalized, and surfactant-treated/untreated. The percentage enhancement in properties for parameters measured at different temperatures and frequencies is listed for the lowest temperature and frequency 50 Hz. Other than AC BDV, other BDV types are explicitly mentioned.

### Nanoparticle band gap

A larger bandgap increases the electrical insulation property of the nanomaterial [124]. Thus, nanoparticles can be classified as insulating, semiconducting, and conducting according to their electronic band structure (Fig. 2a). The significance of the bandgap of nanoparticles in determining the stability, thermal, and dielectric properties of DNFs is further explored.

#### Stability

Effective stabilization of nanoparticles has to take place, since agglomeration and sedimentation of the nanoparticles would be detrimental. Stability is a vital parameter in DNFs, as it directly influences their thermo-dielectric properties. Well-dispersed nanoparticles in BF enable more effective trapping sites, charge scavenging and uniform electric field distribution, which are favorable for enhancing BDV, tan δ, and resistivity [104, 125]. Furthermore, it significantly

**Table 1** Comprehensive review to explore influential factors for stability, dielectric, and thermal properties of dielectric nanofluids

| Nanoparticle (Remark if any) | Size/nm | Filler level range | Filler for listed DNF properties | Base fluid | Prep. method | Sonication | | Surfactant | Stability result/period | Nanofluid properties enhancement compared to base fluid/% | | | | | References |
|---|---|---|---|---|---|---|---|---|---|---|---|---|---|---|---|
| | | | | | | Type | Time | | | BDV/Type | $\mathscr{E}_r$ | Tan δ | $\rho$ | $k$ | |
| Non-modified h–BN | – | 0.03–0.12 g $L^{-1}$ | 0.03 g $L^{-1}$ | NE | Two-step | Bath | 1.5 h | – | 45 days | 15.01 | – | –28.8 | 23.5 | 12.68 | [10] |
| Surface modified h–BN | – | 0.03–0.12 g $L^{-1}$ | 0.03 g $L^{-1}$ | NE | Two-step | Bath | 1.5 h | APTES | 45 days | 19.58 | – | –37.4 | 27.7 | 20.33 | [10] |
| Iron oxide colloidal | 23 nm | 0.1 vol.% | – | Nitro libra | Two-step | Probe | 20 min | – | – | 23.8 | – | – | – | 4.51 | [82] |
| $Fe_3O_4$ | 30 nm | 0.5–2 mass% | 2 mass% | MO | Two-step | – | – | – | – | – | – | – | – | 15.87 | [83] |
| CuO | 30 nm | 0.5–2 mass% | 2 mass% | MO | Two-step | – | – | – | – | – | – | – | – | 24.46 | [83] |
| $Al_2O_3$ | 30 nm | 0.5–2 mass% | 2 mass% | MO | Two-step | – | – | – | – | – | – | – | – | 20.29 | [83] |
| MWCNT | 10–20 nm | 0.001–0.1 mass% | 0.001 mass% | TO | Two-step | Bath | 6 h | Oleic acid | Unstable | –11.9 | – | – | – | 14.48 | [84] |
| MWCNT-OH | 10–20 nm | 0.001–0.1 mass% | 0.001 mass% | TO | Two-step | Bath | 6 h | Stearic acid | 40 days | –4.14 | – | – | – | 15.59 | [84] |
| MWCNTs $TiO_2$-doped | 42–60 nm | 0.05–0.2 mass% | 0.2 mass% | TO | Two-step | Bath | 1 h | Oleic acid | 16 days | –30.38 | – | – | – | 8.6 | [85] |
| Anatase $TiO_2$ | 50–70 nm | 0.0025–0.01 mass% | 0.005 mass% | MO–1 | Two-step | Bath | 2 h | – | 3 months | 11.27 | 6.28 | –13.16 | 216.24 | 210 | [11] |
| Anatase $TiO_2$ | 50–70 nm | 0.0025–0.01 mass% | 0.005 mass% | MO–2 | Two-step | Bath | 2 h | – | 3 months | 11.04 | –6.38 | –25.38 | 20 | 48.5 | [11] |
| $WO_3$–Ag composite | 35–55 nm | 1–4 mass% | High | TO | One-step | – | – | – | Stable | –33.96 | – | – | – | 41 | [36] |
| Anatase $TiO_2$ | 5.9 nm | 0.01–0.05 vol.% | – | T66 | One-step | Bath | 30 min | Stearic acid | 56 days | – | – | – | – | 44.6 | [32] |
| MWCNT-$Fe_3O_4$-doped | – | 0.125–0.5 g $L^{-1}$ | – | MO | One-step | – | 8 h | – | 26 days | – | – | – | – | 50 | [65] |
| $CeO_2$ | 3–7 nm | 0.08–0.7 vol.% | – | TO | One-step | – | 10 min | Oleic acid | 5 months | – | – | – | – | 14.6 | [66] |
| ZnO | 30–50 nm | 0.01–3 mass% | 1 mass% | RBD COO (Dry) | Two-step | Probe | 1 h | – | 1 week | 27.94 | – | 3.03 | 0 | – | [86] |
| ZnO | 30–50 nm | 0.01–0.05 mass% | 0.04 mass% | RBD COO (Wet) | Two-step | Probe | 1 h | Oleic acid | 1 week | 52.84 | – | – | – | – | [86] |
| ZnO | 30–50 nm | 0.01–3 mass% | 1 mass% | COO (Dry) | Two-step | Probe | 1 h | – | 1 week | 39.18 | – | 1.96 | 1.9 | – | [86] |
| ZnO | 30–50 nm | 0.01–0.05 mass% | 0.05 mass% | COO (Wet) | Two-step | Probe | 1 h | Oleic acid | 1 week | 59.02 | – | – | – | – | [86] |
| ZnO | 30–50 nm | 0.01–3 mass% | 1 mass% | MIDEL eN1215 (Dry) | Two-step | Probe | 1 h | – | 1 week | 24.45 | – | 0 | –2.2 | – | [86] |
| ZnO | 30–50 nm | 0.01–0.05 mass% | 0.04 mass% | MIDEL eN1215 (Wet) | Two-step | Probe | 1 h | Oleic acid | 1 week | 61.67 | – | – | – | – | [86] |
| $Fe_3O_4$ | 5 nm | 0.05–0.1 w/V% | 0.05 w/V% | MIDEL eN1204 | Two-step | - | 4 h | Oleic acid | Stable | 14.68 | – | – | – | – | [87] |
| $Fe_3O_4$ | 5 nm | 0.05–0.1 w/V% | 0.1 w/V% | MIDEL 7131 | Two-step | - | 4 h | Oleic acid | Stable | 13.52 | – | – | – | – | [87] |
| SiC | 50 nm | 0.004–0.016 mass% | 0.004 mass% | FR3 | Two-step | Bath | 1.5 h | – | Stable | 35 | – | – | – | – | [44] |

**Table 1** (continued)

| Nanoparticle (Remark if any) | Size/nm | Filler level range | Filler for listed DNF properties | Base fluid | Prep. method | Sonication | | Surfactant | Stability result/period | Nanofluid properties enhancement compared to base fluid/% | | | | | References |
|---|---|---|---|---|---|---|---|---|---|---|---|---|---|---|---|
| | | | | | | Type | Time | | | BDV/Type | $\mathcal{E}_r$ | Tan δ | $\rho$ | $k$ | |
| $TiO_2$ | 21 nm | 0.004–0.016 mass% | 0.004 mass% | FR3 | Two-step | Bath | 1.5 h | – | Less | 4.84 | – | – | – | – | [44] |
| CNT | < 8 nm | 0.01–0.05 g $L^{-1}$ | 0.01 g $L^{-1}$ | MO | Two-step | – | 30 min | – | Stable | 42.4 | – | – | – | – | [88] |
| CNT | > 20 nm | 0.01–0.05 g $L^{-1}$ | 0.01 g $L^{-1}$ | MO | Two-step | – | 120 min | – | Stable | 1.88 | – | – | – | – | [88] |
| h-BN | < 450 nm | 0.005–0.05 mass% | 0.05 mass% | TO | Two-step | Bath | 2 h | – | 1 week | 36 | 0.49 | –31.1 | 342 | 17 | [89] |
| $Al_2O_3$-$TiO_2$ (mix40:40 mg) | 20–30 nm | 0.1 g $L^{-1}$ | 0.1 g $L^{-1}$ | NE | Two-step | Probe | 6 h | Oleic acid | Stable | 58.32 | – | 0 | – | – | [90] |
| $Al_2O_3$-$TiO_2$ (mix40:40 mg) | 30 nm | 0.1 g $L^{-1}$ | 0.1 g $L^{-1}$ | MO | Two-step | Probe | 6 h | Oleic acid | Stable | 69.6 | – | –11.31 | – | – | [90] |
| CdS nanoparticles, nanobelts, and nanosheets | 2.7, 2.3, & 3.1nm | 0.05–0.4 g $L^{-1}$ | 0.3 g $L^{-1}$ | SE | Two-step | Probe | 2 h | – | Stable | 35.5, 37, & 38.3 | – | – | – | – | [91] |
| Rutile $TiO_2$ | 20 nm | 0.2 g $L^{-1}$ | – | MO | Two-step | Probe | 2 h | Oleic acid | – | – | – | 32.7 | – | – | [92] |
| $Al_2O_3$ | 20 nm | 0.2 g $L^{-1}$ | – | MO | Two-step | Probe | 2 h | Oleic acid | – | – | – | 74.2 | – | – | [92] |
| Rutile $TiO_2$ | 20–30 nm | 0.2 g $L^{-1}$ | – | FR3 | Two-step | Probe | 2 h | Oleic acid | – | – | – | –24 | – | – | [92] |
| $Al_2O_3$ | 20–30 nm | 0.2 g $L^{-1}$ | – | FR3 | Two-step | Probe | 2 h | Oleic acid | – | – | – | –31 | – | – | [92] |
| $Al_2O_3$ | 60 nm | 0.002–0.1 mass% | 0.02 mass% | MO | Two-step | – | – | Oleic acid | 1 day | 4.3 | – | – | – | 9.1 | [72] |
| $Al_2O_3$ | 60 nm | 0.002–0.1 mass% | 0.02 mass% | NE | Two-step | – | – | Oleic acid | 1 day | 4.3 | – | – | – | 10.7 | [72] |
| $TiO_2$, ZnO & CNT (Used separately) | 18, 18 & 30 nm | Single concentration | 0.075, 0.01, & 0.01 mass% | MO | Two-step | – | 2 h | – | 7 days | 14, –26, & –68 | – | – | – | – | [93] |
| $Al_2O_3$ | 50 nm | 0.004–0.015 vol.% | 0.015 vol.% | MO | Two-step | – | – | $C_{18}H_{33}NaO_2$ | – | – | – | – | – | 4.4 | [94] |
| $Co_3O_4$ nanoparticles | 16 nm | 0.0002–0.006 mass% | 0.0008 mass% | SKALN 25X | Two-step | – | 2 h | – | Stable | 65.7 | ≈ –4.7 | 0 | 0 | – | [34] |
| $Co_3O_4$ nanobelts | 15 nm | 0.0002–0.006 mass% | 0.0008 mass% | SKALN 25X | Two-step | – | 2 h | – | Stable | 79.4 | ≈ –4.7 | 0 | ≈ 47.9 | – | [34] |
| $Co_3O_4$ nanosheets | 15 nm | 0.0002–0.006 mass% | 0.0008 mass% | SKALN 25X | Two-step | – | 2 h | – | Stable | 62.8 | ≈ –3.2 | 0 | ≈ 47.9 | – | [34] |
| $Fe_3O_4$, $TiO_2$, & Fe-Cu | < 130 nm | 5–20 mg/500mL | 10 mg/500mL | MO | Two-step | Bath | 45 | Oleic acid | Stable | – | 2.7, 2.3, & 1.8 | 40.3, –9.8, & 13.4 | – | – | [95] |
| $Fe_3O_4$, $TiO_2$, & Fe-Cu | < 130 nm | 5–20 mg/500mL | 10 mg/500mL | SE | Two-step | Bath | 45 | Oleic acid | Stable | – | 0.3, 1.3, & 0.9 | 26, –10.9, & 22.2 | – | – | [95] |
| $Fe_3O_4$, $TiO_2$, & Fe-Cu | < 130 nm | 5–20 mg/500mL | 10 mg/500mL | Rapeseed oil | Two-step | Bath | 45 | Oleic acid | Stable | – | 2.6, 1.3, & 1.9 | 8.3, –10.6, & 4.4 | – | – | [95] |
| Graphene | 1–5 nm | 0.01–0.05 mass% | 0.05 mass% | TO | Two-step | – | – | – | – | – | – | 857 | –79.2 | – | [96] |
| $Fe_3O_4$, $Co_3O_4$, & $Fe_3P$ | < 100 nm | 0.0012–0.004 mass% | 0.002 mass% | NE | Two-step | – | 2–3 h | Oleic acid | Stable | 7.3, 9.6 & 13 (M-M) | 4.4, 1.42, & 2.6 | – | – | – | [97] |

**Table 1** (continued)

| Nanoparticle (Remark if any) | Size/nm | Filler level range | Filler for listed DNF properties | Base fluid | Prep. method | Sonication | | Surfactant | Stability result/ period | Nanofluid properties enhancement compared to base fluid/% | | | | | References |
|---|---|---|---|---|---|---|---|---|---|---|---|---|---|---|---|
| | | | | | | Type | Time | | | BDV/Type | $\mathscr{E}_r$ | Tan δ | $\rho$ | $k$ | |
| $Fe_3O_4$, $Co_3O_4$, & $Fe_3P$ | < 100 nm | 0.0012–0.004 mass% | 0.002 mass% | SE | Two-step | – | 2–3 h | Oleic acid | Stable | 20.7, 2 & 20 (M-M) | 4.1, 1.9, & 6.18 | – | – | – | [97] |
| MWCNT | 5–15 nm | 0.001–0.02 g $L^{-1}$ | 0.005 g $L^{-1}$ | MO | Two-step | Probe | 2 h | – | Stable | 40.3 (LI) | 195.6 | –78 | 7400 | – | [98] |
| $TiO_2$ & ZnO (300 h thermal aged base vs. nanofluids) | 45, 60 nm | 0.04 mass% | 0.04 mass% | NE | Two-step | Bath | 7 h | – | $TiO_2$ > ZnO | 26.17 & 14.95 | – | 76.3 & 385.5 | –20.8 & –82 | – | [99] |
| $Al_2O_3$, $MoS_2$, & $TiO_2$ | 60–70 nm | 0.025 mass% | 0.025 mass% | MO | Two-step | – | – | – | Stable | 38.3, 26.1, & 12.8 | – | – | – | – | [100] |
| $TiO_2$ (60-day base vs. natural, forced nano-fluids) | 100 nm | 0.005–0.03 mass% | 0.015 mass% | NYNAS MO | Two-step | – | 30 min | – | Stable | 5.04 & 15.42 | – | – | – | – | [52] |
| $TiO_2$ | 21 nm | 0.005–0.040 vol.% | 0.020 vol.% | NE | Two-step | Bath | 1.5 h | – | Unstable | 22.4 | – | – | – | – | [5] |
| Graphene–$SiO_2$-doped | < 557.6 nm | 0.01–0.10 mass% | 0.10 mass% | MO-palm ester blend | - | Bath | 5 h | – | @pH 10 | –9.58 | – | –78.4 | –94.1 | – | [37] |
| Anatase $TiO_2$ (3 different size nanoparticles) | 9.5, 13.4, & 16.6 nm | 0.05–0.5 g $L^{-1}$ | 0.7 g $L^{-1}$ | MO | Two-step | Probe | 15 min | – | 1 month | 54.6, 109.3, & 85.3 | 16.4, 0.24, 14.6 | – | – | – | [101] |
| $Al_2O_3$ (HCT of DNF under electric field vs. BF) | < 201 nm | 0.1–0.3 vol.% | 0.3 vol.% | TO | Two-step | Bath | 1 h | – | Stable | – | – | – | – | - | [102] |
| Fluorinated BNNs | 5 nm | 0.0025–0.01 mass% | 0.005 mass% | MO-1 | Two-step | Bath | 2 h | – | 1 month | 26 | 1.3 | –11.5 | 161 | 0.9 | [33] |
| Fluorinated BNNs | 5 nm | 0.0025–0.01 mass% | 0.01 mass% | MO-2 | Two-step | Bath | 2 h | – | 1 month | 20 | –4.6 | 31.6 | 0 | – | [33] |
| SiC | 50 nm | 0.002–0.008 mass% | 0.004 mass% | FR3 | Two-step | Bath | 1.5 h | – | Stable | 37.3 | – | –57 | – | – | [103] |
| $SiO_2$, $TiO_2$, & $ZrO_2$ | 25 nm | 0.05–0.4 g $L^{-1}$ | 0.2 g $L^{-1}$ | Nynas MO | Two-step | – | 30 min | – | – | 62.7, 171, & 135.3 | – | – | – | – | [104] |
| Graphene quan-tum dots | 5–17 nm | 0.001 mass% | 0.001 mass% | TO | Two-step | Probe | 30 min | – | Stable | 2.2 | – | – | –2.5 | 3.4 | [105] |
| Graphene sheets | 50–70 nm | 0.0012–0.01mass% | 0.0025 mass% | TRANSOL | Two-step | Probe | 2 h | – | Stable | 40.3 | 0.43 | –21 | 126.9 | 30 | [12] |
| Graphene | 12 nm | 0.01–0.1 mass% | 0.1 mass% | TO | Two-step | Bath | 4 h | – | 3 months | – | – | – | – | ≈ 14 | [106] |
| $Fe_3O_4$, Graphene oxide, & $SiO_2$ | 10, 12, & 5 nm | 0.1 g $L^{-1}$ | 0.1 g $L^{-1}$ | Shell Diala D | Two-step | Probe | 15 min | – | Stable | 12, 12, 20 (DC + ve) 14.5, 8, 90 (DC -ve) | – | – | – | – | [107] |
| $FeO_3$ | < 250 nm | 0.10–0.20 mass% | 0.20 mass% | PKOME | Two-step | Probe | 2 h | – | – | 37.3 | – | – | – | – | [108] |

**Table 1** (continued)

| Nanoparticle (Remark if any) | Size/nm | Filler level range | Filler for listed DNF properties | Base fluid | Prep. method | Sonication | | Surfactant | Stability result/ period | Nanofluid properties enhancement compared to base fluid/% | | | | | References |
|---|---|---|---|---|---|---|---|---|---|---|---|---|---|---|---|
| | | | | | | Type | Time | | | BDV/Type | $\mathscr{E}_r$ | Tan δ | $\rho$ | $k$ | |
| $Fe_3O_4$ | 8.7 nm | 0.07–0.48 vol.% | 0.48 vol.% | Mogul Trafo CZ-A | Two-step | – | – | Oleic acid | 7 years | No change @ RT | – | – | – | – | [109] |
| $Al_2O_3$ nanorods & plates | 15–40 nm | 0.6–1.2 g $L^{-1}$ | 0.6 g $L^{-1}$ | MO | Two-step | – | – | Oleic acid | – | –2.8 & 9 (+ ve LI) | – | – | – | – | [110] |
| $Al_2O_3$ nanoplates | 40 nm | 0.6–1.2 g $L^{-1}$ | 0.6 g $L^{-1}$ | MO | Two-step | – | – | C2 | – | 5.6 (+ ve LI) | – | – | – | – | [110] |
| $Al_2O_3$ nanoplates | 40 nm | 0.6–1.2 g $L^{-1}$ | 0.6 g $L^{-1}$ | MO | Two-step | – | – | C18 | – | 7.2 (+ ve LI) | – | – | – | – | [110] |
| $Al_2O_3$ and Anatase $TiO_2$ | 11–18nm | 0.2–1 mass% | 0.05 mass% | PKEO | Two-step | – | – | Oleic acid | Stable | 38 & 33.3 (DC) | 63 & 89.4 | –97 & –94.4 | – | – | [111] |
| Silicon | 10–30 nm | 0.001–0.005 vol.% | 0.001 vol.% | MO | Two-step | Bath | 4 h | Oleic acid | Stable | 4.3 (AC), 4.2 (LI) | 0 | –18 | – | – | [112] |
| $SiO_2$ & $Al_2O_3$ (Separate) | 12–13 nm | 0.1 mass% | 0.1 mass% | MO | Two-step | – | 2 h | CTAB | Stable | 63 & 53 | – | – | – | – | [113] |
| $Al_2O_3$ & AlN (Sphere) | 13&50 nm | 0.5 vol.% | 0.5 vol.% | TO | Two-step | Bath | – | Oleic acid | Stable | – | – | – | – | 20 & 8 | [41] |
| $ZrO_2$ | 5–10 nm | 0.1–0.5 g $L^{-1}$ | 0.2 g $L^{-1}$ | TO | Two-step | – | 30 min | CTAB | Stable | 25.4 (AC) | – | – | – | 16.6 | [114] |
| $SiO_2$ (DNF without surfactant vs. with three surfactants) | 15 nm | 75 mg $L^{-1}$ | 75 mg $L^{-1}$ | MO | Two-step | – | 2 h | CTAB<br>Oleic acid Span 80 | Stable | 11 (AC), 11 (+DC)<br>17 (AC), 16 (+DC)<br>20 (AC), 22 (+DC) | – | 435.9<br>247.4<br>247.4 | – | – | [115] |
| $Al_2O_3$-$TiO_2$ (Mix 50:50%) (With three different base oils) | <21 nm | 0.2–0.6 mass% | 0.2 mass% | SO<br>COO<br>PAO | Two-step | Bath | 3 h | CTAB | 30 days | – | – | – | – | 11.4<br>15.8<br>48.9 | [116] |
| $Al_2O_3$ | – | 0.2–1mass% | 0.6 mass% | PKEO | Two-step | – | – | Oleic acid | Stable | 100.3 | – | –97 | ≈20 times | – | [117] |
| $TiO_2$ | – | 0.2–1mass% | 0.6 mass% | PKEO | Two-step | – | – | Oleic acid | Stable | 89.4 | – | –94 | ≈8 times | – | [117] |
| ZnO & Anatase $TiO_2$ | 29.5 nm | 0.001–0.009 g $L^{-1}$ | 0.005 g $L^{-1}$ | 80:20 Ester-MO | Two-step | – | – | Oleic acid | Stable | 16 & 17 | – | – | – | – | [118] |
| $Fe_3O_4$ | 50 nm | 0.05–0.4 g $L^{-1}$ | 0.4 g $L^{-1}$ | MIDEL 1204 | Two-step | Probe | 2 h | – | Stable | 7.07 | – | – | – | – | [119] |
| $Al_2O_3$ (2 size) | 13&50 nm | 0.05–0.4 g $L^{-1}$ | 0.05,0.3 g $L^{-1}$ | MIDEL 1204 | Two-step | Probe | 2 h | – | Stable | 7.56 & 6.15 | – | – | – | – | [119] |
| $SiO_2$ | 10–20 nm | 0.05–0.4 g $L^{-1}$ | 0.3 g $L^{-1}$ | MIDEL 1204 | Two-step | Probe | 2 h | – | Stable | 5.76 | – | – | – | – | [119] |
| $SiO_2$ & $WO_3$ | 18, 40 nm | 0.2–1 mass% | 0.2–1 mass% | Neem oil ester | Two-step | – | – | Oleic acid | 48 h | – | – | – | – | Best $SiO_2$ | [120] |
| Anatase $TiO_2$ | 10–20 nm | 0.0045–.00562 mass% | .00562 mass% | MO | Two-step | Probe | 2.5 h | CTAB | Stable | 36 (AC), 43 (DC) | – | – | – | – | [121] |
| Graphene | 3–6 nm | 0.0015–.0.01 mass% | 0.01 mass% | Graphene | Two-step | Probe | 0.5&1 h | SDBS | 90 days | 37.23 & 41.49 | 1.8 & 2.1 | -8.8 & -12.4 | 0.5 & 3.2 | 29,47 time | [122] |
| Nanodiamonds | 4–8 nm | 0.04–0.16 mass% | 0.12 mass% | MO | Two-step | Both | 1&0.5 h | Oleic acid | 3 months | – | – | 0.06 | -2.8 | 14.5 | [123] |

enhances thermal conductivity by maintaining efficient heat transfer pathways [12]. Stability can be accomplished with electrostatic methods (i.e., charging the surface of the nanoparticle induces repulsion profiles) and steric methods (i.e., coating the nanoparticles with polymers or surfactants) to form a steric barrier against particle aggregation [126–128]. For nanofluids to be stable in electrostatic method, the electrostatic repulsive forces between the particles should be greater than the attractive Van der Waals forces [129]. The stability arising from electrostatic stabilization depends upon the surface charge of the dispersed nanomaterial. Moreover, the electrostatic stability increases due to enhanced repulsive forces from highly electronegative or electropositive materials [11]. The charge ($Q_P$) that a nanoparticle develops is dependent on the type of nanoparticle, given by the following equation [104]:

$$Q_P = \begin{cases} -12\Pi E_1 E_0 R^2, & \text{conductive nanoparticles} \\ -12\Pi E_1 E_0 R^2 \dfrac{E_2}{2E_1 + E_2}, & \text{semiconductive and insulative nanoparticles} \end{cases} \quad (1)$$

where $\mathcal{E}_1$ and $\mathcal{E}_2$ are the dielectric constants of base oil and nanoparticles, respectively; $E_0$ is the external electric field strength, and $R$ is the radius of nanoparticles.

As the equation given suggests, the charge accumulation is highest for conductive nanoparticles and the lowest for semiconductive and insulative nanoparticles, which can be explained by a higher electronic polarizability and better dielectric screening of conductive nanoparticles [130, 131]. However, this also entails a significant increase in the contribution toward electrostatic stabilization. Decrease in the electrostatic stabilization contribution with increase in bandgap. Fig. 2b shows how the dielectric constant, charge accumulation, zeta potential, and degree of electrostatic stabilization change with bandgap. Referring to the equations and correlations discussed, Table 2 shows the proposed empirical equations for the stability property (i.e., zeta potential) in relation to bandgap energy based on these correlations.

Nanoparticles' polarization and charge structure can be altered by narrowing their band width. This can lead to increased stability. Bhunia et al. used fluorinated BNN nanosheets to study transformer oil-based f-BNN nanofluids [33]. The bandgap of extremely insulating boron nitride nanosheets was narrowed by adding a small amount of conductive fluorine to their surface. This resulted in high negative charge accumulation on the surface of BNN nanosheets, which contributed to electrostatic stabilization [132]. Thus, nanofluids were stable for up to a month after preparation. Tyndall scattering was used to determine the nanofluid's stability at room temperature. Fig. 3a clearly demonstrates that the scattering intensity remains consistent throughout the entire stability study, suggesting that the nanofluid samples remained stable for the entire duration of one month. In addition, the study conducted by Bhunia et al. found that the $TiO_2$ (i.e., semiconductive with a bandgap of 3.11 eV) DNF based on MO, remained stable for a period of 90 days [11]. Fig. 3b shows the Tyndall scattering images of the nanofluids at different time points: after preparation, 1.5 months, and 3 months. The images guarantee that the scattering intensity remains consistent throughout the stability study. The high electronegativity of $TiO_2$ plays a significant role in facilitating electrostatic stabilization, due to its lower bandgap.

#### Dielectric and thermal properties

The bandgap of the nanoparticles in nanofluids can potentially influence their dielectric and thermal properties [34, 91, 133]. Table 3 compares the range of nanofluid property enhancements compared to BF containing insulative, semiconductive, and conductive nanomaterials, emphasizing how the bandgap influences these properties.

Wider and moderate bandgap insulative and semiconductive nanoparticles have also been used to suppress dielectric breakdown by restricting mobile electrons, leading to substantial advancements in BDV. Charge trapping in nanofluids during breakdown is presented in Fig. 4a. A better understanding of this is achieved by examining the dielectric relaxation time [30]. Dielectric relaxation time $(\tau_{NF})$ of a nanofluid can be expressed as [134]:

$$\tau_{NF} = \frac{2\varepsilon_1 + \varepsilon_2}{2\sigma_1 + \sigma_2} \quad (2)$$

where $\sigma_1$ and $\sigma_2$ are the conductivities of base oil and nanoparticles, respectively.

Insulative nanoparticles exhibit high dielectric relaxation time due to their high dielectric constant and low conductivity. Semiconductive nanoparticles, on the other hand, exhibit moderate dielectric relaxation time due to their moderate dielectric constant and moderate conductivity. Dielectric relaxation time is a good indicator of higher breakdown strength; generally, a higher dielectric relaxation time suggests better insulating properties and thus higher breakdown strength. Therefore, nanofluids infused with insulative and semiconductive nanoparticles showed significant improvements in BDV because of their higher dielectric relaxation time compared to nanofluids with conductive nanoparticles. Bhunia et al. investigated two types of MOs dispersed with semiconductive $TiO_2$ nanoparticles [11]. The relaxation times of the $TiO_2$ nanofluids prepared with these two base oils were calculated as 424 µs and 421 µs, which are significantly higher than the nominal period of streamer propagation (which is of the order of a few nanoseconds). Additionally, at an optimum concentration of 0.005 mass% $TiO_2$ nanofluid with oil 1 exhibited better breakdown strength compared to oil 2, as shown in Fig. 4c. This can be attributed

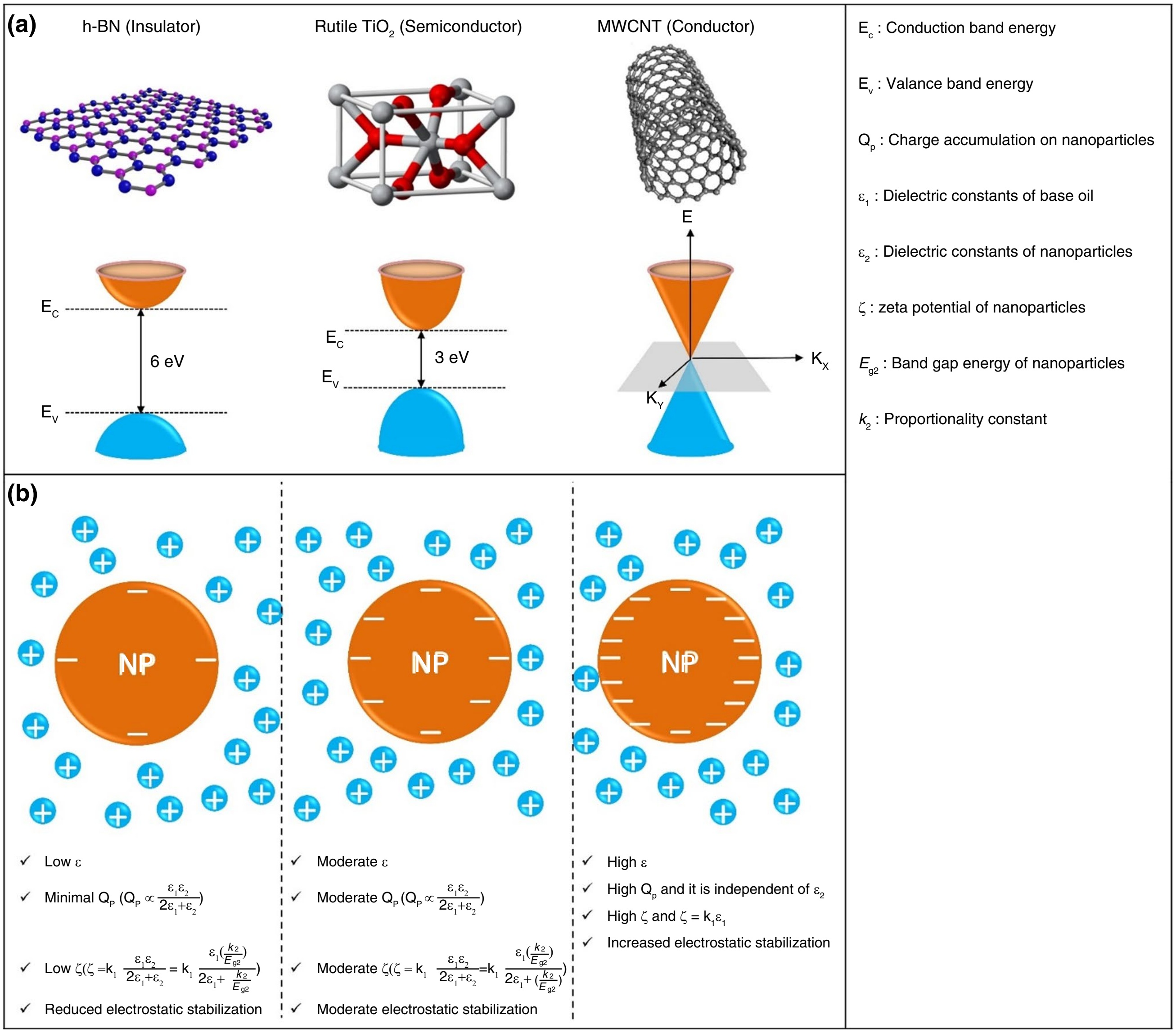


**Fig. 2** **a** Band structure of insulating, semiconductive, and conductive nanoparticles, and **b** Dielectric constant, charge accumulation, zeta potential, and electrostatic stabilization at various bandgaps

**Table 2** Proposed empirical equations for zeta potential for different bandgaps

| Lower bandgap/conductive | | Moderate (semiconductive) and higher bandgap (insulative) | |
|---|---|---|---|
| Correlations | Empirical equations | Correlations | Empirical equations |
| $Q_P$ is independent of $\mathcal{E}_2$ and thus ζ | ζ is independent of $E_{g2}$ and thus $\zeta = k_1\mathcal{E}_1$ | $Q_P \propto \frac{\mathcal{E}_1\mathcal{E}_2}{2\mathcal{E}_1+\mathcal{E}_2}$, thus $\zeta \propto \frac{\mathcal{E}_1\mathcal{E}_2}{2\mathcal{E}_1+\mathcal{E}_2}$ | $\zeta = k_1\frac{\mathcal{E}_1\mathcal{E}_2}{2\mathcal{E}_1+\mathcal{E}_2} = k_1\frac{\mathcal{E}_1(\frac{k_2}{E_{g2}})}{2\mathcal{E}_1+(\frac{k_2}{E_{g2}})}$, since $\mathcal{E}_2 \propto \frac{1}{E_{g2}}$ and $\mathcal{E}_2 = \frac{k_2}{E_{g2}}$ |

where $\zeta$ is the electrostatic or zeta potential of nanoparticles; $E_{g2}$ is the band gap energy of nanoparticles; and $k_1$ and $k_2$ are the proportionality constants

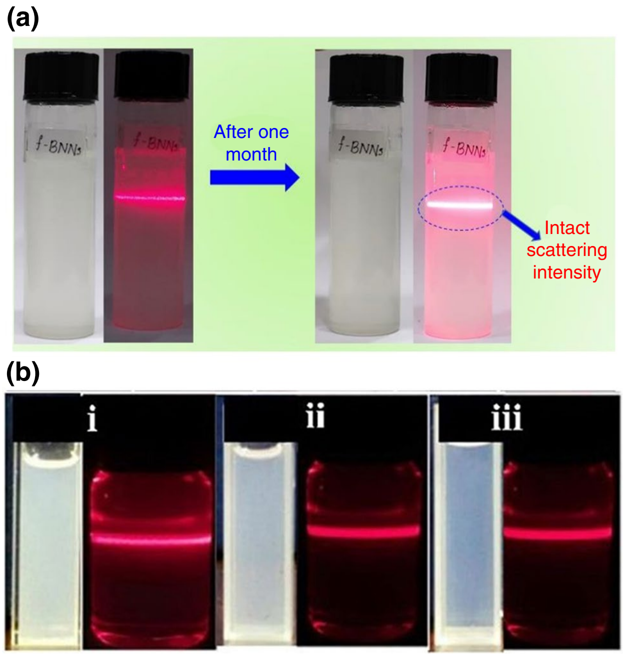


**Fig. 3** **a** Visual comparison of Tyndall scattering in 0.01 mass% nanofluid: freshly prepared vs. after one month—Reprinted under a CC license [33]; and **b** Tyndall scattering of 0.01 mass% nanofluid at different time intervals: after (i) preparation, (ii) 1.5 months, and (iii) 3 months—Reprinted with the license number 6092790346256 [11]

to the higher relaxation time of the $TiO_2$ nanofluid with oil 1 compared to oil 2, as shown in Fig. 4b.

In contrast, conductive nanoparticles with negligible bandgaps offered the highest improvement in dielectric constant of nanofluids due to their high polarization and charge storage capacity [135]. The Maxwell–Garnett equation that can predict the effective dielectric constant of nanofluids $\left(\varepsilon_{NF}\right)$ is as follows [136].

$$\frac{\varepsilon_{NF}-\varepsilon_1}{\varepsilon_{NF}+2\varepsilon_1}=N\frac{\varepsilon_2-\varepsilon_1}{\varepsilon_2+2\varepsilon_1} \quad (3)$$

where $N$ is nanoparticle concentration.

Insulative and semiconductive nanoparticles demonstrated significant reductions in tan δ by reducing dielectric losses through barriers and trapping charge carriers [137]. Therefore, these materials also showed substantial improvements in resistivity. There is no straightforward formula linking the bandgap of nanoparticles directly to the thermal conductivity of nanofluids. However, conductive nanoparticles showed unparalleled improvements in thermal conductivity, likely due to their high intrinsic thermal conductivity, efficient electron–phonon coupling, formation of effective heat pathways, reduced interface thermal resistance, and enhanced Brownian motion from improved electrostatic stabilization.

Bhunia et al. investigated the effect of bandgap reduction in nanoparticles on the thermo-dielectric properties of nanofluids [33]. Attaching a small quantity of conductive fluorine to highly insulating boron nitride nanosheets (functionalization) reduced their bandgap. Fig. 5a illustrates the streamer charges observed for pure BNN and fluorinated BNN with a narrowed bandgap. Fluorinated boron nitride nanosheets created additional charge trapping sites and accomplished surface charge enhancements, which allowed to improved AC BDV. Additionally, improvement of dielectric constant, tan δ, resistivity, and thermal conductivity were observed. Fig. 5b illustrates the improvements in these properties attributable to bandgap reduction, resulting from improved charge trapping, surface charge, and electrostatic stabilization. In summary, this work demonstrates how tuning the bandgap of particles can alter their thermo-dielectric properties, and can provide a pathway toward superior electrical and thermal performance when combined into nanofluids.

Functionalization can change the bandgap of MWCNTs, thus improving the dielectric and thermo-electric properties of transformer oil-based nanofluids by making the nanoparticles more stable and uniformly dispersed. Alizadeh et al. showed that hydroxylated MWCNTs which were covalently functionalized with stearic acid showed better performance than non-covalently functionalized with oleic acid [84]. The covalently modified nanoparticles improved convective heat transfer by up to 30.08% at 0.01 mass% and maintained dielectric strength, with only a 4.1% drop in BDV at 0.001 mass%. This improvement is due to less agglomeration, and better thermal conductivity and better interfacial interaction.

Table 3 also shows that the conductive nanoparticles with very low bandgap values were effective at low filler levels (0.01–0.1 mass% or 0.005–0.4 g $L^{-1}$) because their high conductivity allowed them to significantly enhance properties without requiring high concentrations. On the other hand, semiconductive and insulative nanoparticles, which had moderate to high bandgap values, required higher filler levels (up to 2 mass% or 0.3 g $L^{-1}$) to achieve similar property improvements. This was because their lower intrinsic conductivity necessitated a higher quantity to effectively enhance the material's dielectric properties and achieve the desired performance.

## Nanoparticle size variation and ultrasonic cavitation

Nanoparticle size also affects the stability, dielectric, and thermal properties of nanofluids. Researchers used nanoparticles of various sizes to investigate this effect [88, 119]. Suhaimi et al. studied MO-based CNT nanofluids [88]. Compared to base oil, nanofluids improved AC BDV by 1.88% for CNT size > 20 nm and 42.4% for CNT size < 8 nm. U. Khaled and A. Beroual studied MIDEL 1204-based

**Table 3** Range of nanofluid property enhancements compared to base fluid containing insulative, semiconductive, and conductive nanomaterials

| Material type | Nanomaterials | Filler level range | Range of nanofluid properties enhancement compared to base fluid/% | | | | | References |
|---|---|---|---|---|---|---|---|---|
| | | | BDV | $\mathscr{E}_r$ | Tan δ | ρ | k | |
| Insulative | h–BN, $Al_2O_3$, $SiO_2$, $ZrO_2$, and nanodiamonds | 0.02–2 mass%<br>0.015 vol.%<br>0.03–0.3 g $L^{-1}$ | 4.3 to 135.3 | 0.49 to 63 | −31 to −97 | 23.5 to ≈20 times | 4.4 to 20.33 | [10, 72, 83, 89, 92, 94, 100, 104, 111, 113, 114, 117, 119, 123] |
| Semiconductive | CuO, Anatase $TiO_2$, ZnO, Rutile $TiO_2$, CNT, $Co_3O_4$, $MoS_2$, fluorinated BNNs, SiC, and Si | 0.002–1 mass%<br>0.001–0.02 vol.%<br>0.005–0.2 g $L^{-1}$ | 2 to 171 | 1.3 to 89.4 | −9.8 to −94.4 | 1.9 to 216.24 | 0.9 to 210 | [5, 11, 32, 33, 86, 92, 93, 95, 97, 99, 100, 103, 104, 111, 112, 117, 118, 121] |
| Conductive | $Fe_3O_4$, MWCNT, Fe-Cu, graphene, $Fe_3P$, and graphene quantum dots | 0.01–0.1 mass%<br>0.005–0.4 g $L^{-1}$ | 2.2 to 41.49 | 0.3 to 195.6 | −8.8 to −78 | 0.5 to 126.9 | 3.4 to 47 time | [12, 84, 87, 95–98, 105, 106, 119, 122] |

$Al_2O_3$ nanofluids [119]. Compared to base oil, nanofluids improved AC BDV by 6.15% for 50 nm and 7.56% for 30 nm. In both cases, smaller nanoparticles outperformed larger nanoparticles for AC breakdown.

Conversely, some researchers utilized ultrasonication to study the impact of nanoparticle cluster size on stability, thermal, and dielectric properties [138, 139], as ultrasonication can break nanoparticle clusters into smaller clusters in nanofluids. Fig. 6a to d presents a schematic of breaking cubic and spherical nanoparticle cluster to increase surface area and the number of nanoparticle clusters. Under ideal ultrasonication conditions, increasing the sonication period results in better fragmentation of nanoparticle clusters. Table 4 lists the stability parameter (i.e., zeta potential), dielectric, and thermal properties measured at longer and shorter sonication periods, along with the percentage enhancement in properties at longer sonication periods compared to shorter periods. Longer sonication periods enhanced stability, thermal, and dielectric properties more, due to the increased degree of nanoparticle cluster breakup, compared to shorter durations. Fig. 6e presents percentage improvement in stability, thermal conductivity, and AC BDV, at longer sonication periods compared to shorter periods due to the increased degree of nanoparticle cluster breakup. The zeta potential increased by ≈ 34% and the thermal conductivity improved by ≈ 1% when the sonication time was extended from 30 to 60 min at a concentration of 0.05 vol.% [140]. Meanwhile, the AC BDV saw a 8.88% enhancement when the sonication time was extended from 30 to 120 min at a concentration of 0.01 g $L^{-1}$ [88]. The reasons for the improvement, underlying causes, empirical equations, and exceptions are discussed further.

Smaller size of nanoparticles or nanoparticle clusters improves zeta potential of the nanofluids. The observed enhancement in this case is a result of their increased surface area-to-volume ratio, which increases the interaction with the fluid and decreases agglomeration [145]. Smaller particles also have a higher surface charge density, which means stronger electrostatic repulsion against aggregation [146]. Moreover, smaller nanoparticles exhibit more vigorous Brownian motion, which keeps them suspended and prevents settling [147].

The charge scavenging improves the BDV of dielectric fluids. Infusing nanoparticles in dielectric fluids or EDLs around them creates more fluid trapping sites [33, 148, 149]. These trapping sites result in an increased in BDV [38]. According to the literature, an increase in the BDV caused by smaller size nanoparticles at the specified concentration was attributed to an increase in trapping sites due to additional surface area. The dielectric constant exhibits a direct proportionality to the abundance of liquid molecules and solid nanoparticles or nanoparticle clusters

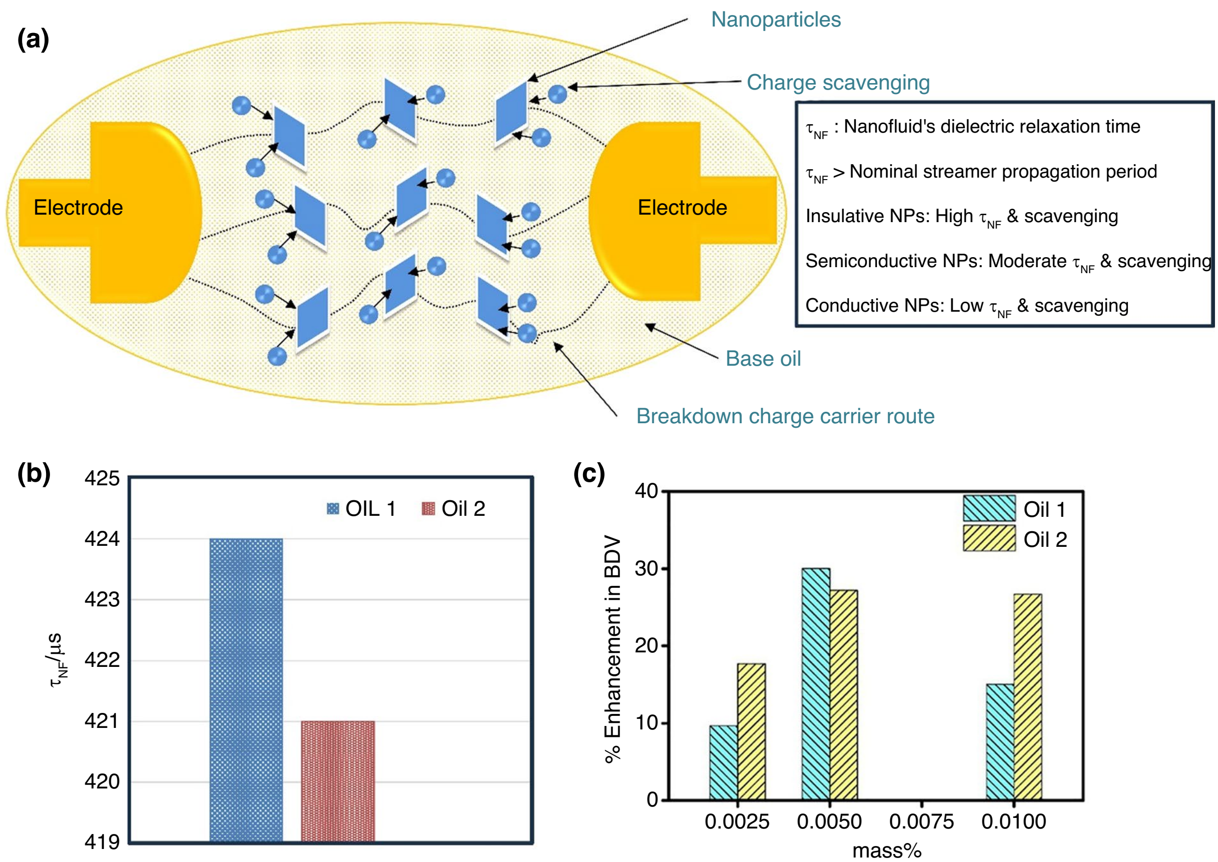


**Fig. 4** **a** Charge trapping phenomenon by nanofluids during breakdown—Reprinted with the license number 6092790876576 [125]; **b** Dielectric relaxation time and **c** enhancement in breakdown voltage of $TiO_2$ nanofluids containing two types of base oils—Reprinted with the license number 6092790346256 [11]

within a given volume [150, 151]. At a specified concentration, the number of liquid molecules per unit volume remains constant, whereas the number of nanoparticles or nanoparticle clusters per unit volume increases with smaller size nanoparticles or nanoparticle clusters [39, 152]. Based on the Clausius–Mossotti model [153], this leads to an enhanced dielectric constant in the nanofluid $(\varepsilon_{\mathrm{NF}})$.

$$\frac{\varepsilon_{\mathrm{NF}}-1}{\varepsilon_{\mathrm{NF}}+2}=\frac{1}{3\varepsilon_0}\left[N_1\alpha_1+N_2\alpha_2+N_2\alpha_3\right] \tag{4}$$

where $\varepsilon_0$ is the permittivity of free space; $N_1$, $N_2$, and $N_3$ are the base fluid molecule counts in free space, number of nanoparticles molecules, and number of liquid-medium molecules at nanoparticle-medium contact, respectively; and $\alpha_1$, $\alpha_1$, and $\alpha_1$ are the polarizability of base fluid, inner polarizability of nanoparticles, orientational polarizability of charged nanoparticles, respectively.

Additionally, improved charge trapping sites, resulting from a decrease in nanoparticle or nanoparticle cluster size at a specified concentration, contribute to increased resistivity (or decreased electrical conductivity). This, in turn, reduces the tan δ of nanofluid, as described by the following equation [60, 154]:

$$\tan\delta=\frac{I_1}{I_{\mathrm{c}}}=\frac{\sigma_{\mathrm{ac}}}{\omega\varepsilon'} \tag{5}$$

where $I_l$ is the effective current, $I_c$ is the charging current, $\sigma_{ac}$ is the AC electrical conductivity, $\omega$ angular frequency, and ε′ is the dielectric constant of nanofluid.

The enhanced thermal conductivity with small sized nanoparticles is governed by phonon transport, Brownian motion, and interaction between nanoparticles due to the EDL [40]. For effective heat transport through phonons, the phonon mean free path must be larger than the size of nanoparticles or nanoparticle clusters [155]. Based on phonon transport, the thermal conductivity term $(K_{\mathrm{p}})$ can be stated as follows [156].

$$K_{\mathrm{p}}=\sum_{\mathrm{i}=1}^{n}C_{\mathrm{i}}(\omega)v_{\mathrm{i}}^2(\omega)\tau_{\mathrm{i}}(\omega)d\omega \tag{6}$$

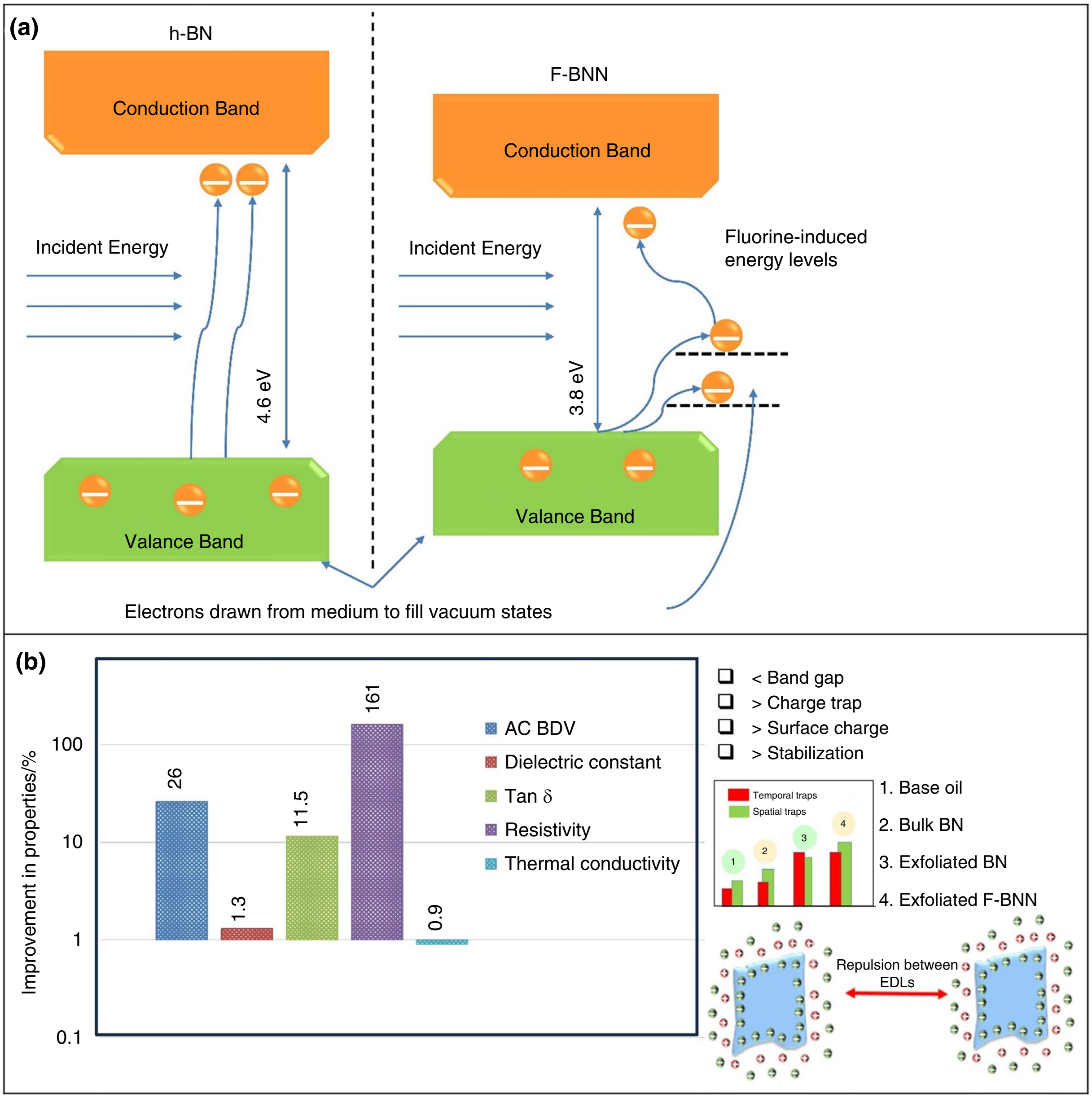


**Fig. 5** **a** Pure BNN and fluorinated BNN streamer charges and bandgap and **b** Percentage improvement in thermo-dielectric properties and enhancement in surface properties resulting from the use of fluorinated BNN—Redrawn under a CC license [33]

where $n$ is the number of phonon polarization branches, $i$ is the branch index, $C_i$ is the mode specific heat, $v_i$ is the phonon group velocity, and $\tau_i$ is the phonon relaxation time.

All terms on the right-hand side of the equation support increased thermal conductivity due to phonon transport in smaller nanoparticles or nanoparticle clusters.

The thermal conductivity due to Brownian motion and EDL, i.e., $K_{Br}$ and $K_{EDL}$, respectively, can be stated as follows [157].

$$K_{Br} = \frac{NL_{np}C_V}{3}\frac{K_B T}{3\pi\mu D_{np}L_{oil}} \tag{7}$$

$$K_{EDL} = \frac{NL_{np}C_V}{3}\sqrt{\frac{Aq^2L_{np}}{\varepsilon_{oil}M_{np}\left(r\varphi^{-1/3}\right)^2}} \tag{8}$$

where $L_{np}$ is the mean free path of nanoparticles, $C_V$ is the specific heat, $K_B$ is the Boltzmann constant, $T$ is the temperature, $\mu$ is the viscosity, $D_{np}$ is the nanoparticle diameter, $L_{oil}$ is the mean free path of oil molecules, $A$ is the Coulomb

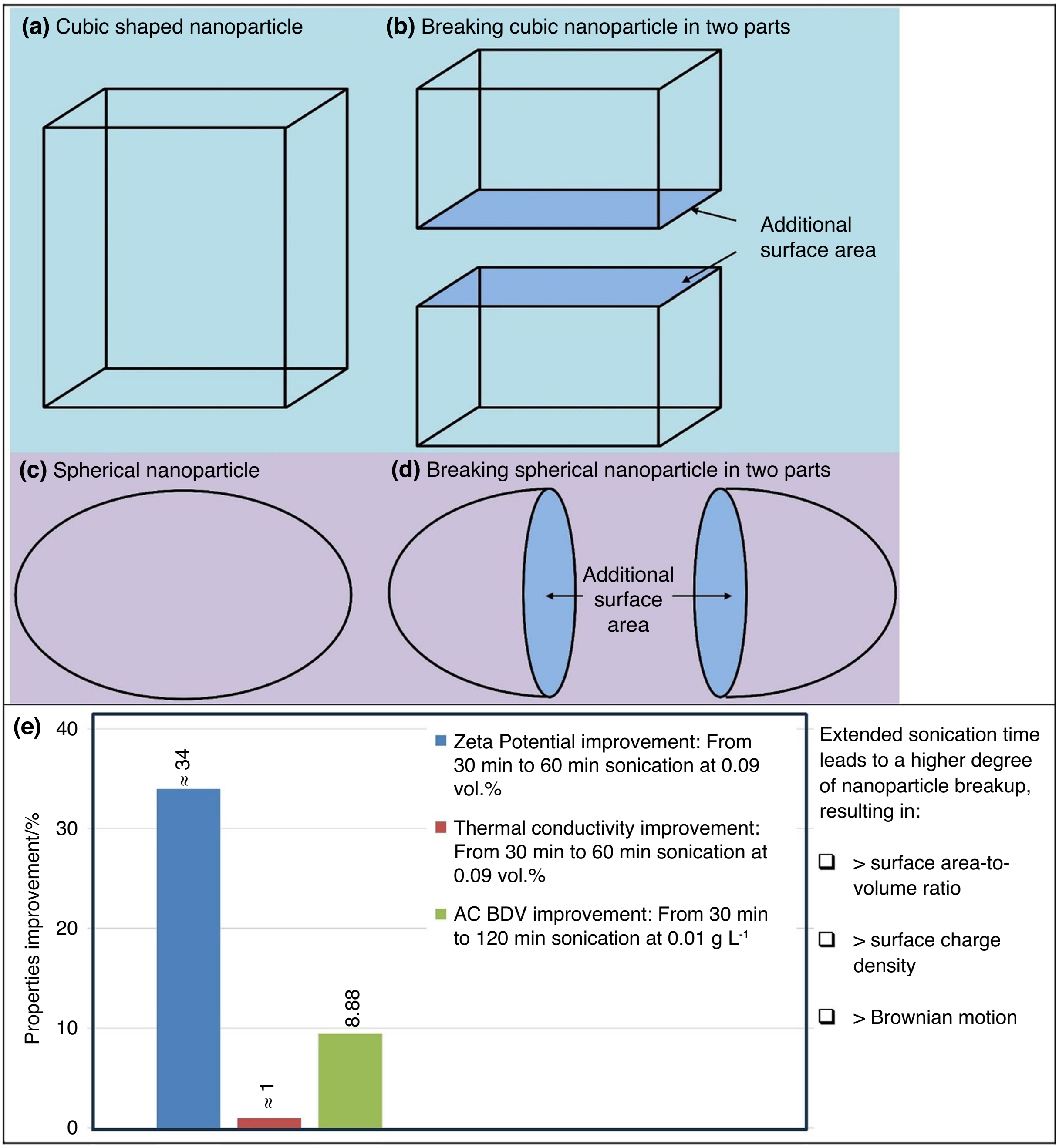


**Fig. 6** **a–d** Schematic of breaking cubic and spherical nanoparticle to increase surface area and number of nanoparticle or nanoparticle cluster; **e** Percentage improvement in zeta potential and thermal conductivity—Redrawn with permission from Elsevier with the license number 6092791305328 [140] and AC breakdown voltage—Redrawn under a CC license [88], at longer sonication periods compared to shorter periods due to the increased degree of nanoparticle cluster breakup

constant, $q$ is the surface charge of nanoparticles, $\varepsilon_{oil}$ is the dielectric constant of oil, $Mnp$ is the nanoparticle mass, $r$ is the radius of nanoparticles, and $\varphi$ is the nanoparticle volume fraction.

Smaller nanoparticles or nanoparticle clusters improve both the thermal conductivity due to Brownian motion and the EDL, as demonstrated by the relationships in these equations.

There are a few exceptions where larger nanoparticles outperformed smaller ones. Elsad et al. investigated MO-based anatase phase $TiO_2$ nanofluids [101]. $TiO_2$ nanoparticles with sizes 9.5, 13.4, and 16.6 nm were studied. Compared to base oil, nanofluids showed 54.6%, 109.3%,

**Table 4** Properties measured at longer and shorter sonication period and percentage enhancement in properties with increased sonication duration

| Property | Nanoparticles | Base liquid | Longer sonication period | Shorter sonication period | Measurement at longer sonication period | Measurement at shorter sonication period | Property improvement in longer sonication time compare to shorter time/% | Assessed condition | Ref |
|---|---|---|---|---|---|---|---|---|---|
| Zeta potential | $CeO_2$ + MWCNTs | Silicon oil | 60 min | 30 min | ǀ40.1ǀ mV | ǀ36.3ǀ mV | 10.5 | Assessed after 30 days | [141] |
| Zeta potential | $Fe_3O_4$ | Liquid paraffin | 4 h | 2 h | − 50 mV | − 42 mV | 19 | – | [142] |
| Thermal conductivity | MWCNTs | Therminol 55 | 60 min | 30 min | 0.137 $Wm^{-1}K^{-1}$ | 0.135 $Wm^{-1}K^{-1}$ | ≈ 1% | 0.09 vol.% | [140] |
| Thermal conductivity | $TiO_2$ | Paraffin oil | 60 min | 20 min | 10.2% | 6.5% | 56.9 | – | [143] |
| AC BDV | CNTs | MO | 120 min | 30 min | 51.9 kV | 47.4 kV | 8.88 | 0.01 g $L^{-1}$ | [88] |
| Nanofluid-to-base fluid thermal conductivity ratio | $Al_2O_3$ | Liquid paraffin | 4 h | 1 h | 1.02 | 1.01 | 1 | 0.01 vol.%, 20 °C | [144] |
| Zeta potential | MWCNTs | Therminol 55 | 60 min | 30 min | ǀ64.2ǀ mV | ǀ47.7ǀ mV | ≈ 34 | 0.09 vol.% | [140] |
| Thermal conductivity | $Fe_3O_4$ | Liquid paraffin | 4 h | 2 h | 0.136 $Wm^{-1}K^{-1}$ | 0.121 $Wm^{-1}K^{-1}$ | 12.1 | 0.005 vol.%, 20 °C | [142] |
| Tan δ | Graphene | CSO | 60 min | 30 min | 0.00762 | 0.00793 | 3.9 | 0.01 mass%, 45 °C | [122] |
| Dielectric constant | Graphene | CSO | 60 min | 30 min | 2.995 | 2.986 | 0.3 | 0.01 mass%, 45 °C | [122] |
| Volume resistivity | Graphene | CSO | 60 min | 30 min | 1.085 (T Ω-cm) | 1.059 (T Ω-cm) | 2.4 | 0.01 mass%, 45 °C | [122] |
| Zeta potential | $CeO_2$ + MWCNTs | Therminol VP-I | 60 min | 30 min | ǀ23.8ǀ mV | ǀ17.9ǀ | 33 | Assessed after 30 days | [141] |

and 85.3% improvement in AC BDV, respectively. This may be due to due to enhanced interfacial zones, better dispersion, reduced agglomeration, and effective water molecule trapping, which delay electrical breakdown. Ultrasonication breaks nanoparticles and nanoparticle clusters; however, excessive ultrasonication periods limit the dispersion stability of nanofluids [144]. Longer ultrasonication periods can also overheat DNFs, reducing their dielectric properties. Moreover, the characteristics of nanofluids typically improve within the first 45 min of sonication [158].

## Phase and shape of nanoparticles

Phase of nanofillers also plays a significant role in improving the ability of heat transfer and dielectric properties of nanofluids. The unit cells of different material phases exhibit varied structures, which influence heat transfer along all three crystallographic axes (a, b, and c), which are perpendicular to each other [159, 160]. For instance, the anatase phase of $TiO_2$ contributes to a greater thermal conductivity in comparison with the rutile phase, because the anatase phase allows low-frequency acoustic phonons along the a and b axes (which are the main contributors to thermal conductivity) to travel longer distances [160, 161], as shown in Fig. 7a and b [160], this results in high thermal conductivity.

Fig. 7c highlights the d-spacing of anatase and rutile phases within a single particle from the $TiO_2$ nanoparticle sample [161]. It uses high-resolution TEM (HR-TEM) to showcase the coexistence of anatase (d-spacing = 0.35 nm) and rutile (d-spacing = 0.248 nm) crystallites. This d-spacing difference indicates changes in lattice structure and also strain, which correlates with thermal conductivity and phonon scattering in the material. Density functional theory (DFT)-derived thermal conductivities as a function of the temperature from 250 to 400 K for the anatase and rutile phases of $TiO_2$ nanoparticles are shown in Fig. 7d [161].

The figure clearly illustrates that the anatase phase of $TiO_2$ has a higher thermal conductivity than the rutile phase at a given temperature. The thermal conductivities of rutile and anatase $TiO_2$ at 300 K were determined to be 4.059 W/m–K and 5.818 W/m–K, respectively.

The rutile phase of $TiO_2$ nanoparticles demonstrates outstanding electrical resistivity, remarkable thermal stability, and strong mechanical strength in comparison with the other common phases of $TiO_2$ nanoparticles, specifically brookite and anatase [162]. The properties of rutile phase of $TiO_2$ nanoparticles present significant benefits for utilizing nanoparticles in DNFs. Fal et al. demonstrated that the phase of $TiO_2$ nanoparticles has a significant impact on the electrical conductivity of ethylene glycol-based nanofluids [163]. Nanofluids containing TiO2 nanoparticles in the anatase phase improve electrical conductivity to 10,727.98 μS/cm, representing a 4,586,400% increase at a concentration of 20 mass%. Nanofluids with rutile phase nanoparticles had the lowest rise in electrical conductivity, measuring at 25.85 μS/cm. This suggests that rutile nanoparticles are more suitable for DNFs than anatase.

Researchers conducted a thorough investigation of anatase and rutile phase $TiO_2$ nanoparticles in DNFs independently. Surprisingly, because of the intricate behavior of nanofluids, both phases of nanoparticles improved the dielectric and thermal properties of their respective BFs. However, there is a lack of research that utilizes both rutile and anatase phase $TiO_2$ nanoparticles with a common BF to comparatively examine their effects on the performance of DNFs. Qin et al. investigated T66-based anatase $TiO_2$ nanofluids [32]. Nanofluid showed dispersion stability for 56 days and thermal conductivity improved by 44.6%. Bhunia et al. investigated two types of MO-based ultra-thin anatase phase $TiO_2$ nanofluids [11]. A MO-based nanofluid demonstrated dispersion stability for 3 months, and improved AC BDV, dielectric constant, tan δ, resistivity, and thermal conductivity by 11.27%, 6.28%, − 13.16%, 216.24%, and 210%, respectively, compared to BF. Other researchers obtained good dispersion stability, dielectric, and thermal properties in transformer oil-based anatase phase $TiO_2$ nanofluids [101, 111, 118, 121]. Chakraborty et al. found that FR3-based rutile phase $TiO_2$ nanofluids improved tan δ by − 24% when compared to the BF [92].

Nanoparticle shape affects nanofluid stability, dielectric, and thermal properties [34, 41, 91, 110]. Their interfacial interactions, charge trap, and thermal conduction due to surface area vary their properties. These shapes can be sphere, cube, rod, nanobelt, and sheet (plate)[164, 165]. In an attempt to enhance the performance of DNFs for use as transformer fluids and in heat transfer applications, researchers often investigated these shapes of nanoparticles. Fasehullah et al. investigated synthetic ester oil-based nanofluids dispersed with CdS spherical nanoparticles, nanobelts, and nanosheets [91]. High-resolution transmission electron microscopy (HR-TEM) images of CdS nanoparticles, nanobelts, and nanosheets along with their corresponding selected area electron diffraction (SAED) patterns are shown in Fig. 8. The nanoparticles (Fig. 8a and c) with spherical morphology and an average crystallite size were 6 nm, SAED pattern (Fig. 8b and d) that was the nature of polycrystalline is further confirmed. The nanobelts (Fig. 8e–g) of sea urchin shape at the length of 200 nm and thickness 8nm and with polycrystalline structure (Fig. 8h). The nanosheets (Fig. 8i–k) show the ultra-thin 2D morphology (800 nm × 700 nm × 3 nm) and the diffraction pattern (Fig. 8l) indicates a hexagonal crystal structure. These CdS spherical nanoparticles, nanobelts, and nanosheets improved AC BDV by 35.5%, 37%, and 38.3% (Fig. 8m), respectively, over BF. Nanosheets improved AC BDV most due to their high surface area, followed by nanobelts and cubic nanoparticles.

Xu et al. investigated SKALN 25X transformer oil-based $Co_3O_4$ nanoparticles, nanobelts, and nanosheets stable nanofluids [34]. Compared to BF, nanofluids showed 65.7%, 79.4%, and 62.8% improvement in AC BDV (Fig. 8n); ≈− 4.7, ≈− 4.7, and ≈− 3.2 improvement in dielectric constant and; 0, ≈47.9, ≈47.9 in volume resistivity, respectively. There is clear evidence of shape-dependent property variation. Rafiq et al. investigated MO-based $Al_2O_3$ nanorods and nanoplates nanofluids [110]. Compare to BF, nanofluids showed − 2.8% and 9% improvement in + ve lightning impulse (LI) voltage, respectively. Choi et al. investigated transformer oil-based $Al_2O_3$ nanospheres and nanorods [41]. Compared to BF, nanofluids showed 20% and 8% improvement in thermal conductivity, respectively.

Lv et al. examined the impact of shape of nanoparticles (i.e., $TiO_2$ nanospheres and nanorods) on the pre-breakdown and breakdown properties of transformer oil-based nanofluids [166]. $TiO_2$ nanorods showed the dominant effect, with up to 55.5% increase in the positive impulse BDV, whereas nanospheres up to 1.23 times. In Fig. 9, characteristics of streamer propagation pre-breakdown reveal that the streamers appear in a tree shape for base oil, whereas in bush shape for nanofluids. With nanorods, more lateral branches are produced that are much denser and the distance between main channels is much closer than those of nanofluid with nanospheres. Interestingly, the nanofluid containing nanorods has a shorter propagation length of the streamer. At the same time, this results in more branches in case of nanorods as larger-streamers are blocked. It is because of the large interfacial layer zone around nanorods and the specific extended charge migration zone for the easy charge migration [167]. In nanofluid with nanorods, the space charges created at the streamer tips are distributed more uniformly, thereby alleviating the distortion of the electric field, which inhibited streamer propagation. As a result, addition of nanorods

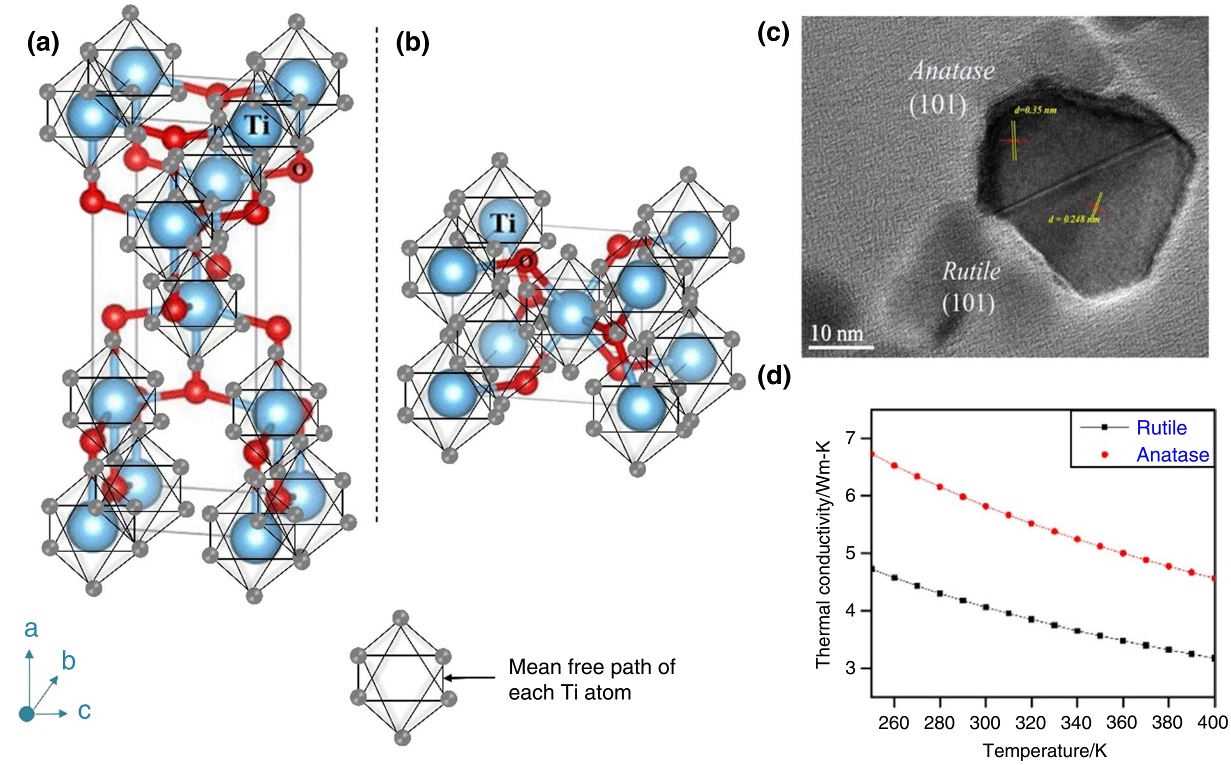


**Fig. 7** Comparison of mean free path of $TiO_2$ unit-cell **a**Anatase and **b** Rutile—Redrawn with permission from Elsevier with the license number 6092800078882 [160]; and **c** HR-TEM picture showing the d spacing of rutile and anatase phases inside a single particle and **d** Temperature-dependent variation of thermal conductivity for anatase and rutile phase nanoparticles—Reprinted with the license number 6092820789790 [161]

compared to nanospheres greatly suppresses pre-breakdown streamer propagation, hence enhancing the BDV.

## Blending and nano-structuring of nanoparticles

Many researchers used single nanoparticles to improve the properties of base dielectric fluid. Blending of nanoparticles is a mixture of multiple nanoparticle types in a predetermined ratio [25, 26]. Researchers have investigated nanoparticle blends in DNFs, demonstrating superior dielectric and thermal properties [90, 116]. These studies described the nanofluid made from the dispersion of two or more nanoparticles which is collectively termed as hybrid nanofluid. The thermal and dielectric properties of insulating fluids can be greatly enhanced by the use of hybrid nanofluids. Despite the fact that most of the studies focus on the single nanoparticle types, the investigation of the hybrid nanofluids is quite scarce for the literature. Such an approach could be beneficial by allowing the complementary advantages of different types of nanoparticles to be combined. For example, $Al_2O_3$ shows better thermal conductivity, and $TiO_2$ shows better BDV when dispersed in transformer oil. The combination of these two nanoparticles can provide an effective way to improve the thermo-dielectric properties of nanofluid [5, 83].

Wanatasanappan et al. investigated coconut, soybean, and palm oil-based nanofluids, dispersed with a blend of $Al_2O_3$-$TiO_2$ (50:50 ratio) nanoparticles [116]. Fig. 10a shows TEM pictures of $Al_2O_3$-$TiO_2$ nanoparticles' blend. The mean particle sizes of $TiO_2$ observed in the TEM image are approximately 21 nm and the diameter of $Al_2O_3$ is about 8 nm. Also, the chains of these small $Al_2O_3$ nanoparticles arrange themselves around the larger $TiO_2$ nanoparticles without significant overlap.

Fig. 10b shows thermal conductivity of soybean, coconut, and palm oil and their respective nanofluids at 0.2 mass% and 30 °C. Soybean, coconut, and palm oil nanofluids increased thermal conductivity over their corresponding BFs by 11.4%, 15.8%, and 48.9%, respectively. This indicates that $Al_2O_3$-$TiO_2$ nanoparticles acted in a synergistic manner to increase the thermal conductivity of the BFs. Among other nanofluids, palm oil-derived nanofluid exhibited the highest enhancement in thermal conductivity, implying that the palm oil BF has better synergy behavior in the presence of $Al_2O_3$-$TiO_2$ hybrid nanoparticles, leading to enhancement of heat transfer property and thermal conductivity. Chakraborty et al. investigated natural ester liquid

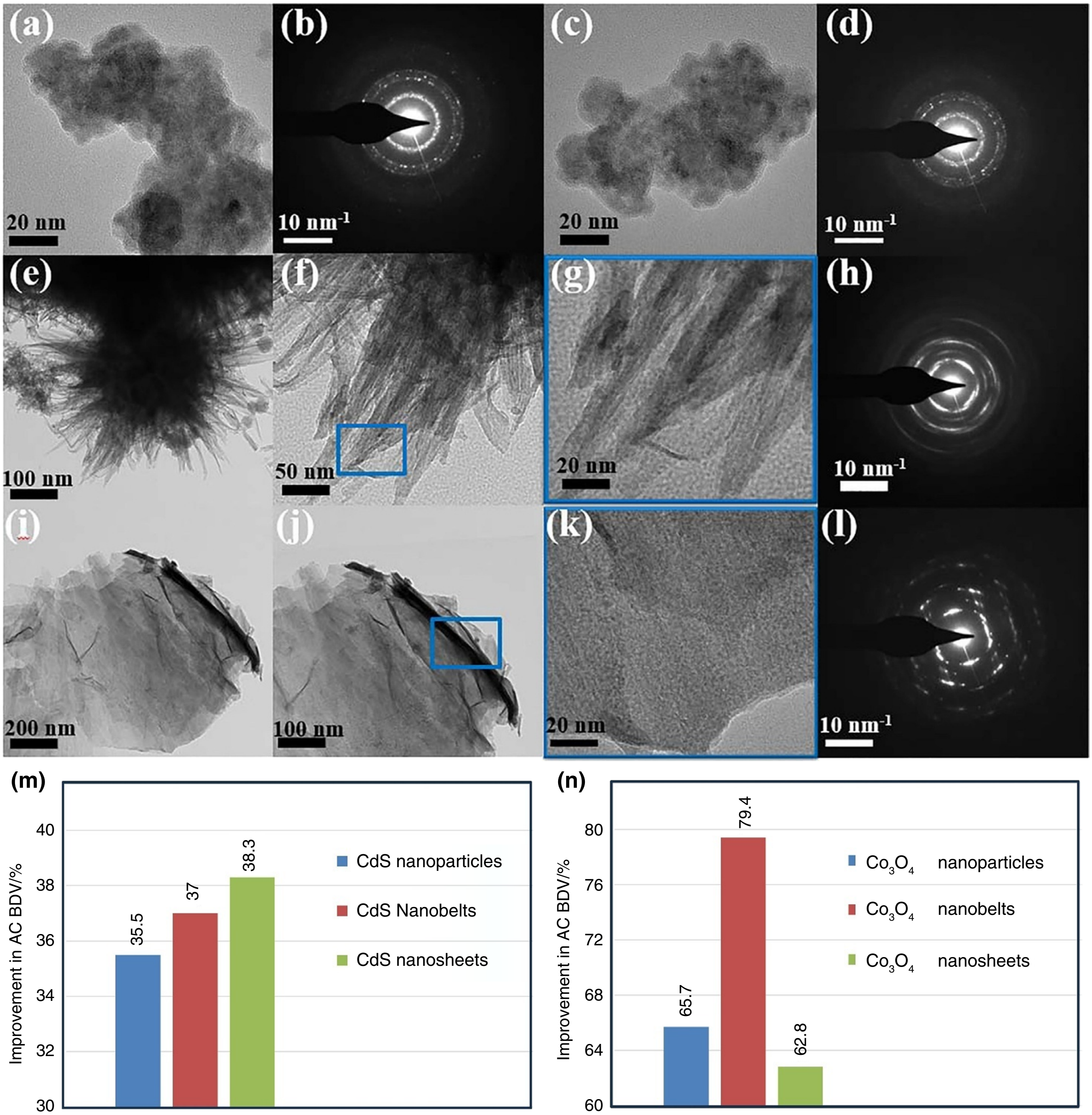


**Fig. 8** High-resolution transmission electron microscopy images and their corresponding selected area electron diffraction patterns of CdS **a**–**d** nanoparticles, **e**–**h** nanobelts, and **i**–**l** nanosheets and **m** percentage improvement in AC BDV using CdS nanoparticles, nanobelts, and nanosheets—Reprinted and redrawn with the license number 5985710352248 [91]; and **n** Percentage improvement in AC BDV using $Co_3O_4$ nanoparticles, nanobelts, and nanosheets—Redrawn [34]

and MO-based nanofluids by dispersing blend of $Al_2O_3$-$TiO_2$ nanoparticles (50:50 ratio) [90]. Compared to base natural ester liquid and MO, nanofluids improved AC BDV by 58.23% and 69.6%, improved tan δ by 0% and − 11.31%, respectively.

Nano-structuring is the process of synthesizing materials at the nanoscale to obtain specific properties. This process includes the heterostructuring (i.e., nanoparticles synthesized by this process can be composite nanoparticles) or doping (i.e., nanoparticles synthesized by this process can be doped nanoparticles).

Composite nanoparticles are synthesized by combining or arranging various materials within a single particle, resulting in nanoparticles with tailored characteristics [168]. S.

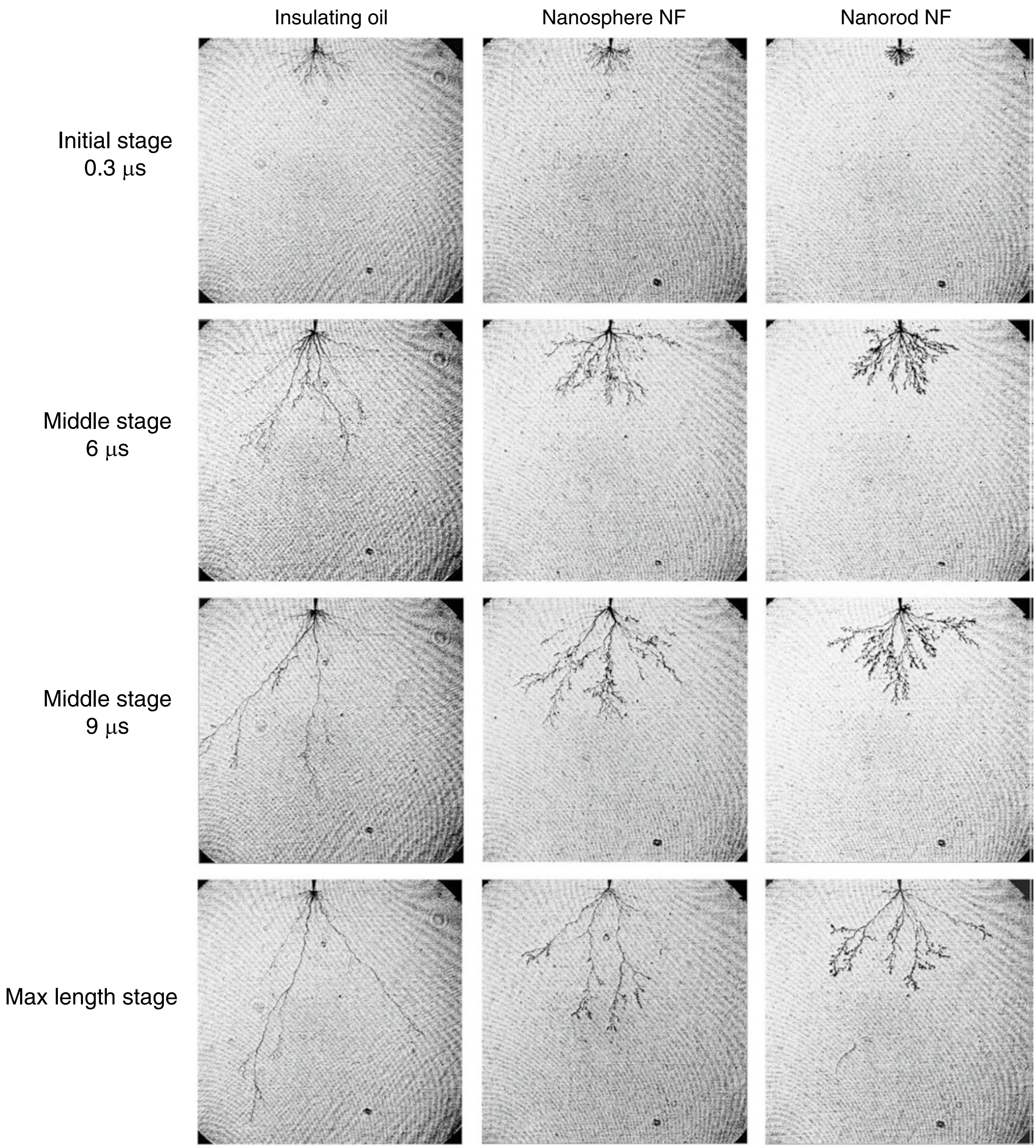


**Fig. 9** Images showing streamer propagation at pre-breakdown for base oil, nanofluid containing nanospheres, and nanorods—Reprinted under a CC license [166]

Aberoumand and A. Jafarimoghaddam investigated transformer oil-based nanofluid, dispersed with $WO_3$–Ag composite [36]. Compared to base oil, nanofluid improved thermal conductivity by 41%.

The concept of doped nanoparticles encompasses the deliberate incorporation of minute quantities of a dopant substance into a host material, hence inducing alterations in its inherent characteristics [169]. Walvekar et al. investigated mineral-palm ester-blend-based nanofluid, dispersed with

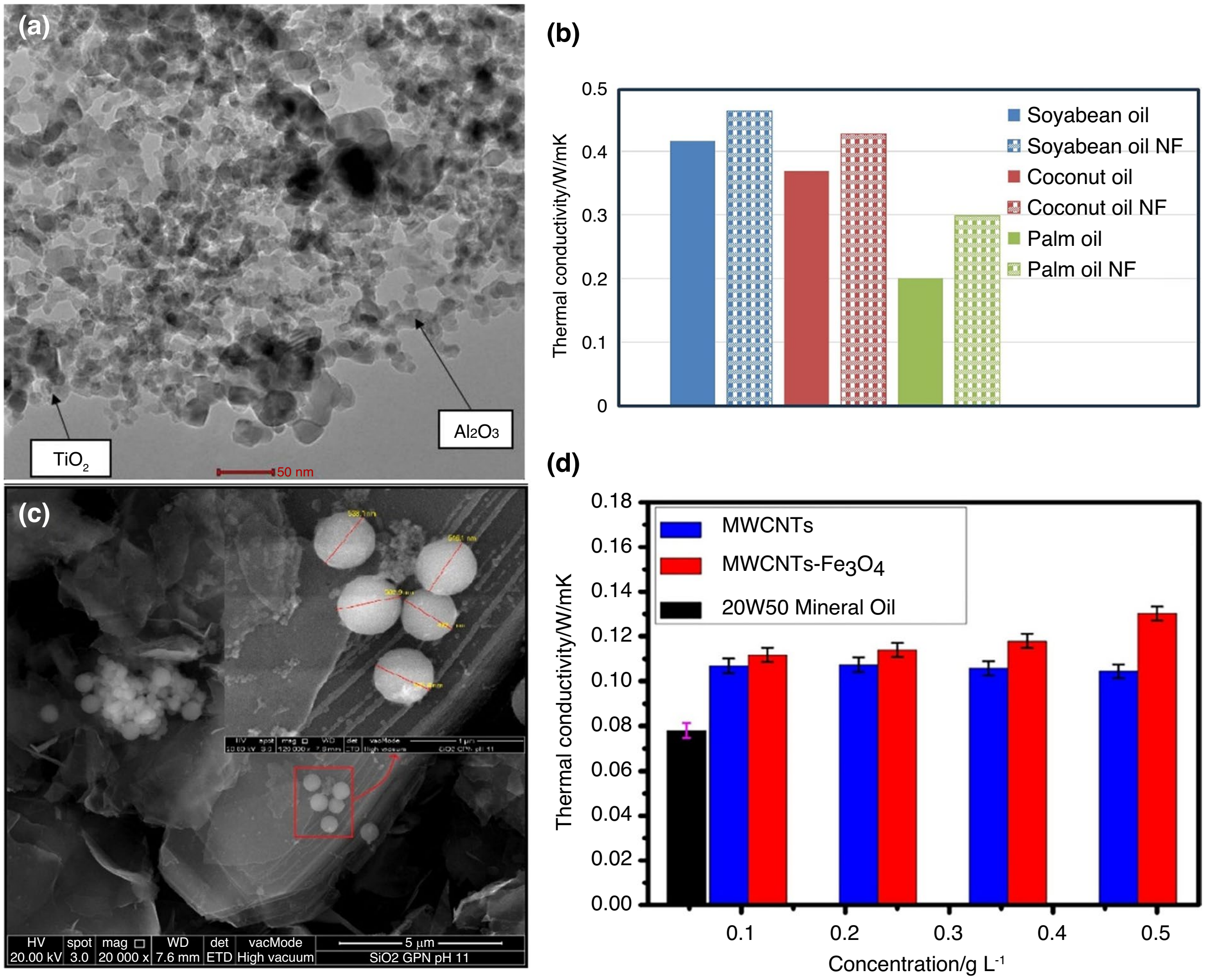


**Fig. 10** **a** Transmission electron microscopy pictures of hybrid $Al_2O_3$-$TiO_2$ nanoparticles and **b** Thermal conductivity of soybean, coconut, and palm oil and their respective nanofluids—Reprinted and redrawn under a CC license [116]; **c** Transmission electron microscopy pictures of $SiO_2$-doped graphene nanoparticles—Reprinted with the license number 6092800683083 [37]; and **d** Base fluid, undoped, and doped nanoparticle dispersed nanofluid thermal conductivity—Reprinted with the license number 6092800959976 [65]

$SiO_2$-doped graphene [37]. Fig. 10c shows TEM pictures of $SiO_2$-doped graphene nanoparticles. The picture shows that the spherical $SiO_2$ nanoparticles (dopant) are well decorated on the surface of the graphene sheets (host). Compared to BF, mineral-palm ester-blend-based nanofluid decreased AC BDV by −9.58%, tan δ by −78.4%, and resistivity by −94.1%. The decreased AC BDV and resistivity may be the result of a higher nanoparticle concentration than the optimal concentration. Hussain et al. investigated MO-based nanofluid dispersed with $Fe_3O_4$-doped MWCNT [65]. Fig. 10d illustrates the comparison of thermal conductivity among the BF, undoped, and doped nanoparticle dispersed nanofluids at varying concentrations of nanoparticles. At every concentration tested, $Fe_3O_4$-doped MWCNTs in nanofluids demonstrated superior thermal conductivity relative to undoped MWCNTs. Compared to BF, MO-based nanofluid improved thermal conductivity by 50% at 0.5 g $L^{-1}$. Pourpasha et al. investigated transformer oil-based nanofluid dispersed with $TiO_2$-doped MWCNTs [85]. Compared to BF, transformer oil-based nanofluid improved thermal conductivity by 8.6%.

In conclusion, the use of hybrid and nanostructured nanoparticle use in nanofluids represents a promising direction for future work in transformer oil enhancement. Various combinations of nanoparticles may facilitate the best advancements in thermal and dielectric properties. Further work is required to explore other combinations of nanoparticles and their effect on the transformer oil performance.

## Nanoparticle concentration

The BDV of DNFs increases with increase in nanofiller concentration until an optimal concentration. Increase in BDV up to the optimal concentration is due to an increase in charge trapping caused by an increase in nanoparticle concentration [30]. Many researchers reported nanoparticle dispersion stability at optimal concentration [11, 86, 87]. Beyond optimal concentration, nanoparticle aggregation decreases the BDV [29, 170]. In some investigations, even beyond the optimal concentration levels, nanofluids were stable without agglomeration and BDV was decreased [171, 172]. This may be due to EDL is unable capture free electrons generated by a powerful electric field at that concentration [173]. Thus, EDL plays a crucial role in the mechanism of breakdown [174]. The nanofluid concentration at and below the optimum concentration distributes nanoparticles uniformly without EDL overlap, increasing trap sites. EDLs of nanoparticles may overlap above the optimal concentration, reducing trap sites. Consequently, BDV decreases beyond the optimal concentration. The electric field distribution along a 2 mm gap between electrodes occupied by base oil and nanofluid is depicted in Fig. 11 [104]. At lower concentrations (up to optimal concentration) of nanoparticles, distortion in the electric field is minimal, allowing charge trapping to dominate, resulting in an increase in BDV. On the other hand, high concentration (above optimal concentration) could lead to breakdown risks due to strong local electric field variations.

The propagation of streamers between electrodes during breakdown is depicted in Fig. 12. The behavior of the streamer propagation channel in the absence of nanoparticles in the base oil is shown in Fig. 12a. The behavior of streamer propagation channel at low concentrations of dispersed nanoparticles is shown in Fig. 12b, where a well-dispersed registry is achieved. As the concentration of nanoparticles increases up to critical concentration, the number of dispersed nanoparticles increases, leading to greater charge trapping and higher BDV. As shown in Fig. 12c, after a critical concentration, the charge trapping zones (specifically, interfacial zone, also known as EDL) of nanoparticles overlap with each other and strengthens the local electric field in the region of overlap [12]. The reduction in the distance between nanoparticles has an impact on the process such that the duration essential for an electrical charge to become trapped in nanoparticles is lengthier than the duration required for an electrical charge to travel through nanoparticles [134]. The critical concentration varies from nanoparticle to nanoparticle, as shown in Table 1. Even for the same nanoparticle, it can differ from one base oil to the other.

Figure 12d illustrates the relation between AC BDV and the concentration of $Al_2O_3$ nanoparticles in the base oil [3]. This graph also shows that the AC BDV values for nanofluids increase at low filler loading and reach a peak before it drops off. However, the AC BDV decreased after a specific concentration. This means that there is such optimal concentration of nanoparticles that enhance the nanofluid BDV to the maximum. Exceeding the critical concentration and adding too much nanoparticles actually has an adverse impact, lowering the BDV.

Table 5 emphasizes the optimal concentration range of nanofluids containing conductive, semiconductive, and insulative nanoparticles and their influence on BDV. Conductive nanoparticles [5] exhibit optimal concentrations as low as 0.002–0.01 mass% due to their high electrical conductivity. Even at minimal concentrations, nanoparticles have significant impact on BDV. Semiconductive nanoparticles [175] display an intermediate critical concentration (0.002–0.04 mass%), indicating their moderate conductivity. These nanoparticles improve BDV up to 61.7%. The critical concentration range (0.02–0.6 mass% or 0.03–0.3 g $L^{-1}$) of insulative nanoparticles is owing to their least conductivity [59]. They exhibit the most profound BDV enhancements (up to 100.3%) despite the higher concentrations. The table highlights the significance of concentrations, since excessive or insufficient concentrations cannot produce optimum effect on the nanofluid.

The nanofluid's dielectric constant can be expressed by the expected polarization. According to the polarization model of oil containing solid particles, there are two forms of polarization: oil molecule polarization and solid particle inner polarization. However, when the size of solid particles is reduced to the nanoscale as in case of nanofluids, a third polarization appeared for base oil molecules located at the nanoparticle/base oil interface due to orientational polarizability. Because of the tight and aligned structure formed in this location, this third polarization has restricted polarizability [126, 127]. The dielectric constant corresponds to liquid molecules and solid nanoparticles/nanosheets per volume [150, 151]. As the concentration increases, the number of solid nanoparticles/nanosheets per unit volume increases, this leads to increase in dielectric constant according to Eq. (4). Moreover, improved charge sites as a result of increased nanoparticle concentration contribute to increased resistivity. The increased resistivity results in decreased electrical conductivity, thereby reducing the dissipation factor of nanofluids as per Eq. (5) [60, 154]. The enhanced thermal conductivity with increase in concentration is intricately regulated by phonon transport, Brownian motion, and interaction between particles due to EDL as discussed in the earlier sub-section [40].

In summary, while there is generally a positive correlation between nanoparticle concentration versus BDV, dielectric constant, dissipation factor, resistivity, thermal conductivity of nanofluids up to certain concentration. Increasing

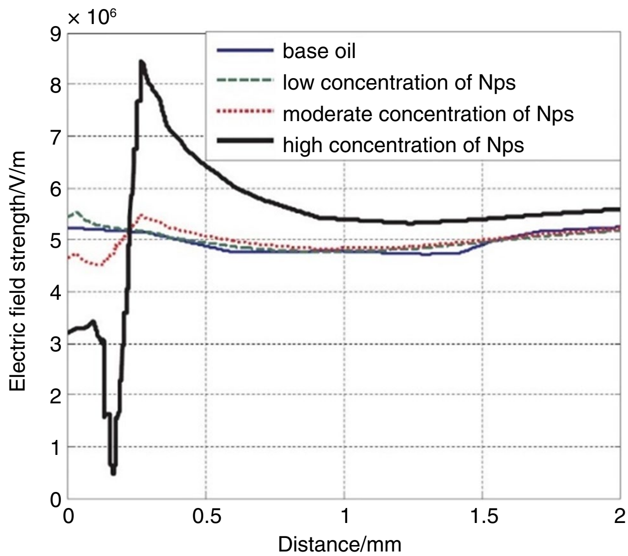


**Fig. 11** Electric field strength along gap length between electrodes—Reprinted with the license number 6092801409773 [104]

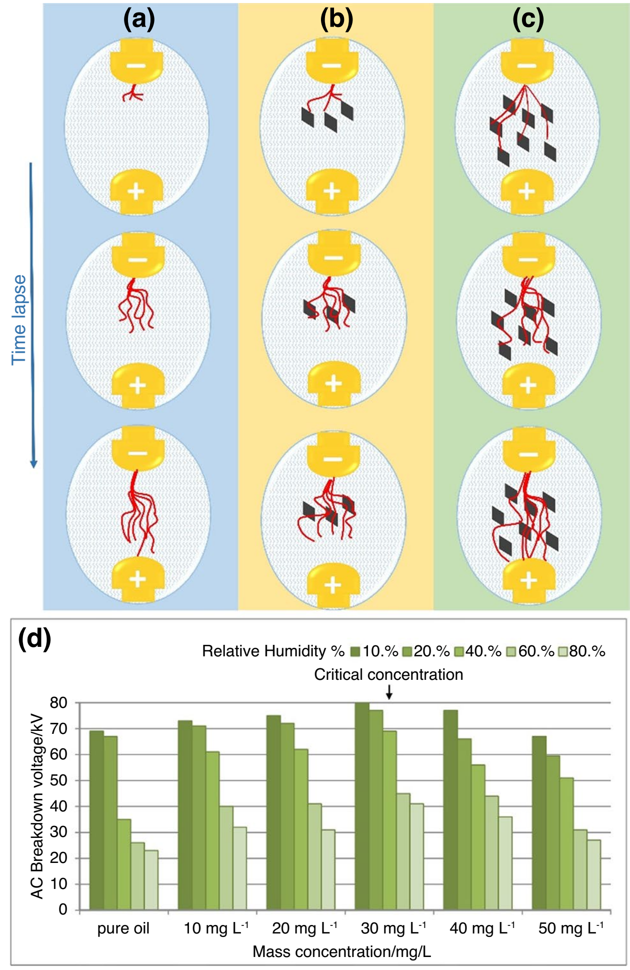


**Fig. 12** Propagation of streamers in **a** Pure dielectric oil **b** Nanofluid up to and **c** Nanofluid beyond critical concentration during breakdown for trapping free electrons; and **d** AC breakdown voltage depending on concentration at various relative humidity—Reprinted with the license number 6092810187720 [3]

nanoparticle concentration enhances the BDV up to certain concentration [176, 177], due to increase in charge trapping sites. Increasing nanoparticle concentration enhances the dielectric constant up to certain concentration [11, 97, 178], due to their high permittivity and interfacial polarization effects. Increasing nanoparticle concentration enhances the resistivity up to certain concentration [12, 97, 178], due to charge trapping effects. Nanoparticles decrease tan δ to a specific concentration [11, 98], by alleviating charge carrier movement via charge trapping. Elevating the concentration of nanoparticles within a dielectric fluid significantly boosts thermal conductivity [12, 33, 89]. This enhancement is attributed to the superior intrinsic thermal conductivity of nanoparticles relative to the BF, facilitated by mechanisms such as direct thermal conduction, Brownian motion, and the percolation effect. The ideal concentration is contingent upon the particular combination of nanoparticle and BF, as well as the intended characteristics. It is essential to weigh these enhancements against possible agglomeration and sedimentation challenges at elevated concentrations [3, 20].

## Surfactant treatment

Surfactants modify nanoparticle surfaces in DNFs, improving their dispersion by enhancing oil affinity [10, 61]. Surfactnts prevent agglomeration and ensure stability in nonpolar insulating oils. Surfactants locates at the interface between nanoparticles and the BF [179]. Fig. 13a dipicts, ionic surfactants possess either negative or positive charge accumulation on their head, an amphoteric surfactant accumulates both, while a nonionic surfactant not have any charge group [180]. Surfactants contribute to the stability of nanofluids by electrostatic and steric mechanisms [181]. Ionic surfactants stabilize electrostatically. Fig. 13b shows the EDL around a positively charged nanoparticle, including the potential on its surface and EDL. A good dispersion stability results from a high zeta potential [171]. Zeta potential of DNFs depends on surfactant type and concentration, nanoparticle concentration, and temperature [182–184]. Nonionic and amphoteric surfactants primarily stabilize nanoparticles sterically. Fig. 13c and d illustrates the schematic diagrams of electrostatic and stearic stabilization, respectively. In electrostatic stabilization, nanoparticles are surrounded by charged layers, while in steric stabilization, nanoparticles are coated with surfactant layers.

Table 6 lists various surfactants, their types, and the studied nanoparticles. The absence of amphoteric surfactants in

**Table 5** Optimal concentration range of nanoparticle types, BDV range, and notable observations

| Nanoparticle type | Nanoparticles | Optimal concentration range/mass% | BDV range/% | Notable observations | References |
|---|---|---|---|---|---|
| Conductive | $Fe_3O_4$, $Fe_3P$, and graphene | 0.002–0.01 mass% | 7.3–41.49 | Minimal optimal concentrations resulting from the exceptional conductivity of nanoparticles | [12, 97, 122] |
| Semiconductive | Anatase TiO2, ZnO, Co3O4, MoS2, fluorinated-BNNs, and SiC | 0.002–0.04 mass% 0.005 g $L^{-1}$ | 2–61.7 | Moderate optimal concentrations resulting from the moderate conductivity of nanoparticles | [11, 33, 86, 97, 99, 100, 103, 111, 118, 121] |
| Insulative | h–BN, $Al_2O_3$, $SiO_2$, and $ZrO_2$ | 0.02–0.6 mass% 0.03–0.3 g $L^{-1}$ | 4.3–100.3 | High optimal concentrations resulting from the low conductivity of nanoparticles | [10, 72, 89, 100, 104, 111, 113, 114, 117, 119] |

the investigated surfactant–nanoparticle systems indicates a potential research gap. Unlike anionic, cationic, and non-ionic surfactants, the amphoteric surfactants may provide stability and compatibility in various DNFs. The dual charge of amphoteric surfactants may further promote the dispersion of the nanoparticles, as well as their better interaction with BFs, and may also be particularly advantageous for applications requiring tuneable surface properties. Studies on amphoteric surfactants—betaines [187], amino acid-based surfactants [188], and phospholipids [189]—could provide new insights into optimizing DNFs for enhanced performance.

Table 7 shows the stability of DNFs treated with surfactants by various base fluids and nanoparticles. Oleic acid and cetyl trimethyl ammonium bromide (CTAB) surfactants are the most dominant surfactants used in DNFs, with oleic acid retaining remarkable time stability (up to 7 years) for $Fe_3O_4$ in MO [109]. This is succeeded by carboxylic acid modified $Fe_3O_4$ in natural ester over a period of 10 months and SDBS-treated graphene in cotton seed oil for 90 days [47, 122]. Conversely, nanofluids treated with CTAB exhibited remarkable stability for up to 1 month for $Al_2O_3$ and $TiO_2$ in COO, palm oil, & soybean oil [116]. In a similar manner, $TiO_2$ treated with Triton X-100 in canola oil (CNO) and $TiO_2$ treated with span 20 in natural ester liquids demonstrated stability for 1 month [195, 218]. Many of the alternative surfactants, including SDBS, SDS, and Span 20, demonstrate a level of stability ranging from 4 to 12 weeks. This indicates that nanofluids with surfactant treatment have considerable potential to produce stable and long-term nanofluids. It is certain that future studies focusing on temporal stability can be applied as a new dimension to improve the effectiveness of DNFs.

Surfactant concentration influences the stability of DNFs [113, 182, 195]. Sedimentation of $Al_2O_3$ nanofluids with different concentrations of CTAB surfactant in 0.1 mass% of nanoparticles is depicted in Fig. 14a [113]. Sedimentation tests on $Al_2O_3$ nanofluids at different CTAB concentrations over 24 h showed that sample with no surfactant and with 0.025 and 0.05 mass% exhibited sedimentation level of 160 mL. At 0.075 mass% CTAB, sedimentation reduced to 150 mL, while 0.1 mass% CTAB showed the most compact sedimentation at 110 mL. This trend indicates that the increase of CTAB concentration increases dispersion and stability of nanoparticles. At 0.1 mass%, stable micelles by CTAB could either have increased electrostatic repulsion or steric hindrance. Zeta potential measured for various concentrations of silica nanoparticles and span 80 surfactant in the synthetic ester fluid is shown in Fig. 14b [182]. Untreated nanofluids presented electrostatic repulsion, as evidenced by their positive values, and span 80-treated nanofluids showed negative zeta potential which indicates the surfactant adsorption and charge modification. It appears that this trend holds for all measured concentrations and may suggest stabilization of the equilibria. With zeta potential magnitudes, above $\pm$30 mV exhibits better long-term dispersion and reduced sedimentation. The span 80-treated nanofluids likely demonstrate long-term stability and reduced sedimentation.

The peak absorbance over a 30-day period for both CNO-based heat transfer oil with and without Triton X-100 surfactant, and for varying $TiO_2$: Triton X-100 mass ratios (1:2, 1:3 and 1:4) is illustrated in Fig. 14c [195]. The ratio of 1:3 exhibited a maximum absorbance and the minimum decrease in absorbance, suggesting that the 1:3 ratio has the highest dispersion stability compared to the other ratios and the surfactant-free sample. The absorbance for the 1:3 ratio decreased by only 5.74% after 30 days, the other ratios showed higher decrease.

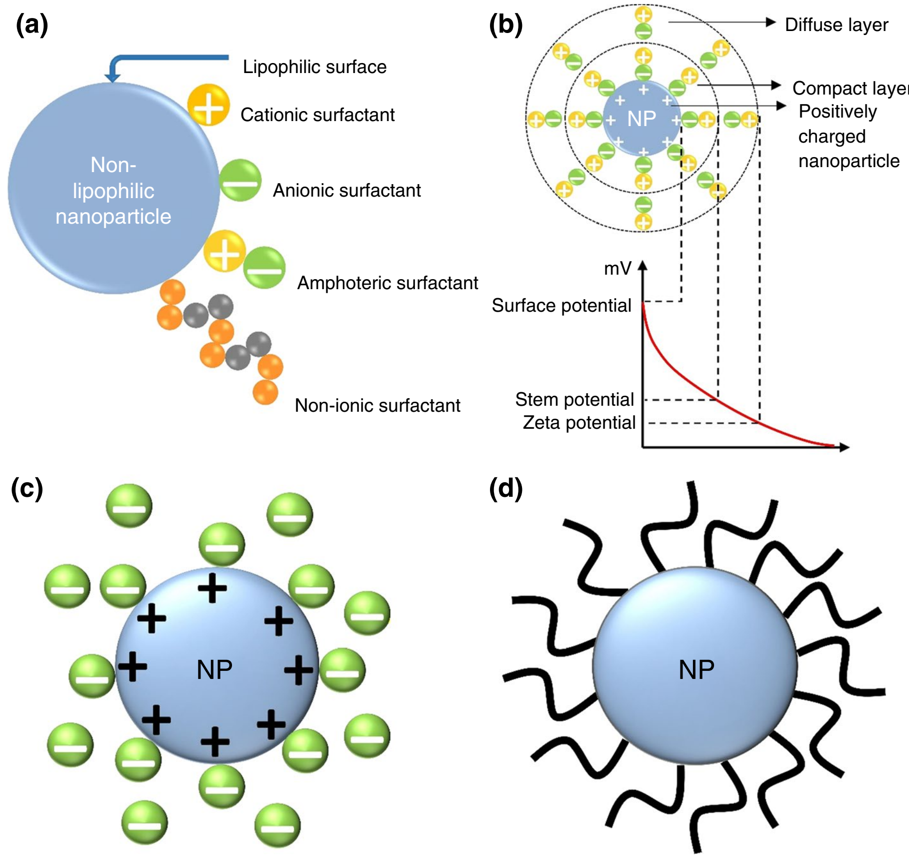


**Fig. 13** **a** Types of surfactants based on their head group polarity, **b** EDL around positively charged nanoparticle and potential on nanoparticle surface and EDL—Redrawn under a CC license [185]; and Schematic illustration: **c** Electrostatic and **d** Steric stabilization of nanoparticles—Redrawn with the license number 6092810415991 [186]

Nanofluids treated with surfactants improved dielectric and thermal characteristics in comparison with their untreated nanofluids [110, 174, 210]. Chen et al. investigated natural ester liquids-based h–BN nanofluids as depicted in Fig. 14d [10]. Compared to base liquid, non-surfactant-treated nanofluids showed 15.01%, −28.8%, 23.5%, 12.68% improvement and nanofluids treated with surfactant γ-amino-propyl triethoxysilane (APTES) showed 19.58%, −37.4%, 27.7%, and 20.33% improvement; in AC BDV, tan δ, resistivity, and thermal conductivity, respectively, at 0.03 g $L^{-1}$ nanoparticle concentration. Surfactant-treated nanofluids demonstrated superiority. This is because homogeneously dispersed nanoparticles produce more uniform charge trapping sites which hinder streamer growth by scattering and neutralizing electrons [125]. Nanoparticle surface modification increases their electrostatic potential, allowing them to adsorb more charged particles from base oil. Adsorption of charged particles traps free electrons in oil, limiting streamer growth [10]. These reasons contribute to improve the BDV and resistivity. Ultimately, an increase in resistivity leads to a reduction in tan δ, as expressed by the equation $\tan\delta = \frac{\sigma_{ac}}{\omega\varepsilon\prime}$ [60, 154]. Such uniformly dispersed nanoparticles in surfactant-treated nanofluids augment interfacial polarization due to rigid structure of interfacial zone [197, 219], ultimately resulting in enhancement of dielectric constant. Nanoparticle surface modification improves base oil compatibility. The nanoparticle–base oil interfacial interaction tightens and thickens due to this compatibility. Tighter and thicker interfacial binding reduces thermal resistance between nanoparticles and base oil, improving thermal conductivity in surfactant-treated nanofluids compared to untreated nanofluids [10]. The uniform registry of nanoparticles in surfactant-treated nanofluid is also a reason for their superiority [125].

Limited research has explored multiple surfactants to identify the most effective one for a specific nanofluid. Rafiq et al. investigated MO-based $Al_2O_3$ nanofluids [110]. Surfactant oleic acid, C2, and C18 treated nanofluids showed 9%, 5.6%, and 7.2% improvement in positive LI BDV, respectively, compared to base oil. Surfactant oleic acid-treated nanofluids outperformed C2 and C18 treated nanofluids due to increased nanoparticle interfacial volume that introduced more traps to capture high-energy electrons. Amizhtan et al. investigated MO-based $SiO_2$ nanofluids [115]. Surfactant CTAB, oleic acid, and span 80-treated nanofluids showed 11%, 17%, and 20% in AC BDV; and 11%, 16%, and 22% improvement in DC BDV, respectively, compared to base oil. Span 80-treated nanofluids outperformed CTAB and oleic treated nanofluids due to increased

**Table 6** Surfactant used in dielectric nanofluids-type, concentration, and studied nanoparticles

| Surfactant | Type | Studied nanoparticles |
|---|---|---|
| Brij-35 | Nonionic [190] | $SiO_2$ [191], and $TiO_2$ [191] |
| C2 | Nonionic [192] | $Al_2O_3$ nanorods [110] |
| SDS | Anionic [193] | Graphene oxide [151] |
| Span 20 | Nonionic [194] | $TiO_2$ [19] |
| Triton X-100 | Nonionic [193] | $TiO_2$ [195] |
| SDBS | Anionic [196] | $Al_2O_3$ [197] and graphene [122] |
| C18 | Nonionic [198] | $Al_2O_3$ nanorods [110] |
| Sodium docusate | Anionic [199] | α-FeO(OH) [200] |
| CTAB | Cationic [193] | $SiO_2$ [113], $Al_2O_3$ [113, 201], $Fe_3O_4$ [201], $ZrO_2$ [114], $TiO_2$ [174, 202], CuO [201], TiC [203], and $ZnFe_2O_4$ [203] |
| Oleic acid | Anionic [204] | $TiO_2$ [90, 111, 118, 205–207], $TiO_2$ nanosphere [166], $TiO_2$ nanorod [166], $Co_3O_4$, ZnO [86, 118], FeP [97], $Al_2O_3$ [90, 111, 205, 206, 208], $Al_2O_3$ nanoplate [209], $Al_2O_3$ nanorods [209, 210], $Fe_3O_4$ [97, 133, 207, 211], $Fe_2O_3$ [206], $SiO_2$ [212], silicon [112], and iron oxide [213] |
| Polysorbate 80 or Tween 80 | Nonionic [214] | $SiO_2$ [191] and $TiO_2$ [191] |
| Glycerol monooleate | Nonionic [215] | $SiO_2$ [191] and $TiO_2$ [191] |
| Stearic acid | Nonionic [216] | MWCNTs [84] |
| Span 80 | Nonionic [216] | MgO [217] and $SiO_2$ [115] |
| Carboxylic acid | Anionic [215] | $Fe_3O_4$ [47] |

**Table 7** Temporal stability of surfactant-driven dielectric nanofluids

| Base fluid | Nanoparticle | Nanoparticle concentration | Nanoparticle size | Surfactant | Stability analysis | Stability time | References |
|---|---|---|---|---|---|---|---|
| SE | $Fe_2O_3$ | 0.02 mass% | 50–110 nm | Oleic acid | Visual inspection | 72 h | [206] |
| SE | $TiO_2$ | 0.02 mass% | 80–110 nm | Oleic acid | Visual inspection | 72 h | [206] |
| MO | $Fe_3O_4$ | 0.07–0.48 vol.% | 8.7 nm | Oleic acid | Visual inspection | 7 years | [109] |
| MO | $Al_2O_3$ nanoplate | 0.8 g $L^{-1}$ | $L \times W$: 100 × 40 nm | Oleic acid | Visual inspection | 30 days | [209] |
| SE | $Al_2O_3$ | 0.02 mass% | 100–130 nm | Oleic acid | Visual inspection | 72 h | [206] |
| MO | $Al_2O_3$ | 0.1 mass% | 13 nm | CTAB | Visual inspection | 24 h | [113] |
| MO | $Al_2O_3$ nanorod | 0.8 g $L^{-1}$ | $D \times L$: 15 × 150 nm | Oleic acid | Visual inspection | 1 month | [209] |
| COO, PAO, & SO | $Al_2O_3$ | 0.2 mass% | < 13 nm | CTAB | Visual inspection | 1 month | [116] |
| MO | $SiO_2$ | 0.1 mass% | 12 nm | CTAB | Visual inspection | 24 h | [113] |
| MO | $ZnFe_2O_4$ | 2.5 mg $L^{-1}$ | 8–28 nm | CTAB | Visual inspection | 1 month | [203] |
| COO, PAO, & SO | $TiO_2$ | 0.2 mass% | < 21 nm | CTAB | Visual inspection | 30 days | [116] |
| MO | $TiO_2$ | 0.3 mass% | 21 nm | HLB 10.5 | Visual inspection | 1week | [191] |
| MO | $MoO_3$ | 2.5 mg $L^{-1}$ | 8–75 nm | Oleic acid | Visual inspection | 1 month | [203] |
| CSO | Graphene oxide | 0.01 mass% | – | SDS | UV–Vis | 6 weeks | [151] |
| NE | $TiO_2$ | 0.004–0.020 mass% | 21 nm | Span 20 | Visual inspection | 1 month | [218] |
| CSO | Graphene | 0.0015 mass% | Lateral: 5–10 µm Thickness: 3–6 nm | SDBS | UV–Vis | 90 days | [122] |
| CSO | $Al_2O_3$ | 0.01 mass% | 15–25 nm | SDBS | Visual inspection | 4 weeks | [197] |
| CNO | $TiO_2$ | 0.04 vol.% | 13 nm | Triton X-100 | UV–Vis | 30 days | [195] |
| NE | $Fe_3O_4$ | 0.1 g $L^{-1}$ | 10 nm | Carboxylic acid | Visual inspection | 10 months | [47] |

nanoparticle interfacial volume that introduced more traps to capture high-energy electrons.

In addition, very few studies presented non-improved dielectric properties for surfactant-treated nanofluids compared to untreated nanofluids. Jin et al. investigated that surface modified silica nanofluids using Z6011 surfactant decreased AC BDV (almost half the value without surfactant), but unmodified nanofluids increased the AC BDV of MO [220]. The primary reason for this is that unmodified silica nanoparticles possess a hydrophilic surface that can

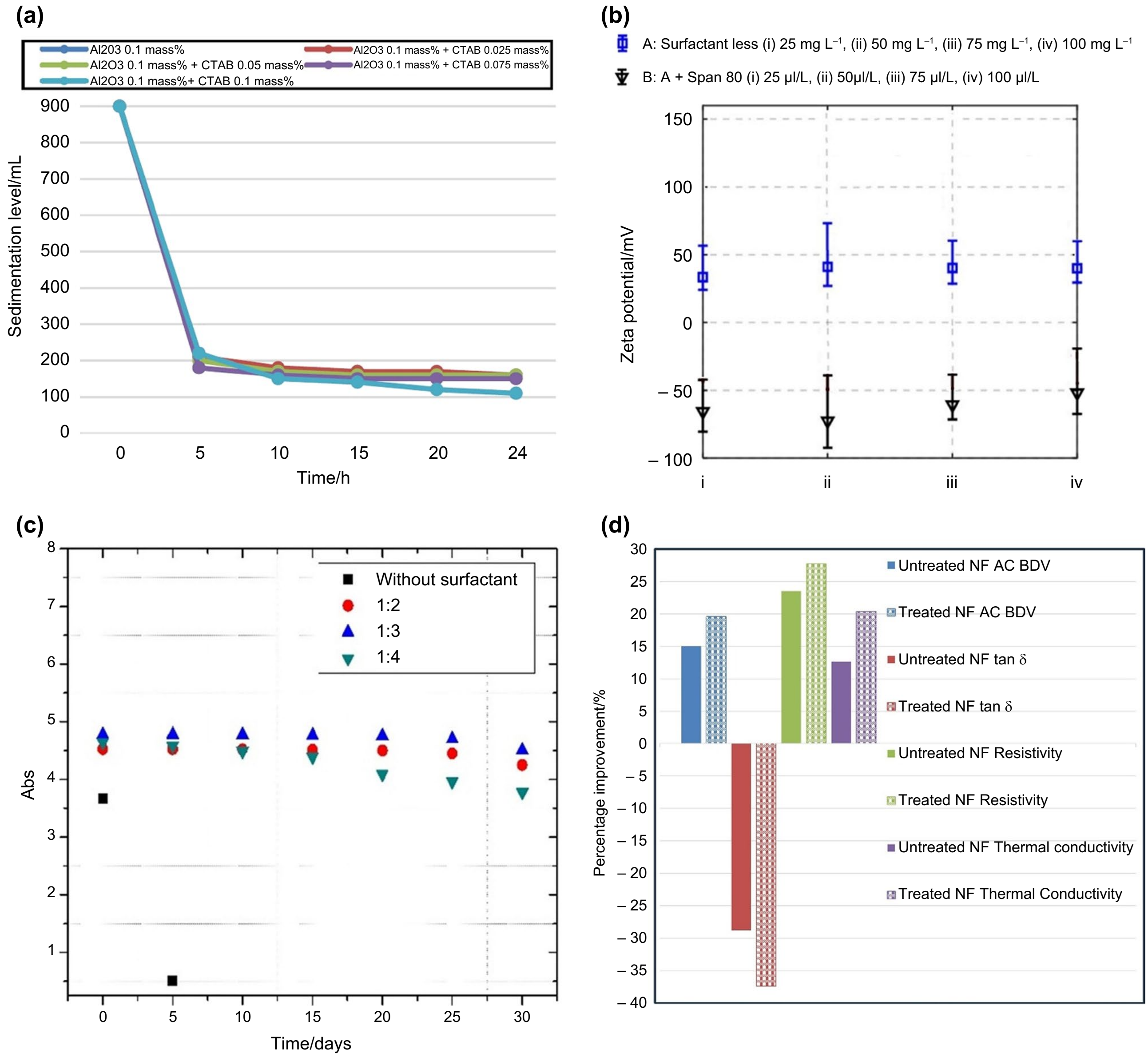


**Fig. 14** **a** Sedimentation of $Al_2O_3$ nanofluids at different CTAB concentration—Reprinted with the license number 6092810615652 [113]; **b** Zeta potentials of span 80-treated and untreated nanofluids at different concentration and surfactant levels—Reprinted under a CC license [182]; **c** Absorbance of Triton X-100 treated $TiO_2$ nanofluids at varying concentration over 30 days—Reprinted with the license number 6092810810644 [195]; and **d** Percentage enhancement in dielectric and thermal properties of surfactant-treated and untreated nanofluids—Redrawn with the license number 6092810976814 [10]

bind water in the oil [221], resulting in an enhancement of the AC BDV. In contrast, following Z6011 treatment, the silica nanoparticles adsorb it and transform into a hydrophobic state, which inhibits their ability to bind with water. This leads to a reduction in the AC BDV. In another study [109], a magnetic nanofluid containing oleic acid surfactant-coated iron oxide nanoparticles exhibited either the same level of AC BDV as that of base transformer oil or a slightly lower level. Again, the reason for this is because surfactant coating inhibits the efficacy of water bonding around nanoparticles in transformer oil. The addition of oleic acid-coated iron oxide nanoparticles raised the tan δ of transformer base oil, rather than reducing it [109]. The reason for this is the coated nanoparticles' dielectric relaxation around the frequency of 50 Hz, which reduces charge trapping and increases polarization losses and charge mobility at the nanoparticle–oil interface.

Moreover, Rajnak et al. reported four-time increase in the tan δ for transformer oil-based oleic acid-coated iron oxide nanofluids [175]. The reason for this might be the increase in AC conductivity as a result of charge carriers produced by impurities or moisture. A moderate increase in dielectric constant is beneficial in transformer insulation and high-voltage applications. Several studies found that surfactant-treated DNFs showed increased dielectric constants [95, 97, 122]. However, no encompassed studies on surfactant-treated DNFs have reported a decrease in dielectric constant. The screening effect can lower the thermal conductivity of nanofluids with high surfactant concentrations [41]. Numerous studies have indicated that the ideal low surfactant amount enhances the thermal conductivity of DNFs [41, 114, 116]. However, no encompassed studies on surfactant-treated DNFs have reported decreased thermal conductivity.

### Moisture content

The common contaminant present in transformer oil is moisture [222, 223], and its form (i.e., either molecules, dimers, or clusters) in DNFs depends on level of moisture present as shown in Fig. 15 [48]. Nanofluid with low moisture ('dry nanofluid') contains moisture in the form of water molecules or dimers, with high moisture content ('wet nanofluid') contains moisture in the form of water clusters [224]. Similar to solid-material defects, nanoparticles in nanofluids with varying moisture content bind water molecules or ions and create an expanded two-layer structure in an electric field [225]. In dry nanofluids, nanoparticles at low concentration hold solitary water molecules or dimers as depicted in Fig. 15a, but as the concentration of nanoparticles increases, some nanoparticles may not have dimers on their surfaces, as shown in Fig. 15b. The breakdown strength of nanofluids depends on moisture levels [86, 226]. The mechanism of enhancement of BDV by nanoparticles is different, based on dry or wet nanofluids. In dry nanofluids, nanoparticles augment the BDV of insulating oil up to a critical nanofiller level, after which it decreases. This phenomenon can be explained by EDL theory [173]. Nanoparticle surfaces attract counter ions and form compact and diffuse layers. EDL is essential for nanofluid BDV improvement over base oil [174]. EDL traps high-voltage-generated fast electrons. However, nanoparticle concentrations above the critical concentration overlap EDLs, creating conductive channels and reducing BDV.

In wet nanofluids, the BDV is usually low at lower nanoparticle concentration. This is because water molecules, dimers, or clusters tend to align and form a bridge across the distance between electrodes, which may cause the oil gap to prematurely fail under electric stress, as shown in Fig. 15c. At higher nanoparticle concentration, nanoparticles catch water clusters or smaller water elements until their surface is saturated with water molecules. This effectively hinders the alignment of water molecules to form a bridge over the gap of the electrode, and hence increases BDV, as shown in Fig. 15d. Lyutikova et al. and Das found that the higher the moisture content of the oil, the more nanoparticles are needed to capture it [86, 226].

A.K. Das investigated BDV of dry and wet nanofluids [86]. Fig. 16a and b shows the influence of ZnO nanoparticle filler level on the AC BDV for both dry and wet nanofluids, respectively. For wet nanofluids at lower filler concentration, 0.01 to 0.02 mass% BDV is less and it is increased at higher higher filler concentration 0.03 to 0.05 mass%. Also, critical concentation (shown by arrows) for wet nanofluids is lesser than dry nanofluids and at 0.01 and 0.05 mass% dry nanofluids showed better BDV than wet nanofluids. At optimal concentration, compared to their base oils, dry refined, bleached and deodorized (RBD) COO, COO, and MIDEL eN1215-based ZnO nanofluids improved AC BDV by 27.94%, 39.18%, and 24.45%, and wet by 52.84%, 59.02%, and 61.67%.

Although the wet nanofluids performed better than the dry nanofluids in terms of BDV at optimal concentrations, the moisture in wet nanofluids is harmful to the safe operation and service life of the power transformer. Furthermore, there exist only a few studies covering the effects of moisture on various characteristics of DNF [227, 228]. Consequently, it is necessary to carry out more research to study the effect of moisture presence on DNF characteristics.

### Temperature variation

DNFs are proposed as potential replacements for conventional transformer oils, and their performance under operating temperature conditions and over time is essential for practical applications.

Many studies investigated DNF dispersion stability at room temperature [13, 37, 72, 76]. However, transformer fluids are often exposed to 30–110 °C in service. At the elevated temperature, dispersion stability of oil-based nanofluids decreases due to accelerated nanoparticle aggregation [229]. Higher temperatures enhance Brownian motion, increasing collision probability, while reduced fluid viscosity lowers drag forces, further promoting aggregation. The literature on dispersion stability of DNFs particularly at the service temperature is very limited. Primo et al. presented an experimental study that evaluates the stability of DNFs under realistic transformer temperature [47]. Two $Fe_3O_4$ commercial nanoparticle dispersions (Abbreviated as F1 and F2) were dispersed in Bioelectra natural ester and Nytro 4000X MO. Nanofluids were subjected to temperatures ranging from 50 to 110 °C for up to 10 months. Visual inspection and particle size measurement were used to evaluate the stability. Zeta potential was not found to be a suitable method for characterizing the stability of these nonpolar, oil-based fluids. The results show that all nanofluid formulations lose stability when subjected to high temperature (i.e.,

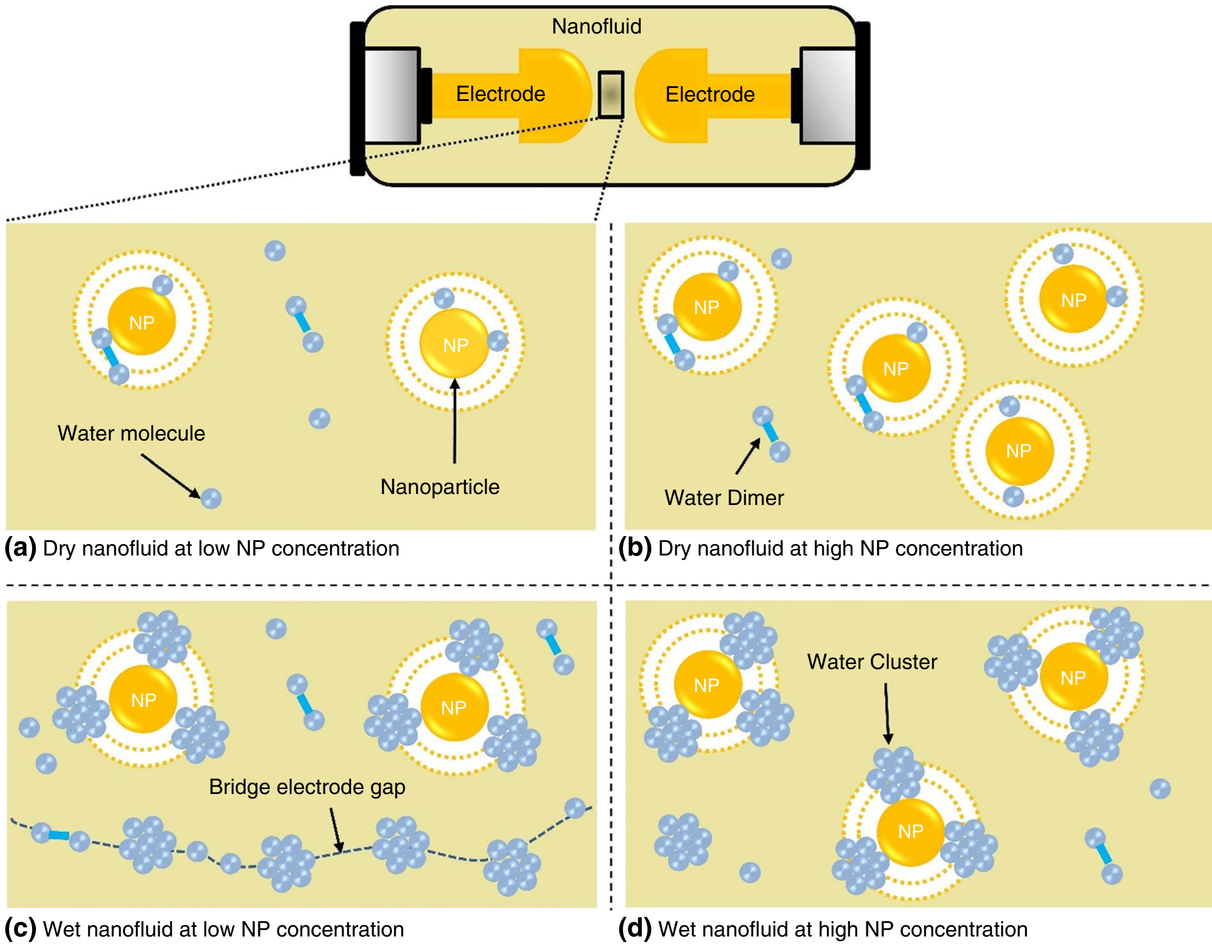


**Fig. 15** Schematic diagram of AC breakdown phenomenon in dry and wet nanofluids at low and high nanoparticle concentrations—Redrawn with the license number 6092811395180 [86]

80°C) within few days, while FF1 dispersed in Bioelectra maintained good stability even for 2 months. It indicates the choice of BF and nanoparticle used also significantly impacts the long-term stability. Consequently, additional research on variations in temperature is essential to evaluate the long-term performance and stability of DNFs.

There are limited studies on the BDV of DNFs across different temperatures. Rajňák et al. reported an increase in BDV with increase in temperature up to 70 °C and a decrease in BDV at 80 °C as shown in Fig. 17a [109]. A similar trend was observed when Katiyar et al. investigated MO-based ZnO, $ZrO_2$, and $Al_2O_3$ nanofluids [230]. The BDV was increased up to 90 °C and then decreased at 100 °C. The observed trend may be attributed to the rising temperature causing the emulsified water in the transformer oil to dissolve [48, 49] and the water dissolved in the oil content increases with temperature. The effect of dissolved water on the BDV is negligible compared to that of emulsified water and that is the reason in increasing the BDV. Nonetheless, at the elevated temperatures, the exceptional viscosity drops induced by the high thermal energy diminish the hindering effects on the water and space charge transport to form conductive pathways [109]. That leads to a drop of the BDV at the highest temperatures.

Most of the experimental studies showed that nanofluids' dielectric constant decreased with increase in temperature [150, 197, 231–233]. Thermal energy reduces charge storage by increasing charge carrier mobility, potentially increasing leakage currents at higher temperatures. The dielectric constant decreases with increase in temperature due to the inverse relationship between dipolar orientation polarization and thermal agitation [234, 235], which disrupts dipole alignment. The dielectric constant of groundnut oil-based ZnO nanofluids at nanoparticle concentrations of 0.0, 0.1, and 0.2 g $L^{-1}$, measured across various temperatures, is illustrated in Fig. 17b [232]. This study demonstrates a notable reduction in dielectric constant as the temperature rises from 45 to 85 °C. Few studies have found nanofluid's dielectric constant unchanged with small increase in temperature [11]. The reason for this could be that a slight rise

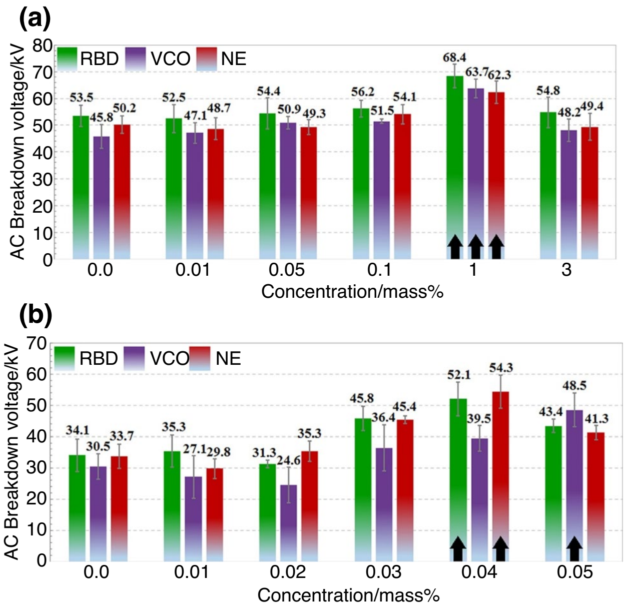


**Fig. 16** AC BDV in (**a**) dry and (**b**) wet nanofluids, at different ZnO concentrations—Reprinted with the license number 6092811395180 [86]

in temperature might not enhance charge carrier mobility enough to lower the dielectric constant.

The studies reported that the nanofluid dissipation factor increased with increase in temperature. The dissipation factor for nanofluids with varying concentrations of silica-coated $TiO_2$ nanoparticles is depicted in Fig. 17c [3]. The dissipation factor exhibited an increase with temperature across all concentrations. However, Liu et al. observed a similar increase in dissipation factor for ZnO nanofluids from 25 to 100 °C [236]. Taha-Tijerina et al. reported increased dissipation for h-BN and graphene nanofluids [237]. Additionally, Du et al. (for vegetable oil-based h-BN nanofluids) and Michal et al. (for vegetable oil-based $Al_2O_3$ nanofluid) found higher dielectric losses at elevated temperatures [238, 239]. This increase in dissipation factor with increase in temperature is attributed to nanoparticle thermal motion that increases energy dissipation [92, 240]. However, at lower frequencies, dissipation factor decreased as temperature rose from 25 to 50 °C due to de-trapping [92], where reduced free charge generation promotes charge bonding with nanoparticles [241]. Overall, studies have reported pure increases [3, 236–239], pure decreases [197], and mixed trends (i.e., increased at certain temperatures and decreased at others) [12, 242], driven by nanoparticle thermal motion and de-trapping effects.

Khan et al. investigated the resistivity of synthetic ester oil-based $Fe_2O_3$, $TiO_2$, and $Al_2O_3$ nanofluids at 0.02 mass% [206]. Resistivity decreased with increase in temperature up to 40°C and then remained relatively constant; except for $TiO_2$ nanofluids, where resistivity increased from 60 °C to 80 °C. Bhunia et al. studied the resistivity of optimized nanofluids with 0.005 mass% anatase-$TiO_2$ nanosheets, as shown in Fig. 17d [11]. Oil-1 and Oil-2 are two types of commercial MOs that are used as BFs in the preparation of nanofluids. Resistivity of both base oil and nanofluids decreased as temperature increased from 60 °C to 90°C. Prasath et al. investigated MO-based $CaCu_3Ti_4O_{12}$ nanofluids [243]. The resistivity was increased at 90 °C compared to lower temperature. Maneerat et al. investigated resistivity of FR3-based $BaTiO_3$ and $TiO_2$ nanofluids [244]. At 110 °C and 130 °C, both nanofluids showed decreased resistivity. Michal et al. investigated ENVITRAFOL based $Al_2O_3$ nanofluids [239]. Volume resistivity of nanofluids decreased with increase in temperature from 30 °C to 90 °C. Increase and decrease in resistivity of DNFs with increase in temperature can be attributed to thermal activation of charge carriers and nanoparticles' ability to trap charges, respectively [50, 245, 246].

Emara et al. studied the effect of temperature variation (10 °C to 100 °C) on the thermal and dielectric properties of natural ester-based MgO nanofluids [247]. It demonstrates that, at lower temperatures, the addition of MgO nanoparticles improves thermal conductivity and dielectric strength; however, as temperature rises, thermal conductivity and dielectric constant decrease and electrical conductivity increases. These trends are the result of mechanisms such as decreased dipolar orientation, increased EDL thickness, and enhanced Brownian motion. The findings highlight the temperature-sensitivity of nanofluid performance, as well as the importance of balancing thermal effects for optimal nanofluid behavior.

Table 8 shows the enhancement of thermal conductivity among several nanofluids with increase in temperatures. The trends in the table imply that temperature is quite important in changing the thermal transport characteristics of nanofluids. Thermal conductivity of most nanofluids increases with temperature. This can be explained by: high Brownian motion of nanoparticles at higher temperatures [248], so improving thermal transfer; lowering of BF viscosity results in improved nanoparticle dispersion and less aggregation [249]; and enhanced phonon transport brought on by higher thermal energy. The decrease in thermal conductivity of nanofluids in [250, 251], and [24] with increase in temperature is likely due to the declining thermal conductivity of the BFs, which in turn influences the overall nanofluid behavior. This highlights the importance of choosing BFs with stable or increasing thermal conductivity with increase in temperature when designing nanofluids for high-temperature applications.

In summary, DNFs operate within service temperatures of 30–110 °C, demanding careful designing design of DNFs at this temperature range to assure not only the stability of

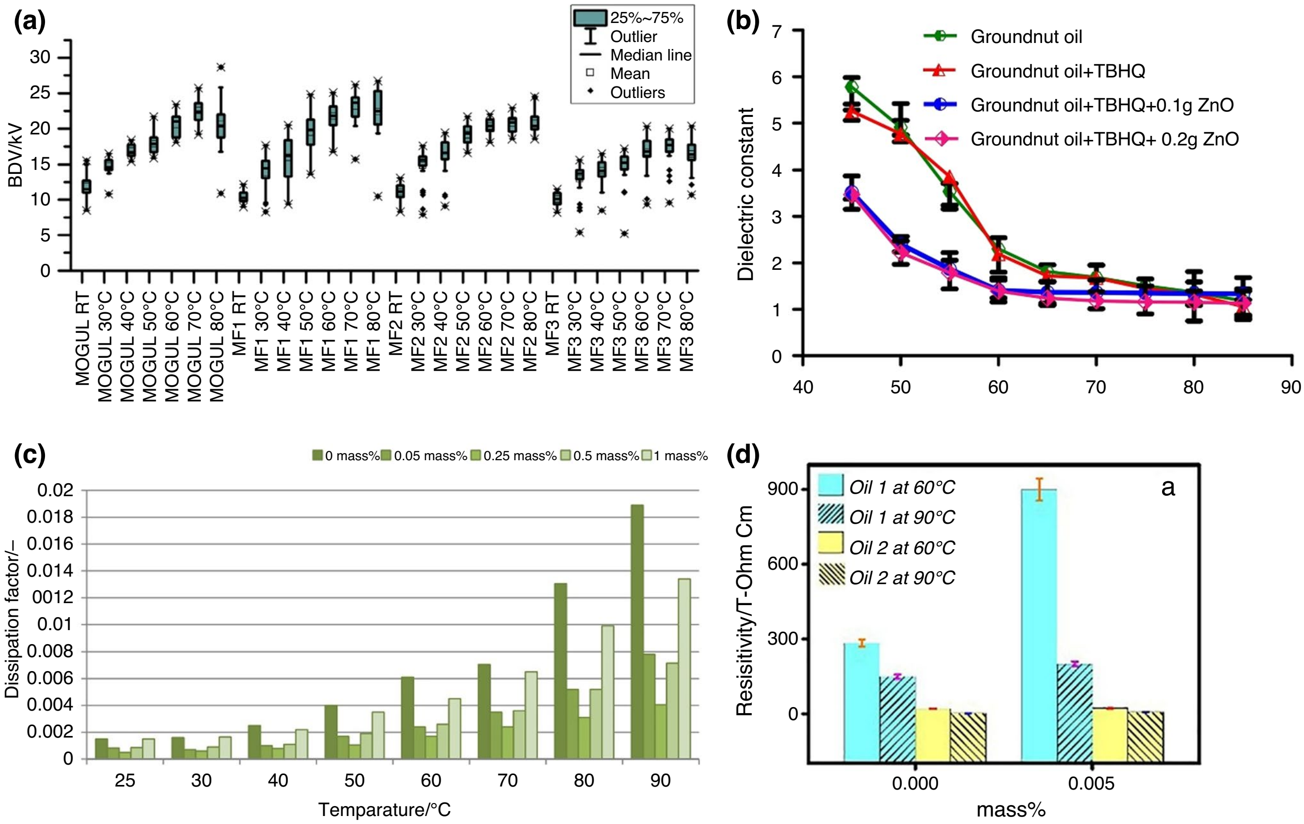


**Fig. 17** Dielectric properties of nanofluids measured across various temperatures: **a** AC breakdown voltage (base oil MOGUL and nanofluids MF1-MF3)—Reprinted with the license number 6092820073965 [109]; **b** dielectric constant [232]; **c** dissipation factor—Reprinted with the license number 5985720519027 [3]; and **d** resistivity—Reprinted with the license number 6092790346256 [11]

nanofluid, but also BDV, dielectric constant, dissipation factor, resistivity, and thermal conductivity. Therefore, a detailed assessment of these properties under diverse temperatures is necessary to avoid degradation, ensure reliable insulation, and optimize the thermal performance in practical applications.

## Thermal aging

Thermal aging may decrease the properties of dielectric BFs. Amalanathan et al. conducted the thermal aging test by heating natural ester oil with copper-wrapped pressboard at 90 °C, 140 °C, and 160 °C in a nitrogen atmosphere [256]. Oil samples were analyzed at 100-h intervals up to a total aging duration of 500 h. This study found thermal aging decreased AC, DC, and impulse BDV of base natural ester liquid. The decrease was greater at the investigated higher temperature (160 °C) than at the lower temperature (90 °C). The response of DNFs to thermal aging is quite intriguing. Singha et al. conducted the thermal aging test at a constant temperature of 150°C for a duration of 3000 h using a sealed tube setup containing natural ester or MO along with solid insulation materials [257]. After aging, MO's BDV dropped by over 50% due to increased moisture, acidity, and oxidation. In contrast, natural ester liquid maintained a stable BDV despite a sharp rise in acidity, as its higher acid solubility prevented dielectric degradation. On the other hand, Amalanathan et al. found that BDV of natural ester liquids decreased with thermal aging [256], particularly at higher temperatures (140°C and 160°C), and attributed this decline to oxidation byproducts such as carboxylic acids and ketones. The contradiction in the natural ester liquid BDV likely arises due to differences in oil composition and experimental conditions. More comparative studies under controlled conditions are needed to determine the true impact of thermal aging on natural ester liquid BDV.

Studies on the aging of DNFs have revealed both possible challenges and interesting results. Fernández et al. studied thermally aged natural ester-based $TiO_2$ and ZnO nanofluids [99]. Fig. 18a shows the evolution of AC BDV over time for vegetable oil, vegetable oil-based $TiO_2$ and ZnO nanofluids. Nanofluids were thermally aged at 150 °C for 312 h. Aged nanofluids showed lower AC BDV than freshly prepared nanofluids but better AC BDV than aged base oil.

Additionally, aged nanofluids showed higher tan δ than fresh nanofluids and aged base oil.

Koutras et al. conducted thermal aging in situ for 28 days to simulate real transformer operating conditions and evaluate the long-term stability and dielectric properties of natural ester-based nanofluids containing $TiO_2$ and SiC nanoparticles [44]. Two sets of experiments one at ambient temperature (25°C) and one at 90°C were conducted to simulate real operating conditions of power transformers. Dynamic light scattering, AC BDV, and partial discharge were performed. SiC nanofluids exhibited better stability and dielectric performance compared to $TiO_2$ nanofluids under similar conditions. At 0.004 mass%, SiC nanoparticles showed the best dielectric properties and longest stability under both ambient and elevated temperature aging. Fig. 18b illustrates the potential well distribution around the SiC and $TiO_2$ nanoparticles under the influence of an external electric field. SiC nanoparticles have a higher ability to capture charge carriers in deeper traps compared to the $TiO_2$ nanoparticles, resulting in best dielectric properties. The results show that ambient temperature studies alone cannot accurately predict nanofluid stability and dielectric performance, as in situ high-temperature experiments revealed significant differences.

Prasath et al. conducted thermal aging at 115 °C using ASTM D1934 method, where nanofluids were aged with copper catalyst under rotation at 8 rpm [243]. This study found that the aged nanofluids demonstrated superior dielectric properties compared to the aged base MO. This indicates that $CaCu_3Ti_4O_{12}$ nanoparticles help control the deterioration of the oil during aging. CCTO nanoparticles enhance aged MO's dielectric properties by increasing BDV (up to 70.7%), reducing tan δ (up to 12%), and slightly raising the dielectric constant (6.75%). These improvements stem from electron trapping and insulating boundaries. Maharana et al. studied the MO-based $TiO_2$ and exfoliated h-BN nanofluids with an optimized concentration of 0.01 mass% [258]. Thermal aging experiment was performed at 115°C for 164, 328, and 492 h using an open beaker oxidative aging setup as per ASTM D1934 standard. Fig. 18c shows the comparative analysis of the AC BDV for the fresh and aged insulating oil samples. The introduction of nanoparticles improves the aging resistance of MO. Exfoliated h-BN nanoparticles are more effective than $TiO_2$ in enhancing and maintaining BDV over aging time. Additionally, the exfoliated h-BN dispersed nanofluid exhibited higher thermal conductivity and better insulation properties compared to base oil and $TiO_2$ nanofluid even after aging. This is due to high thermal conductivity and insulating nature of the exfoliated h-BN.

Thus, studying thermal aging in DNFs is essential for assessing their long-term performance, stability, and suitability for use in transformers and other high-power applications. In conclusion, the aging behavior of DNFs is complex and depends on various factors such as nanoparticle type, BF, and aging conditions. The introduction of nanoparticles improved the aging resistance and properties of BFs [243, 258]. While some nanofluids show improved stability and performance after aging [44]. Fewer studies have focused on the thermal aging of DNFs. Further research is needed to fully understand and optimize the long-term performance of thermally aged nanofluids.

Koutras et al. examined the impact of one-month natural aging (at ambient temperature) on natural ester-based nanofluids containing low concentrations of $TiO_2$ and SiC nanoparticles [259]. It shows that natural thermal aging leads to a decline in thermal diffusivity and conductivity, primarily due to nanoparticle agglomeration. The sample with 0.004% SiC, which initially showed the highest thermal enhancement (up to 58%), exhibited the greatest degradation after aging. These findings highlight the critical role of nanoparticle dispersion stability over long-term in maintaining performance of DNFs.

#### Forced circulation

Forced oil circulation can significantly improve the stability of nanoparticles in transformer oil, leading to better BDV and thermal performance compared to natural cooling systems. M. E. Ibrahim et al. examined the effect of forced oil circulation on the dielectric and thermal performance of the transformer oil-based $TiO_2$ nanofluid at the optimal concentration of 0.015 mass% [52]. The natural-cooled system (no oil circulation) and forced-cooled system (with oil circulation) average BDV over 60 days are shown in Fig. 19a. For the natural-cooled system, the average BDV starts at 15.5 kV at the start of the test period but drops to 10.83 kV after 60 days. This lowers the mean BDV by 30%. On the other hand, the forced-cooled system showed 15.5 kV BDV for all of the 60-day experiment. For the transformer oil, the forced oil circulation serves to stabilize the $TiO_2$ nanoparticles and limits the reduction in BDV. On the other side, the temperatures of the base oil, natural-cooled nanofluid and forced-cooled nanofluid oil changes over the 60-min cooling periods, as illustrated in Fig. 19b. The forced-cooled nanofluid reduces in temperature more than the natural-cooled and base oil. This implies that the thermal performance of oil circulation is better with forced oil circulation. This is due to circulation in the forced-cooled system, which leads to better dispersion of the $TiO_2$ nanoparticles, thus improving the thermal conductivity and cooling performance of the oil.

Pourpasha et al. investigated the natural convective heat transfer (NCHT) and forced convective heat transfer (FCHT) coefficients of $TiO_2$-doped MWCNT nanofluids modified with oleic acid in transformer oil [85]. The experimental setup (Fig. 19c) included a fluid tank, thermocouples (2 on the walls, 4 inside the fluid), variac transformers, two 36 W

**Table 8** Thermal conductivity enhancement of nanofluids at different temperatures

| Temp. /°C | Base fluid | Nanoparticle | | | Thermal conductivity/W/mK | | Thermal conductivity enhancement/% | References |
|---|---|---|---|---|---|---|---|---|
| | | Name | Size/nm | Concentration | Base fluids | Nanofluids | | |
| 35 | MO | ZnO | ≈160 | 0.0015 vol.% | 0.132 | 0.138 | 4.5 | [252] |
| 45 | MO | ZnO | ≈160 | 0.0015 vol.% | 0.133 | 0.139 | 4.5 | – |
| 25 | MO | Graphene | 60 (thick) | 0.01 mass% | – | – | 0.79 | [37] |
| 80 | MO | Graphene | 60 (thick) | 0.01 mass% | – | – | 26.4 | – |
| 25 | MO | Graphene | 60 (thick) | 0.05 mass% | – | – | 1.75 | [37] |
| 80 | MO | Graphene | 60 (thick) | 0.05 mass% | – | – | 29.3 | – |
| 25 | MO | Graphene | 60 (thick) | 0.10 mass% | – | – | 1.80 | [37] |
| 80 | MO | Graphene | 60 (thick) | 0.10 mass% | – | – | 33.3 | – |
| 10 | MO | CuO | 30 | 0.5 mass% | 0.133 | 0.138 | 3.8 | [82] |
| 60 | MO | CuO | 30 | 0.5 mass% | 0.129 | 0.142 | 10.1 | – |
| 100 | MO | CuO | 30 | 0.5 mass% | 0.126 | 0.146 | 15.9 | – |
| 10 | MO | $Fe_3O_4$ | 30 | 0.5 mass% | 0.133 | 0.137 | 3 | [82] |
| 60 | MO | $Fe_3O_4$ | 30 | 0.5 mass% | 0.129 | 0.136 | 5.4 | – |
| 100 | MO | $Fe_3O_4$ | 30 | 0.5 mass% | 0.126 | 0.136 | 7.9 | – |
| 20 | MO | $Al_2O_3$ | 20 | 0.5 φ.% | 0.116 | 0.122 | 5.20 | [253] |
| 30 | MO | $Al_2O_3$ | 20 | 0.5 φ.% | 0.125 | 0.135 | 8.00 | – |
| 50 | MO | $Al_2O_3$ | 20 | 0.5 φ.% | 0.159 | 0.17 | 6.90 | – |
| 20 | MO | MWCNT | 10–20 | 0.01 mass% | 0.109 | 0.110 | 0.90 | [254] |
| 40 | MO | MWCNT | 10–20 | 0.01 mass% | 0.107 | 0.111 | 3.74 | – |
| 60 | MO | MWCNT | 10–20 | 0.01 mass% | 0.104 | 0.112 | 7.70 | – |
| 20 | MO | MWCNT | 10–20 | 0.001 mass% | 0.109 | 0.109 | 0.00 | [254] |
| 40 | MO | MWCNT | 10–20 | 0.001 mass% | 0.107 | 0.1095 | 2.34 | – |
| 60 | MO | MWCNT | 10–20 | 0.001 mass% | 0.104 | 0.11 | 5.77 | – |
| 20 | MO | AlN | 40 | 0.159 vol.% | 0.1052 | 0.1108 | 5.30 | [250] |
| 70 | MO | AlN | 40 | 0.159 vol.% | 0.0998 | 0.1064 | 6.60 | – |
| 20 | MO | AlN | 40 | 0.079 vol.% | 0.1052 | 0.1089 | 3.50 | [250] |
| 70 | MO | AlN | 40 | 0.079 vol.% | 0.0998 | 0.104 | 4.20 | – |
| 40 | MO | $TiO_2$ | 21 | 0.816 g $L^{-1}$ | 0.132 | 0.135 | 2.27 | [251] |
| 80 | MO | $TiO_2$ | 21 | 0.816 g $L^{-1}$ | 0.127 | 0.129 | 1.57 | – |
| 40 | SE | $TiO_2$ | 21 | 0.816 g $L^{-1}$ | 0.156 | 0.160 | 2.56 | [251] |
| 80 | SE | $TiO_2$ | 21 | 0.816 g $L^{-1}$ | 0.151 | 0.154 | 1.99 | – |
| 30 | MO | $Fe_3O_4$ | 10.55 | 0.2 Mass.% | 0.122 | 0.123 | 0.8 | [24] |
| 50 | MO | $Fe_3O_4$ | 10.55 | 0.2 Mass.% | 0.113 | 0.115 | 1.8 | – |
| 70 | MO | $Fe_3O_4$ | 10.55 | 0.2 Mass.% | 0.106 | 0.107 | 0.9 | – |
| 40 | TO | $TiO_2$ | 58 | 0.02 mass% | 0.108 | 0.111 | 2.8 | [255] |
| 80 | TO | $TiO_2$ | 58 | 0.02 mass% | 0.106 | 0.108 | 1.9 | – |

blowers (1400 rpm, placed 20 cm from the large transformer walls), and a heating element. Heat transfer performance was assessed at nanoparticle concentrations of 0.05–0.2 mass% and input powers of 50.5–124 W. The NCHT (Fig. 19d) and FCHT (Fig. 19e) coefficients increased with concentration and power, with peak enhancements of 23.08% and 24.68%, respectively, at 0.2 mass% and 50.5 W. Higher FCHT coefficient (at 0.2 mass% and 50.5 W) is attributed to more turbulent enforced convection, improving heat dissipation.

Amiri et al. examined the influence of forced convection on the thermal characteristics of transformer oil-based amine-treated graphene quantum dots (AGQD) nanofluid [105]. The FCHT coefficient for both the base oil and nanofluids exhibits an upward trend with increase in input power. The FCHT coefficient for the transformer oil-based AGQD nanofluid was markedly superior to that of pure transformer oil, demonstrating an enhancement of 21–32% at a minimal concentration of 0.001 mass%. The FCHT coefficients of

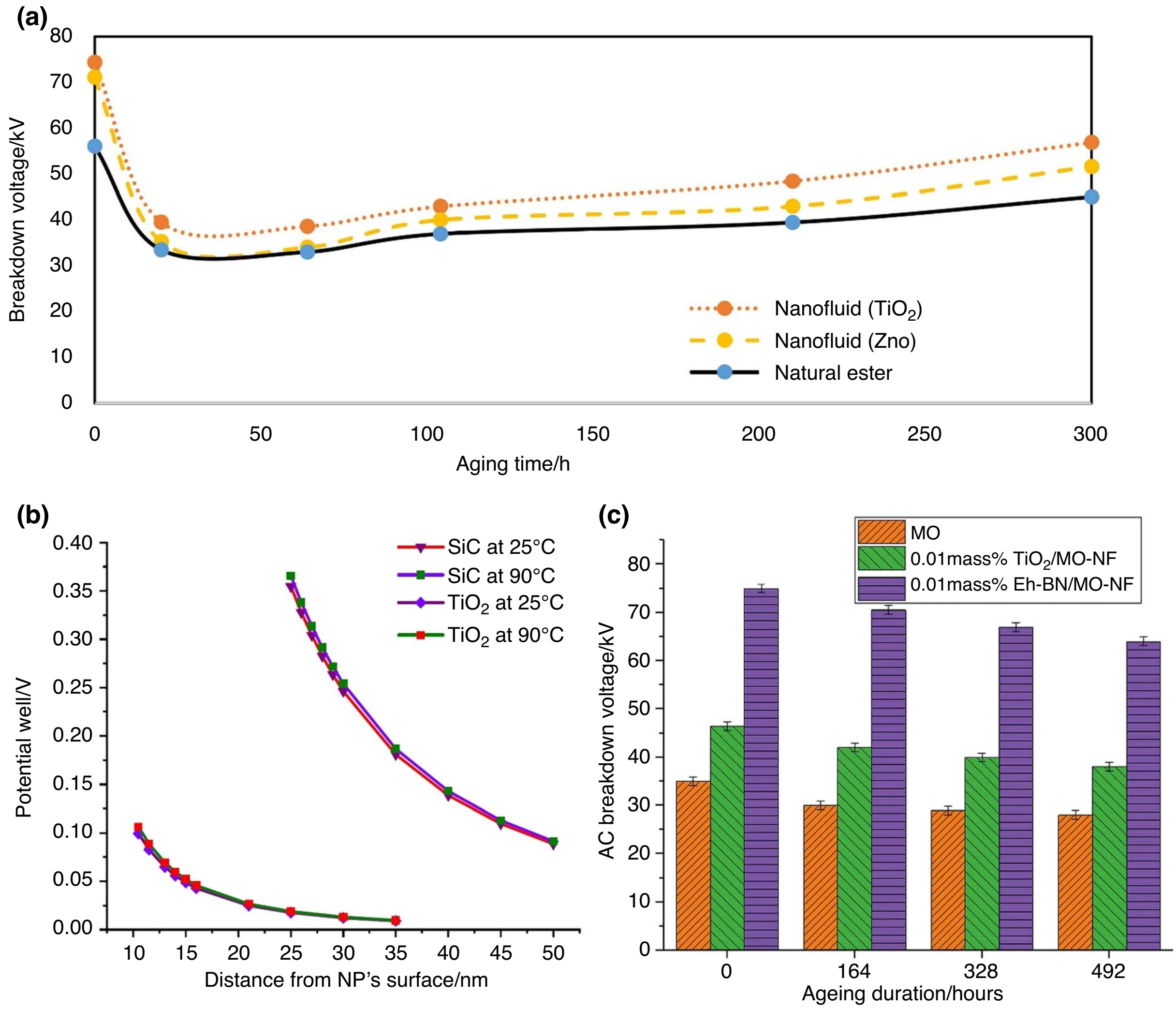


**Fig. 18** **a** AC Breakdown voltage progression over time at 150 °C—Reprinted under a CC license [99]; **b** Potential well distribution vs. nanoparticle surface distance under a 20 kV/mm field—Reprinted with the license number 6092820966250 [44]; and **c** AC breakdown voltage of mineral oil, mineral oil-based $TiO_2$, and exfoliated h-BN nanofluids over aging time—Reprinted under a CC license [258]

transformer oil, both with and without AGQD, significantly exceed those observed under natural convection conditions. Furthermore, Hussein et al. investigated the augmentation of FCHT using $TiO_2$ nanoparticles dispersed in palm oil [260]. The maximum enhancement in heat transfer was approximately 6% relative to the pure palm oil BF.

This considerable enhancement in the dielectric properties and heat transfer of nanofluid suggests that forced circulation conditions can markedly improve the dielectric and cooling efficiencies of transformer systems. This may result in more compact, efficient, and reliable transformer designs. However, investigations carried out on the effect of forced oil circulations on various parameters are inadequate, which requires the need for more research studies on the forced oil circulation.

#### External magnetic and electrical field

An external magnetic field can be used for forced circulation of magnetic nanofluid [51]. Thus, a magnetic field reduces magnetic nanoparticle agglomeration and improves dispersion [261]. It also influences iron oxide nanoparticle polarization and charge trapping, which improves the dielectric properties of nanofluids [213, 262, 263].

Lee et al. studied the BDV of nanofluids without and with magnetic fields [264]. In Fig. 20, it is clear that the BDV of transformer oil was greatly increased by the addition of magnetic nanoparticles. When the external magnetic field is supplied, the average BDV further increases to about 40.2 kV. It is 30% higher than that without applied field, it might be due to the improvement of dispersion of nanoparticles. This is because an external magnetic field can successfully disperse magnetic nanoparticles and also enhances charge trapping [265]. Rajnak et al. found that the thermal conductivity of transformer oil-based magnetic nanofluids improved by incorporation of iron oxide nanoparticles (9.2% increase at 2.198 vol.%) [266]. The anisotropic thermal conductivity is revealed by comparing the radial and axial directions under an external magnetic field, in which higher thermal conductivity is obtained in radial direction due to the effect of gradient magnetic field redistributing the nanoparticles and constructing heat conduction pathways. On the other hand, dielectric permittivity increased gradually from 2.12 (pure oil) to 2.45 (at 2.198 vol.%). Under an external magnetic field, a magnetic field dependent permittivity is observed, leading to a magneto-dielectric anisotropy, in which the permittivity is anisotropic with respect to the electric and magnetic fields. This effect is attributed to nanoparticle alignment and charge accumulation at chain terminals.

Kosterec et al. used a magneto-hydrodynamic model for obtaining the simulation results for the magnetic fluid under magnetic field [51]. The thermal distribution and fluid flow were obtained using the ANSYS Workbench software. TO fluid flow streamline at 1500 s is shown in Fig. 21a. Oil is causing natural convection due to the heat from the wire spiral. Based on the flow pattern, it appears that hot oil is convectively rising and cold oil is falling. Here, since no other forces are present, circulation is driven by the effects of buoyancy from temperature differences. Fig. 21b shows magnetic fluid flow streamline at 1500 s. This flow is affected by thermomagnetic and natural convection, unlike transformer oil fluid flow streamline. Natural convection pushes heated fluid above the spiral toward the container walls due to its lower magnetic permeability. It cools at the walls and is drawn back to the heating spiral by the magnetic field, forcing circulation. This improved circulation boosts magnetic fluid cooling efficiency over transformer oil.

DNFs are subjected to electric fields for their practical applications in real time. The influence of the electrical field on their performance is significant. Applying an electrical field with a periodically changing direction effectively resuspends deposited nanoparticles, addressing a key challenge in the practical use of nanofluids. Over time, nanoparticles tend to settle on heat transfer surfaces, forming a sediment layer that increases thermal resistance and degrades heat transfer performance. Figure 21c illustrates [102], in the absence of an electric field, adhesive forces ($F_a$) and gravity ($F_g$) keep nanoparticles in place. As illustrated in Fig. 21d [102], under the influence of an alternating electrical field, adhesive forces are opposed by electrophoretic and dielectrophoretic forces ($F_e$) and aided by drag force ($F_c$) from the BF in lifting the nanoparticles. By preventing long-term accumulation, the nanofluid can be stable and have high thermal conductivity during long operations.

Furthermore, it illustrates the velocity contours based on numerical simulations [267]. Fig. 21e and f [102] shows the applied electric field causes movement in the BF, thus generating convective currents that improve dispersion and therefore avoid particle sedimentation. This higher fluid velocity disturbs the temperature boundary layer, therefore enhancing heat transfer efficiency. The technique preserves better thermal performance by eliminating nanoparticle deposition, which is especially advantageous for long-term uses like transformer cooling or higher voltage, where more nanoparticle concentration, and longer switching periods for the electrical field direction help to maximize heat transfer enhancement. This method guarantees consistent, effective heat dissipation, which makes nanofluids more practical for engineering uses needing consistent temperature control.

The possibility to improve BDV using a magnetic field implies that active management of insulation characteristics might be achieved in real time [264], thus providing fresh approaches to maximize high-voltage insulation. The results might be utilized to create adaptive insulation fluids wherein dynamic adjustment of insulation qualities in response to varying operating circumstances could be accomplished using external magnetic fields [51]. Magnetic fluids can enhance transformer system cooling efficiency, creating a thermomagnetic convection, which supports regular convection. This helps to bring down temperature gradients so transformer life span and reliability are increased by improved heat dissipation. In addition, external magnetic field regulated fluid flow is a potential approach for enhanced thermal management in limited spaces or for high-power electrical applications.

Periodically changing electrical field prevents nanoparticle deposition, ensuring stable nanofluid thermal conductivity and enhancing natural convection heat transfer, which is critical for applications like transformer cooling and electronic heat dissipation [102]. It complements this by using the lattice Boltzmann method (LBM) to numerically analyze electric field interactions with natural convection, highlighting the roles of electrophoretic and dielectrophoretic forces in modifying velocity fields [267].

## Practical implications

This in-depth review explores the profound effect of multiple factors on the dispersion stability and their thermo-dielectric characteristics of DNFs. This review outlines the following practical implications.

### Nanoparticle bandgap

- Conductive nanoparticles increase charge accumulation [104], improving electrostatic stabilization. Bandgap tun-

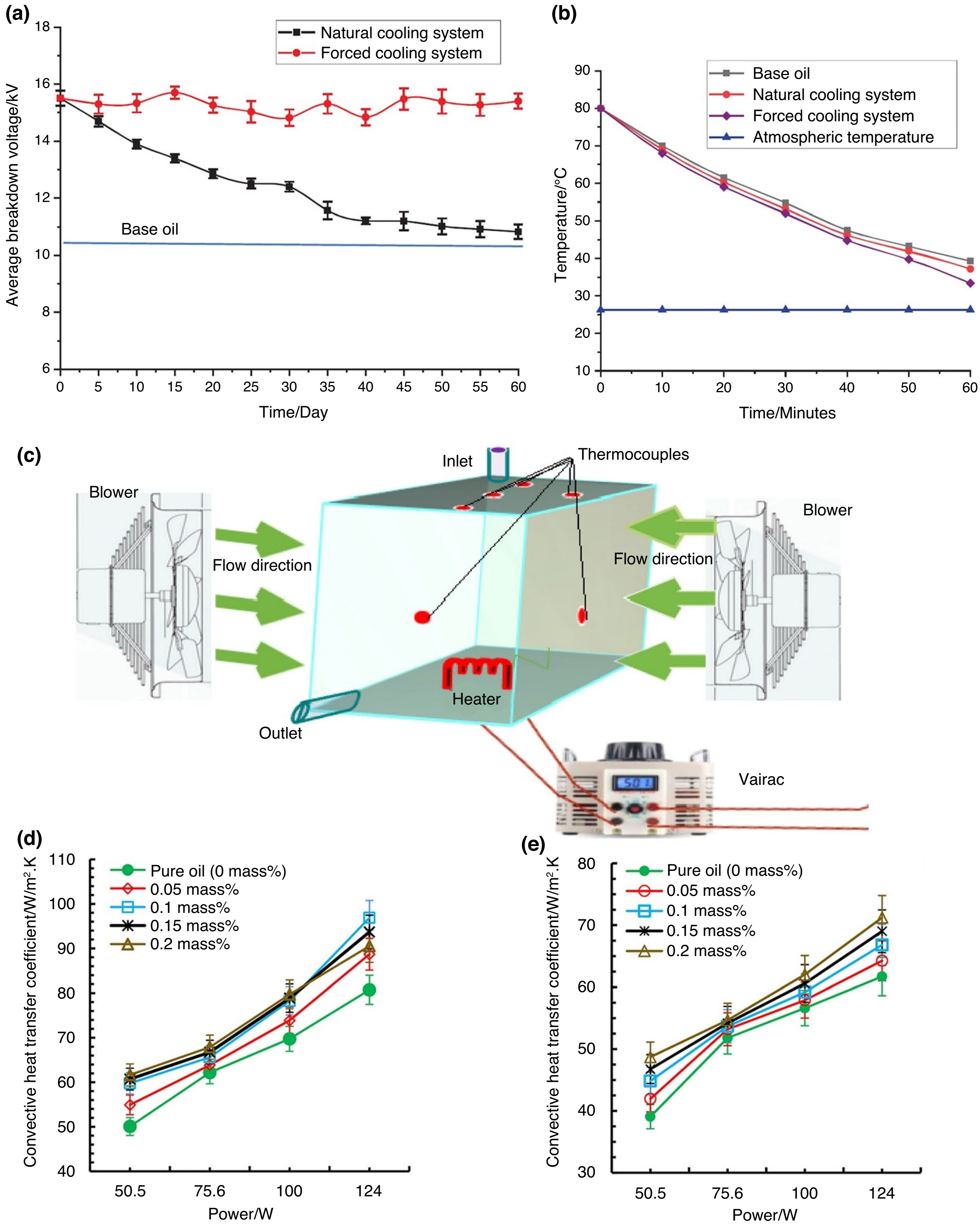


**Fig. 19** Natural and forced circulation nanofluids: **a** 60-day average breakdown voltage and **b** 60-min temperature variation—Reprinted under a CC license [52]; and **c** schematic diagram of the experimental setup, and convective heat transfer coefficient: **d** natural and **e** forced—Reprinted under a CC license [85]

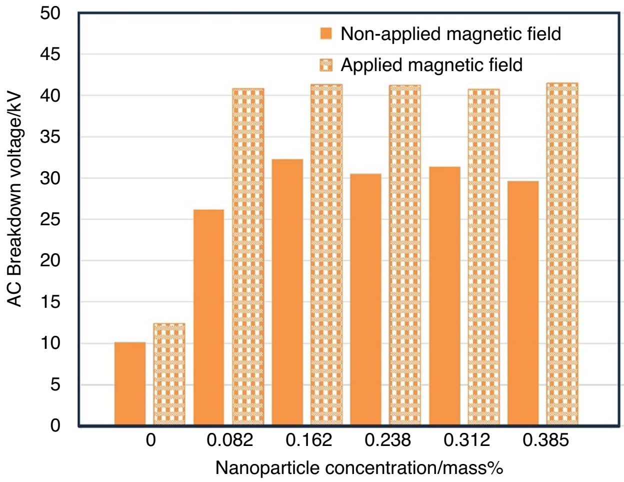


**Fig. 20** Breakdown voltage of nanofluids under with and magnetic field at different nanoparticle concentration—Redrawn license number 6092820316448 [264]

ing (e.g., fluorination [33]) enhances stability by modifying surface charge.

- Insulative/semiconductive nanoparticles improve dielectric relaxation, enhancing BDV [134]. Charge trapping reduces tan δ, improving resistivity. Conductive nanoparticles increase polarization and charge storage [135].
- There is no straightforward formula linking the bandgap of nanoparticles directly to the thermal conductivity of nanofluids. However, conductive nanoparticles showed unparalleled improvements in thermal conductivity, likely due to their high intrinsic thermal conductivity.
- Conductive nanoparticles are effective at low concentrations (0.01–0.1 mass%). Insulative/semiconductive nanoparticles require higher filler levels (up to 2 mass%) (refer to Table 3).

## Nanoparticle size variation and ultrasonic cavitation

- Higher zeta potential from smaller nanoparticles improves dispersion [140]. Optimized sonication prevents sedimentation; excessive sonication reduces performance [125].
- Smaller nanoparticles enhance BDV by increasing charge trapping sites and surface area. Ultrasonication improves BDV by breaking clusters and enhancing dispersion [125].
- Smaller nanoparticles boost conductivity via phonon transport, Brownian motion, and EDL effects [122]. Ultrasonication further enhances conductivity by preventing agglomeration.
- Controlled sonication improves dielectric and thermal characteristics [125]; too long duration may reduce nanofluid stability.
- Some studies found larger nanoparticles perform better [101], because of improved interfacial effects and dispersion. Optimization specific to nanofluid is absolutely vital.

## Phase and shape of nanoparticles

- Comparative investigation on anatase $TiO_2$ enhanced thermal conductivity by 43.3% (i.e., 5.818 W/m–K vs. 4.059 W/m–K for rutile) [161], due to longer mean free path of low-frequency acoustic phonons along the a and b axes in dielectric fluids. In DNFs, anatase $TiO_2$ achieved maximum improvements of 11.27% in AC BDV [11], also maintained 56-day stability [32].
- CdS nanosheets improve AC BDV up to 38.3%, outperforming nanobelts (37%) and spheres (35.5%), indicating Nanosheets > Nanobelts > Spheres for AC BDV enhancement in DNFs [91]. Nanosheets achieved maximum improvements.

## Blending and nano-structuring of nanoparticles

- One can find a harmonic balance of dielectric and thermal improvements in blended nanoparticles [90, 116]. Blended nanoparticles reportedly enhanced BDV up to 69.6% [90], lowered tan δ up to 11.31% [90], and raised thermal conductivity up to 48.9% [116].
- Composite and doped nanoparticles among other nanostructuring techniques enable fine-tuning of several properties. Studies showed that nanostructured nanoparticles raised thermal conductivity up to 50% [65] and lowered tan δ up to 78.4% [37].

## Nanoparticle concentration

- Optimizing nanoparticle concentration in DNFs enhances key electrical and thermal properties [268], but exceeding the critical concentration leads to performance degradation.
- Conductive nanoparticles required 0.002–0.01 mass% for BDV improvements up to 41.49%, semiconductive nanoparticles optimized between 0.002–0.04 mass%, increasing BDV up to 61.7%, while insulative nanoparticles required 0.02–0.6 mass% and achieved the highest BDV enhancement (up to 100.3%) (refer to Table 5).

## Surfactant treatment

- Surfactant treatment enhances DNF stability by preventing nanoparticle agglomeration, leading to improved long-term dispersion, maximum stability duration of

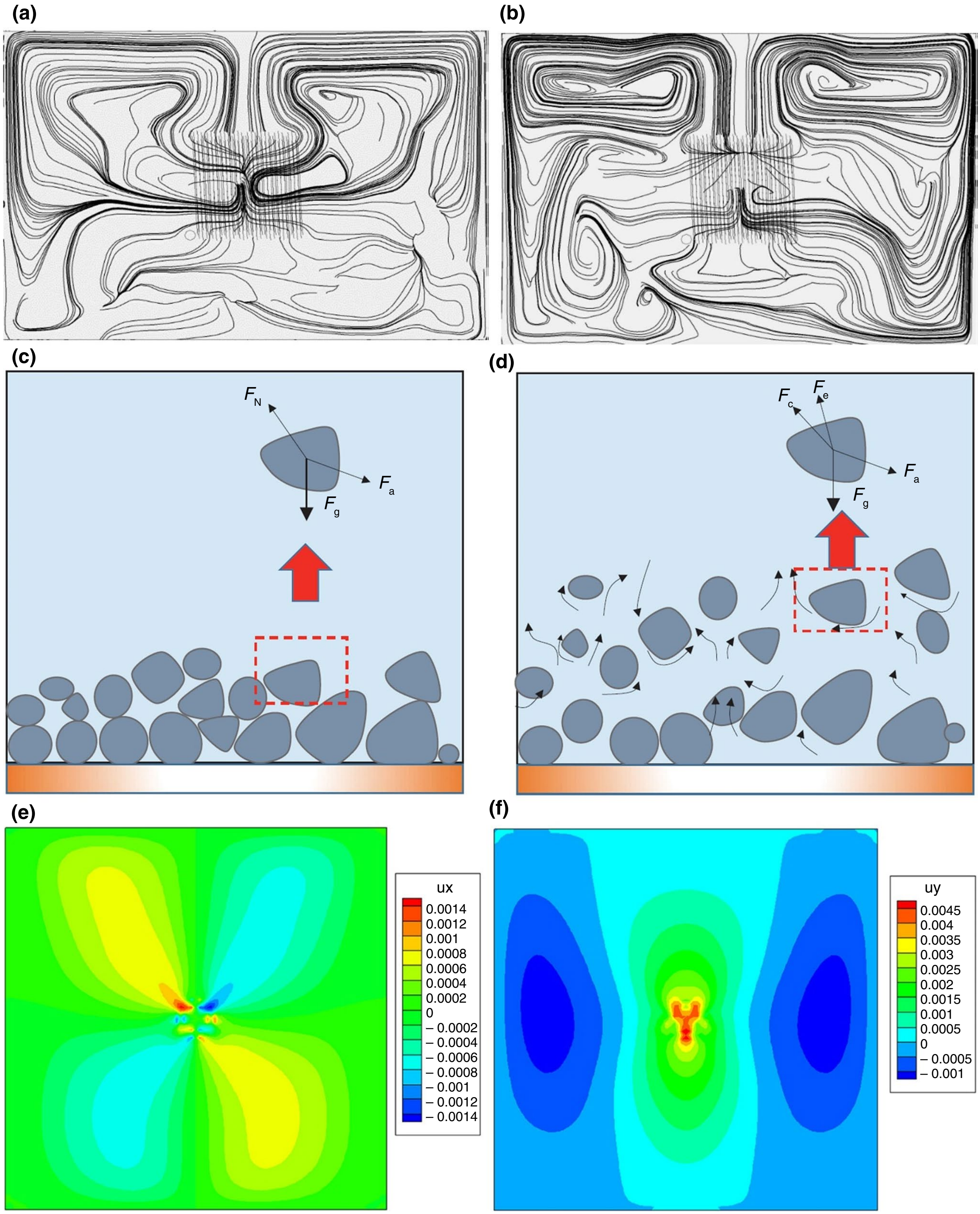


**Fig. 21** Fluid flow streamline: **a** transformer oil **b** magnetic fluid [51]; and schematic of nanoparticle: **c** deposit and **d** suspension without and with external electrical field, respectively, base fluid velocity contours under electrical field **e** and **f**—Reprinted with the license number 6092820479454 [102]

7 years observed in oleic acid-treated $Fe_3O_4$ nanofluids [109].
- Surfactants significantly improve dielectric and thermal properties, with treated nanofluids demonstrated up to 20% higher AC BDV, 27.7% higher resistivity, 37.4% lower tan δ, and 20.33% increased thermal conductivity compared to untreated counterparts [10, 115].

### Moisture content

- The findings indicate that moisture content significantly influences the BDV of DNFs, with wet nanofluids showing a higher BDV improvement (up to 61.67%) compared to dry nanofluids (up to 39.18%) [86].
- Nanoparticles effectively mitigate moisture-induced degradation by capturing water clusters, excessive moisture still poses risks to transformer performance and longevity.

### Temperature variation

- DNFs operate within service temperatures of 30–110 °C, in accordance with IEEE Standard C57.91, demanding careful designing design of DNFs at this temperature range to assure not only the stability of nanofluid, but also BDV, dielectric constant, dissipation factor, resistivity and thermal conductivity.
- A detailed assessment of these properties under diverse temperatures is necessary to avoid degradation, ensure reliable insulation, and optimize the thermal performance in practical applications.

### Thermal aging

- Thermal aging significantly impacts the dielectric properties of BFs and nanofluids [256], with AC BDV reductions exceeding 50% in MO due to oxidation and moisture accumulation [257].
- Nanoparticles enhance aging resistance, with $CaCu_3Ti_4O_{12}$ boosting BDV by 70.7% and reducing tan δ by 12% [243], while exfoliated h-BN sustains BDV and thermal conductivity after aging [258]. This highlights their role in improving transformer oil longevity under thermal stress.

#### Forced circulation

- Forced circulation improved transformer oil performance over longer time. $TiO_2$ nanofluid under forced cooling retained BDV at 15.5 kV over time, while natural cooling caused a 30% drop [52]. Heat transfer coefficients (HTCs) increased up to 24.68% in forced convection with $TiO_2$-doped MWCNT nanofluids, indicating higher thermal efficiency [85].
- The forced circulation enhances nanofluid stability, cooling, and dielectric performance, enabling more efficient transformer designs. Further research is needed to optimize its effects across different conditions.

#### External magnetic and electrical field

- External magnetic and electric fields enhanced transformer oil by improving dielectric strength and thermal management. A magnetic field increased BDV by 30% through better nanoparticle dispersion and improved thermal conductivity by 9.2% via anisotropic heat conduction [264, 266]. An alternating electric field prevented nanoparticle sedimentation, ensured long-term stability, and enhanced thermal conduction.
- These findings support the development of adaptive insulation fluids that dynamically adjust their properties for improved nanofluid performance.

## Challenges in practical applications

- Key challenges in nanoparticle bandgap tuning and DNF applications include precise control over modifications and designing scalable-cost-effective synthesis methods.
- Optimizing and standardizing nanoparticle size and ultrasonication parameters to enhance the properties of DNFs during their preparation remains a challenge.
- The trade-off between thermal efficiency and electrical insulation is a key challenge in material phase selection. For example, anatase $TiO_2$ enhances thermal conductivity but may reduce insulation, while rutile $TiO_2$ improves dielectric performance but lowers thermal conductivity. Optimized blending can help balance both properties.
- Systematic research is crucial for optimization, particularly in the careful selection of nanoparticles and precise adjustment of their ratios. This ensures the mitigation of negative impacts on dielectric strength while maximizing thermal advantages through blending and nano-structuring techniques for multi-property enhancement.
- The main challenges related to concentration in practical applications of DNFs are maintaining long-term stability, preventing sedimentation, and determining the optimal concentration for desired properties. Overcoming these challenges is essential for the commercial acceptance and widespread use of DNFs
- The main challenges related to concentration in practical applications of DNFs include maintaining long-term stability, preventing sedimentation, and accurately determining the optimal concentration for desired properties.

Addressing these issues is crucial for their commercial viability and widespread adoption.

- Surfactants are essential for improving the stability of DNFs, their impact on other critical properties presents a significant challenge for practical applications. Balancing the positive effects of improved stability against potential negative impacts on dielectric and thermal properties requires careful optimization.
- Moisture can cause dielectric degradation and accelerate the aging of BFs, negatively affecting dielectric and thermal performance over time, ultimately reducing transformer efficiency and lifespan.
- Elevated temperatures accelerate nanoparticle aggregation, degrade surfactants, and impact insulation. While thermal conductivity improves, reduced viscosity and increased charge mobility may lead to electrical failure. Ensuring stability and reliability across operational temperatures remains a key challenge.
- Thermal aging can lead to nanoparticle aggregation and surfactant degradation, resulting in inconsistent improvements in dielectric and thermal properties over time.
- The implementation of forced circulation in large-scale transformer systems entails balancing energy efficiency, maintenance costs, and reliability. Standardizing testing techniques and real-world validation are necessary for wider adoption.
- Current research indicates that magnetic fields primarily enhance nanofluids with magnetic nanoparticles, while electric fields can influence both magnetic and nonmagnetic nanofluids. However, material compatibility and scalability to full transformer systems require extensive validation.
- A significant challenge in advancing DNFs lies in the absence of standardized testing protocols. Variability in sample preparation, measurement techniques, and test conditions contributes to inconsistent and noncomparable results across published studies, hindering meaningful benchmarking and industrial acceptance.

## Future research directions

- Optimizing bandgap can improve charge trapping, BDV, and thermal conductivity. Future research should focus on bandgap tuning. Advanced characterization techniques are needed to correlate bandgap variations and nanofluid properties.
- Optimized nanoparticle size selection and ultrasonication parameters can enhance stability, dielectric, and thermal performance. Additionally, application-specific tailoring such as power transformers and thermal management systems needed using theoretical and empirical validation.
- More studies are needed on phase and shape effects to systematically compare stability, dielectric properties, and thermal conductivity using a common BF for consistency in experimental findings.
- Systematic studies should explore new hybrid and nanostructured nanoparticle combinations that optimize dielectric and thermal properties. Long-term stability assessments are essential for practical applicability. Machine learning and computational modeling can streamline nanoparticle formulation by reducing experimental trial and error.
- Develop ultra-stable nanofluids with high-performance reliability while addressing sedimentation issues through optimized nanoparticle concentration.
- Despite advancements, amphoteric surfactants remain underexplored, yet they offer tuneable surface properties and improved compatibility with dielectric fluids. Future research should focus on developing novel surfactants that are nontoxic, biodegradable, and recyclable while enhancing stability without compromising the key properties of nanofluids.
- Studies on the effect of moisture on DNFs have been limited to BDV investigations; studies on other dielectric and thermal properties of DNFs are lacking. Additional research is required to fully understand and mitigate the effects of moisture on DNFs.
- Future research should develop advanced surfactants and functionalized nanoparticles to improve nanofluid stability at high temperatures and thermal aging condition while examining viscosity, insulating, and thermal properties for reliable performance in high-power applications.
- Developing energy-efficient forced circulation systems and predictive models for performance assessment. Standardized testing protocols and real-world validation of forced circulation systems in transformer applications are critical for commercialization.
- Advancing the design, creating predictive models for evaluating performance, and the real-world validation are essential for successful commercialization of energy-efficient forced circulation systems.
- Optimize electric and magnetic field parameters, assess nonmagnetic nanoparticle behavior, and assess long-term stability for large-scale use. AI-driven models can enhance predictions.
- Optimize electric and magnetic field parameters, study nonmagnetic nanoparticle behavior, and evaluate long-term stability for large-scale use. AI-powered models can improve predictions.
- Future research should prioritize the development and adoption of standardized protocols for nanofluid preparation, characterization, and performance evaluation. Establishing such guidelines would enhance reproduc-

ibility, comparability, and accelerate translation into practical applications.

- DNFs exhibit superior thermal and electrical stability during thermal and electrical fault conditions such as overheating and arcing faults, due to enhanced heat dissipation and dielectric strength [269, 270]. Future research should enhance nanoparticle stability and create optical sensing for real-time monitoring [271].

**Acknowledgements** The authors extend their appreciation to the Deanship of Research and Graduate Studies at King Khalid University for funding this work through Large Research Project under grant number RGP2/34/46. This work is supported by the University Putra Malaysia under Grant GP-GPB/2021/9706100.

**Author contributions** Rizwan A. Farade was involved in conceptualization, data curation, formal analysis, investigation, methodology, validation, visualization, writing—original draft, and writing—review & editing. Noor Izzri Abdul Wahab helped in conceptualization, funding acquisition, supervision, and validation. Muhammad Rafiq contributed to writing—original draft, and writing—review & editing. Nehad Ali Shah helped in writing—original draft, and writing—review & editing. T. M. Yunus Khan contributed to writing—original draft, and writing—review & editing. Syed waheedullah Ghori was involved in writing—original draft, and Writing—review & editing.

**Funding** Open access funding provided by The Ministry of Higher Education Malaysia and Universiti Putra Malaysia.

## Declarations

**Conflict of interest** The authors declare that they have no known competing financial interests or personal relationships that could have appeared to influence the work reported in this paper.



## References

1. Ghaffarkhah A, Afrand M, Talebkeikhah M, Sehat AA, Moraveji MK, Talebkeikhah F, et al. On evaluation of thermophysical properties of transformer oil-based nanofluids: a comprehensive modeling and experimental study. J Mol Liq. 2020;300: 112249.
2. Rafiq M, Shafique M, Azam A, Ateeq M. The impacts of nanotechnology on the improvement of liquid insulation of transformers: emerging trends and challenges. J Mol Liq. 2020;302: 112482.
3. Karatas M, Bicen Y. Nanoparticles for next-generation transformer insulating fluids: a review. Renew Sustain Energy Rev. 2022;167: 112645.
4. Kurimský J, Rajňák M, Šárpataky M, Čonka Z, Paulovičová K. Electrical and acoustic investigation of partial discharges in two types of nanofluids. J Mol Liq. 2021;341: 117444.
5. Koutras KN, Naxakis IA, Antonelou AE, Charalampakos VP, Pyrgioti EC, Yannopoulos SN. Dielectric strength and stability of natural ester oil based $TiO_2$ nanofluids. J Mol Liq. 2020;316: 113901.
6. Souza RR, Gonçalves IM, Rodrigues RO, Minas G, Miranda JM, Moreira ALN, et al. Recent advances on the thermal properties and applications of nanofluids: from nanomedicine to renewable energies. Appl Therm Eng. 2022;201: 117725.
7. Shen Z, Wang F, Wang Z, Li J. A critical review of plant-based insulating fluids for transformer: 30-year development. Renew Sustain Energy Rev. 2021;141: 110783.
8. Cimbala R, Havran P, Király J, Rajňák M, Kurimský J, Šárpataky M, et al. Dielectric response of a hybrid nanofluid containing fullerene $C_{60}$ and iron oxide nanoparticles. J Mol Liq. 2022;359: 119338.
9. Das AK, Shill DC, Chatterjee S. Coconut oil for utility transformers – environmental safety and sustainability perspectives. Renew Sustain Energy Rev. 2022;164: 112572.
10. Chen R, Qiu Q, Peng X, Tang C. Surface modified h-BN towards enhanced electrical properties and thermal conductivity of natural ester insulating oil. Renew Energy. 2023;204:185–96.
11. Bhunia MM, Panigrahi K, Naskar CB, Bhattacharjee S, Chattopadhyay KK, Chattopadhyay P. 2D square nanosheets of Anatase TiO2: a surfactant free nanofiller for transformer oil nanofluids. J Mol Liq. 2021;325: 115000.
12. Bhunia MM, Panigrahi K, Das S, Chattopadhyay KK, Chattopadhyay P. Amorphous graphene – Transformer oil nanofluids with superior thermal and insulating properties. Carbon N Y. 2018;139:1010–9.
13. Lv Y, Li C, Sun Q, Huang M, Li C, Qi B. Effect of dispersion method on stability and dielectric strength of transformer oil-based $TiO_2$ nanofluids. Nanoscale Res Lett. 2016;11:515.
14. Farade RA, Wahab NIA, Mansour DA, Soudagar MEM. The effect of nanoadditives in natural ester dielectric liquids: a comprehensive review on stability and thermal properties. IEEE Trans Dielectr Electr Insul. 2023;30:1478–92.
15. A N, Kuan TM, Mansour D-EA, Farade RA, Ariffin AM, Rahman MSA, et al. Innovative Approaches for Augmenting Dielectric Properties in Cross-Linked Polyethylene (XLPE): A Review. Heliyon 2024:e34737.
16. Šárpataky M, Kurimský J, Rajňák M, Krbal M, Adamčák M. Dielectric performance of natural- and synthetic-ester-based nanofluids with fullerene nanoparticles. Energies. 2022;16:343.
17. Hussain M, Mir FA, Ansari MA. Nanofluid transformer oil for cooling and insulating applications: a brief review. Appl Surf Sci Adv. 2022;8: 100223.
18. IEEE. IEEE Guide for Acceptance and Maintenance of Natural Ester Insulating Liquid in Transformers IEEE Std C57.147–2018. New York, USA: IEEE; 2018.
19. Dombek G, Nadolny Z, Marcinkowska A. Effects of nanoparticles materials on heat transfer in electro-insulating liquids. Appl Sci. 2018;8:2538.
20. Asadi A, Aberoumand S, Moradikazerouni A, Pourfattah F, Żyła G, Estellé P, et al. Recent advances in preparation methods and thermophysical properties of oil-based nanofluids: a state-of-the-art review. Powder Technol. 2019;352:209–26.
21. Hrkac M, Papageorgiou P, Kosmoglou I, Miatto G. BIOTEMP® transformer technology for innovative compact substation. IET Conf Publ. 2010;2010:1–6.

22. Adekunle AA, Oparanti SO. A review on physicochemical and electrical performance of vegetable oil-based nanofluids for high voltage equipment. Electr Power Syst Res. 2023;214: 108873.
23. Mehta DM, Kundu P, Chowdhury A, Lakhiani VK, Jhala AS. A review on critical evaluation of natural ester vis-a-vis mineral oil insulating liquid for use in transformers: Part 1. IEEE Trans Dielectr Electr Insul. 2016;23:873–80.
24. Rajňák M, Paulovičová K, Kurimský J, Tóthová J, Cimbala R, Kónyová K, et al. Comparison of physical properties of ferrofluids based on mineral transformer oil and bio-degradable gas-to-liquid oil. J Magn Magn Mater. 2024;589: 171628.
25. Rahman A, Chowdhury MA, Hossain N. Green synthesis of hybrid nanoparticles for biomedical applications: A review. Appl Surf Sci Adv. 2022;11: 100296.
26. Khan U, Shafiq A, Zaib A, Baleanu D. Hybrid nanofluid on mixed convective radiative flow from an irregular variably thick moving surface with convex and concave effects. Case Stud Therm Eng. 2020;21: 100660.
27. Pourpasha H, Zeinali Heris S, Javadpour R, Mohammadpourfard M, Li Y. Experimental investigation of zinc ferrite/insulation oil nanofluid natural convection heat transfer, AC dielectric breakdown voltage, and thermophysical properties. Sci Rep. 2024;14:20721.
28. Pourpasha H, Zeinali Heris S, Mousavi SB. Thermal performance of novel ZnFe2O4 and TiO2-doped MWCNT nanocomposites in transformer oil. J Mol Liq. 2024;394: 123727.
29. Atiya EG, Mansour D-EA, Khattab RM, Azmy AM. Dispersion behavior and breakdown strength of transformer oil filled with $TiO_2$ nanoparticles. IEEE Trans Dielectr Electr Insul. 2015;22:2463–72.
30. Sima W, Shi J, Yang Q, Huang S, Cao X. Effects of conductivity and permittivity of nanoparticle on transformer oil insulation performance: experiment and theory. IEEE Trans Dielectr Electr Insul. 2015;22:380–90.
31. Liu C, Qiao Y, Du P, Zhang J, Zhao J, Liu C, et al. Recent advances of nanofluids in micro/nano scale energy transportation. Renew Sustain Energy Rev. 2021;149: 111346.
32. Qin Z-B, Tan L, Liu Z-Q, Chen S, Qin J-H, Tang J-J, et al. One-pot synthesis of ultrafine $TiO_2$ nanoparticles with enhanced thermal conductivity for nanofluid applications. Adv Powder Technol. 2016;27:299–304.
33. Bhunia MM, Chattopadhyay KK, Chattopadhyay P. Ultra-stable transformer oil nanofluids with significant AC breakdown voltage enhancement at ultra-low filler fraction of functionalized boron nitride nanosheets 2022:1–23.
34. Xu F, Wang H, Xing S, Tang M, Zhang H, Wang Y. Seeking optimized transformer oil-based nanofluids by investigation of the modification mechanism of nano-dielectrics. J Mater Chem C. 2020;8:7336–43.
35. Ahmed W, Kazi SN, Chowdhury ZZ, Bin JMR, Mehmood S, Soudagar MEM, et al. Heat transfer growth of sonochemically synthesized novel mixed metal oxide $ZnO+Al_2O_3+TiO_2$/DW based ternary hybrid nanofluids in a square flow conduit. Renew Sustain Energy Rev. 2021;145:111025.
36. Aberoumand S, Jafarimoghaddam A. Tungsten (III) oxide ($WO_3$) – silver/transformer oil hybrid nanofluid: preparation, stability, thermal conductivity and dielectric strength. Alexandria Eng J. 2018;57:169–74.
37. Walvekar R, Zairin DA, Khalid M, Jagadish P, Mubarak NM, Tcsm G. Stability, thermo-physical and electrical properties of naphthenic/POME blended transformer oil nanofluids. Therm Sci Eng Prog. 2021;23: 100878.
38. Ise N, Sogami IS, Sogam I, Sogami IS, Sogam I, Sogami IS, et al. Structure Formation in Solution: Ionic Polymers and Colloidal Particles. Berlin/Heidelberg: Springer-Verlag; 2005.
39. Asadi A, Pourfattah F, Miklós Szilágyi I, Afrand M, Żyła G, Seon Ahn H, et al. Effect of sonication characteristics on stability, thermophysical properties, and heat transfer of nanofluids: a comprehensive review. Ultrason Sonochem. 2019;58: 104701.
40. Rodríguez-Laguna MR, Castro-Alvarez A, Sledzinska M, Maire J, Costanzo F, Ensing B, et al. Mechanisms behind the enhancement of thermal properties of graphene nanofluids. Nanoscale. 2018;10:15402–9.
41. Choi C, Yoo HS, Oh JM. Preparation and heat transfer properties of nanoparticle-in-transformer oil dispersions as advanced energy-efficient coolants. Curr Appl Phys. 2008;8:710–2.
42. Olmo C, Méndez C, Ortiz F, Delgado F, Ortiz A. Titania nanofluids based on natural ester: cooling and insulation properties assessment. Nanomaterials. 2020;10: 603.
43. Abd-Elhady AM, Ibrahim ME, Taha TA, Izzularab MA. Effect of temperature on AC breakdown voltage of nanofilled transformer oil. IET Sci Meas Technol. 2018;12:138–44.
44. Koutras KN, Antonelou AE, Naxakis IA, Charalampakos VP, Pyrgioti EC, Yannopoulos SN. In-situ high temperature study of the long-term stability and dielectric properties of nanofluids based on $TiO_2$ and SiC dispersions in natural ester oil at various concentrations. J Mol Liq. 2022;359: 119284.
45. Mu-tian C, Yue-fan D, Yu-zhen L, Jian-quan Z, Xiao-xin L, Cheng-rong L. Effect of nanoparticles on the dielectric strength of aged transformer oil. 2011 Annu. Rep. Conf. Electr. Insul. Dielectr. Phenom., IEEE; 2011, pp. 664–7.
46. Amalanathan AJ, Harid N, Griffiths H, Sarathi R. Impact of adding activated bentonite to thermally aged ester-based $TiO_2$ nanofluids on insulation performance. IET Nanodielectr. 2021;4:63–74.
47. Primo VA, Pérez-Rosa D, García B, Cabanelas JC. Evaluation of the stability of dielectric nanofluids for use in transformers under real operating conditions. Nanomaterials. 2019;9:143.
48. Mladenov E, Staykov S, Cholakov G. Water saturation limit of transformer oils. IEEE Electr Insul Mag. 2009;25:23–30.
49. Bartnikas R. Electrical Insulating Liquids. vol. 3. 1994.
50. Du B, Li X, Xiao M. High thermal conductivity transformer oil filled with BN nanoparticles. IEEE Trans Dielectr Electr Insul. 2015;22:851–8.
51. Kosterec M, Kurimský J, Cimbala R, Čonka Z, Kruželák L, Rajňák M, et al. Analysis of thermal field in mineral transformer oil based magnetic fluids. Acta Phys Pol A. 2017;131:937–9.
52. Ibrahim ME, El-Behiry SM, Hussien AA, Izzularab MA, Abd-Elhady AM. Breakdown voltage and thermal performance of nanofilled transformer oil considering natural and forced cooling systems. IET Gener Transm Distrib. 2021;15:339–46.
53. Gürdal M, Arslan K, Gedik E, Minea AA. Effects of using nanofluid, applying a magnetic field, and placing turbulators in channels on the convective heat transfer: a comprehensive review. Renew Sustain Energy Rev. 2022;162: 112453.
54. Alsabery AI, Abosinnee AS, Al-Hadraawy SK, Ismael MA, Fteiti MA, Hashim I, et al. Convection heat transfer in enclosures with inner bodies: a review on single and two-phase nanofluid models. Renew Sustain Energy Rev. 2023;183: 113424.
55. Karpets M, Rajnak M, Petrenko V, Gapon I, Avdeev M, Bulavin L, et al. Electric field-induced assembly of magnetic nanoparticles from dielectric ferrofluids on planar interface. J Mol Liq. 2022;362: 119773.
56. Chakraborty S, Shukla D, Kumar PP. A review on coolant selection for thermal management of electronics and implementation of multiple-criteria decision-making approach. Appl Therm Eng. 2024;245: 122807.

57. Behera US, Sangwai JS, Byun H-S. A comprehensive review on the recent advances in applications of nanofluids for effective utilization of renewable energy. Renew Sustain Energy Rev. 2025;207: 114901.
58. Rafiq M, Lv YZ, Zhou Y, Ma KB, Wang W, Li CR, et al. Use of vegetable oils as transformer oils-a review. Renew Sustain Energy Rev. 2015;52:308–24.
59. Ahmad F, Khan AALI, Khan Q, Hussain MR, Member S, Khan AALI, et al. State-of-art in nano-based dielectric oil: A review. IEEE Access. 2019;7:13396–410.
60. Farade RA, Wahab NIA, Mansour DA. The effect of nano-additives in natural ester dielectric liquids: a comprehensive review on dielectric properties. IEEE Trans Dielectr Electr Insul. 2023;30:1502–16.
61. Rafiq M, Shafique M, Azam A, Ateeq M. Transformer oil-based nanofluid: the application of nanomaterials on thermal, electrical and physicochemical properties of liquid insulation-a review. Ain Shams Eng J. 2021;12:555–76.
62. Huang Z, Li J, Yao W, Wang F, Wan F, Tan Y, et al. Electrical and thermal properties of insulating oil-based nanofluids: a comprehensive overview. IET Nanodielectr. 2019;2:27–40.
63. Wen D, Lin G, Vafaei S, Zhang K. Review of nanofluids for heat transfer applications. Particuology. 2009;7:141–50.
64. Hameed A, Mukhtar A, Shafiq U, Qizilbash M, Khan MS, Rashid T, et al. Experimental investigation on synthesis, characterization, stability, thermo-physical properties and rheological behavior of MWCNTs-kapok seed oil based nanofluid. J Mol Liq. 2019;277:812–24.
65. Hussain S, Mottahir Alam M, Imran M, Zouli N, Aziz A, Irshad K, et al. $Fe_3O_4$ nanoparticles decorated multi-walled carbon nanotubes based magnetic nanofluid for heat transfer application. Mater Lett. 2020;274: 128043.
66. Sreeremya TS, Krishnan A, Peer Mohamed A, Hareesh US, Ghosh S. Synthesis and characterization of cerium oxide based nanofluids: An efficient coolant in heat transport applications. Chem Eng J. 2014;255:282–9.
67. Li W, Zou C, Li X. Thermo-physical properties of waste cooking oil-based nanofluids. Appl Therm Eng. 2017;112:784–92.
68. Hwang Y, Lee J-K, Lee J-K, Jeong Y-M, Cheong S, Ahn Y-C, et al. Production and dispersion stability of nanoparticles in nanofluids. Powder Technol. 2008;186:145–53.
69. Joseph A, Thomas S. Energy, exergy and corrosion analysis of direct absorption solar collector employed with ultra-high stable carbon quantum dot nanofluid. Renew Energy. 2022;181:725–37.
70. Farade RA, Mansour D-EA, Wahab NIA, Ariffin MKA, Emara RF, Emara MM, et al. Deeper insight into thermal conductivity, size, sedimentation, band gap, and moisture effect of nanoparticles on thermo-dielectric performance of nanofluids. J Mol Liq. 2025;434: 127986.
71. Amalanathan AJ, Sarathi R, Harid N, Griffiths H. Investigation on flow electrification of ester-based $TiO_2$ nanofluids. IEEE Trans Dielectr Electr Insul. 2020;27:1492–500.
72. Jacob J, Preetha P, Sindhu TK. Stability analysis and characterization of natural ester nanofluids for transformers. IEEE Trans Dielectr Electr Insul. 2020;27:1715–23.
73. Lusas EW, Alam MS, Clough RC, Riaz MN. Animal and Vegetable Fats, Oils, and Waxes. Handb. Ind. Chem. Biotechnol., Boston, MA: Springer US; 2012, pp. 1323–402.
74. Fukumori Y, Nomura T, Adschiri T, Ohara S, Saito F, Naito M, et al. Structural Control of Nanoparticles. Nanoparticle Technol. Handb. Second Edi: Elsevier; 2012. p. 49–112.
75. Mansour DA, Shaalan EM, Ward SA, El Dein AZ, Karaman HS, Ahmed HM. Multiple nanoparticles for improvement of thermal and dielectric properties of oil nanofluids. IET Sci Meas Technol. 2019;13:968–74.
76. Majeed NS, Abdulmajeed BA, Yaseen AK. The influence of the preparation and stability of nanofluids for heat transfer. J Eng. 2019;25:45–54.
77. Transformers Committee IEEE. IEEE Std C57.147™-2008, IEEE Guide for Acceptance and Maintenance of Natural Ester Fluids in Transformers. 2008.
78. Rafiq M, Lv YZ, Zhou Y, Ma KB, Wang W, Li CR, et al. Use of vegetable oils as transformer oils – a review. Renew Sustain Energy Rev. 2015;52:308–24.
79. Abdelwahab SAM, Dessouky SS, Shaaban M. Experimental investigation for the maintenance of molded case circuit breaker using nano oil. Electr Eng. 2021;103:429–37.
80. Beroual A, Duzkaya H. AC and lightning impulse breakdown voltages of natural ester based fullerene nanofluids. IEEE Trans Dielectr Electr Insul. 2021;28:1996–2003.
81. Sarkar J, Ghosh P, Adil A. A review on hybrid nanofluids: Recent research, development and applications. Renew Sustain Energy Rev. 2015;43:164–77.
82. Nazari M, Jafarmadar S, Gohari S. Convective heat transfer behavior and AC dielectric breakdown voltage of electric power transformer oil with magnetic colloidal nano-fluid: an experimental study. Case Stud Therm Eng. 2023;45: 103017.
83. Taghikhani Z, Taghikhani MA, Gharehpetian GB. Comprehensive comparative analysis of metal-oxide nanoadditives impacts on oil-filled finemet and vitroperm alloy core transformers HST concerning nanofluid thermophysical properties accurate estimation. Energy Convers Manag. 2022;260: 115594.
84. Alizadeh H, Pourpasha H, Zeinali Heris S, Estellé P. Experimental investigation on thermal performance of covalently functionalized hydroxylated and non-covalently functionalized multi-walled carbon nanotubes/transformer oil nanofluid. Case Stud Therm Eng. 2022;31: 101713.
85. Pourpasha H, Zeinali Heris S, Mohammadpourfard M. The effect of $TiO_2$ doped multi-walled carbon nanotubes synthesis on the thermophysical and heat transfer properties of transformer oil: a comprehensive experimental study. Case Stud Therm Eng. 2023;41: 102607.
86. Das AK. Investigation of electrical breakdown and heat transfer properties of coconut oil-based nanofluids. Ind Crops Prod. 2023;197: 116545.
87. Šárpataky M, Kurimský J, Rajňák M, Paulovičová K, Krbal M, Pelikán L. Synthetic and natural ester-based nanofluids with fullerene and magnetite nanoparticles – an experimental AC breakdown voltage study. J Mol Liq. 2022;368: 120802.
88. Suhaimi NS, Din MFM, Ishak MT, Rahman ARA, Wang J, Hassan MZ. Performance and limitation of mineral oil-based carbon nanotubes nanofluid in transformer application. Alexandria Eng J. 2022;61:9623–35.
89. Bhunia MM, Chattopadhyay KK, Chattopadhyay P. Transformer oil nanofluids by two-dimensional hexagonal boron nitride nanofillers. Electr Eng. 2023;105:813–25.
90. Chakraborty B, Maur S, Kumar Pradhan A, Chatterjee B, Dalai S. Investigations on dielectric characteristics of hybrid nanofluids through time and frequency domain spectroscopic measurement. J Mol Liq. 2022;366: 120347.
91. Fasehullah M, Wang F, Jamil S. Significantly elevated AC dielectric strength of synthetic ester oil-based nanofluids by varying morphology of CdS nano-additives. J Mol Liq. 2022;353: 118817.
92. Chakraborty B, Raj KY, Pradhan AK, Chatterjee B, Chakravorti S, Dalai S. Investigation of dielectric properties of $TiO_2$ and $Al_2O_3$ nanofluids by frequency domain spectroscopy at different temperatures. J Mol Liq. 2021;330: 115642.
93. Hamed A, Mahmood M, Amangaldi G, Seyyedbarzegar S, Ghorbanzadeh M. Partial Discharge Elimination in

Transformer Oils by Nanofluids: From Theory to Practice. Arab J Sci Eng 2022.

94. Khoza MM, Huan Z, Sithebe T, Vasudeva V. Experimental study of specific heat capacity and thermal conductivity of $Al_2O_3$-nanotransformer oil. Mater Today Proc. 2023. https://doi.org/10.1016/j.matpr.2023.05.486.
95. Khan SA, Tariq M, Khan AA, Alamri B. Effect of Iron/Titania-based nanomaterials on the dielectric properties of mineral oil, natural and synthetic esters as transformers insulating fluid. IEEE Access. 2021;9:168971–80.
96. Almeida C, Paul S, Godson Asirvatham L, Manova S, Nimmagadda R, Raja Bose J, et al. Experimental studies on thermophysical and electrical properties of graphene–transformer oil nanofluid. Fluids. 2020;5:172.
97. Hussain MR, Khan Q, Khan AA, Refaat SS, Abu-Rub H. Dielectric performance of magneto-nanofluids for advancing oil-immersed power transformer. IEEE Access. 2020;8:163316–28.
98. Suhaimi NS, Md Din MF, Ishak MT, Abdul Rahman AR, Mohd Ariffin M, Hashim NI, et al. Systematical study of multi-walled carbon nanotube nanofluids based disposed transformer oil. Sci Rep. 2020;10:20984.
99. Fernández I, Valiente R, Ortiz F, Renedo CJ, Ortiz A. Effect of $TiO_2$ and ZnO nanoparticles on the performance of dielectric nanofluids based on vegetable esters during their aging. Nanomaterials. 2020;10:692.
100. Sumathi S, Rajesh R. Improvement on the characteristics of transformer oil using nanofluids. Curr Sci. 2020;118:29–33.
101. Elsad RA, Mansour SA, Izzularab MA. Loading different sizes of titania nanoparticles into transformer oil: a study on the dielectric behavior. J Sol-Gel Sci Technol. 2020;93:615–22.
102. Chen Y, Luo P, Tao Q, Liu X, He D. Natural convective heat transfer investigation of nanofluids affected by electrical field with periodically changed direction. Int Commun Heat Mass Transfer. 2021;128: 105613.
103. Koutras KN, Tegopoulos SN, Charalampakos VP, Kyritsis A, Gonos IF, Pyrgioti EC. Breakdown performance and partial discharge development in transformer oil-based metal carbide nanofluids. Nanomaterials. 2022;12:269.
104. Samy AM, Ibrahim ME, Abd-Elhady AM, Izzularab MA. On electric field distortion for breakdown mechanism of nanofilled transformer oil. Int J Electr Power Energy Syst. 2020;117: 105632.
105. Amiri A, Shanbedi M, Ahmadi G, Rozali S. Transformer oils-based graphene quantum dots nanofluid as a new generation of highly conductive and stable coolant. Int Commun Heat Mass Transf. 2017;83:40–7.
106. Alicia CPY, Rashmi W, Khalid M, Rasheed AK, Gupta T. Synthesis and thermo-physical characterization of graphene based transformer oil. J Eng Sci Technol. 2016;11:140–52.
107. Cavallini A, Karthik R, Negri F. The effect of magnetite, graphene oxide and silicone oxide nanoparticles on dielectric withstand characteristics of mineral oil. IEEE Trans Dielectr Electr Insul. 2015;22:2592–600.
108. Asse JB, Mengounou GM, Imano AM. Impact of FeO3 on the AC breakdown voltage and acidity index of a palm kernel oil methyl ester based nanofluid. Energy Rep. 2022;8:275–80.
109. Rajňák M, Kurimský J, Cimbala R, Čonka Z, Bartko P, Šuga M, et al. Statistical analysis of AC dielectric breakdown in transformer oil-based magnetic nanofluids. J Mol Liq. 2020;309: 113243.
110. Rafiq M, Lv Y, Li C. Effect of shape, surface modification and concentration of $Al_2O_3$ nanoparticles on breakdown performance of transformer oil. J Electr Eng Technol. 2020;15:457–68.
111. Oparanti SO, Khaleed AA, Abdelmalik AA. Nanofluid from palm kernel oil for high voltage insulation. Mater Chem Phys. 2021;259: 123961.
112. Hiremath VK, Muduli RC, Kale P. Investigation of the stability and insulating properties of mineral oil-based surface modified silicon nanofluid. IEEE Trans Dielectr Electr Insul. 2023;30:1040–7.
113. Baharuddin MF, Zakaria IH, Ahmad MH, Aulia NZ, Sidik MAB, et al. Effect of surfactant on breakdown strength performance of transformer oil-based nanofluids. J Electr Eng Technol. 2019;14:395–405.
114. Vaishnav H, Navin K, Kurchania R, Ball RJ. Synthesis of $ZrO_2$ based nanofluids for cooling and insulation of transformers. IEEE Trans Dielectr Electr Insul. 2022;29:199–205.
115. Amizhtan SK, Amalanathan AJ, Babu MS, Sarathi R, Kumar G, Sangwai JS, et al. Experimental study and ANN analysis of rheological behavior of mineral oil-based $SiO_2$ nanofluids. IEEE Trans Dielectr Electr Insul. 2022;29:956–64.
116. Wanatasanappan VV, Rezman M, Abdullah MZ. Thermophysical properties of vegetable oil-based hybrid nanofluids containing $Al_2O_3$-$TiO_2$ nanoparticles as insulation oil for power transformers. Nanomaterials. 2022;12:3621.
117. Oparanti SO, Khaleed AA, Abdelmalik AA. Ac breakdown analysis of synthesized nanofluids for oil-filled transformer insulation. Int J Adv Manuf Technol. 2021;117:1395–403.
118. Siddique ZB, Basu S, Basak P. Dielectric behavior of natural ester based mineral oil blend dispersed with $TiO_2$ and ZnO nanoparticles as insulating fluid for transformers. J Mol Liq. 2021;339: 116825.
119. Khaled U, Beroual A. Statistical investigation of AC dielectric strength of natural ester oil-based $Fe_3O_4$, $Al_2O_3$, and $SiO_2$ nano-fluids. IEEE Access. 2019;7:60594–601.
120. Oparanti SO, Abdelmalik AA, Khaleed AA, Abifarin JK, Suleiman MU, Oteikwu VE. Synthesis and characterization of cooling biodegradable nanofluids from non-edible oil for high voltage application. Mater Chem Phys. 2022;277: 125485.
121. Raja S, Koperundevi G. Titania-based transformer nanofluid: a study on the synthesis for enhanced breakdown strength and its humidity ageing. IET Nanodielectr. 2020;3:138–46.
122. Farade RA, Wahab NIA, Mansour D-EA, Azis NB, Jasni JB, Veerasamy V, et al. Investigation of the effect of sonication time on dispersion stability, dielectric properties, and heat transfer of graphene based green nanofluids. IEEE Access. 2021;9:50607–23.
123. Shukla G, Aiyer H. Thermal conductivity enhancement of transformer oil using functionalized nanodiamonds. IEEE Trans Dielectr Electr Insul. 2015;22:2185–90.
124. Phogat P, Shreya JR, Singh S. Synthesis of novel ZnO nanoparticles with optimized band gap of 1.4 eV for high-sensitivity photo electrochemical detection. Mater Today Sustain. 2024;27:100823.
125. Farade RA, Abdul Wahab NI, Mansour D-EA, Junaidi N, Soudagar MEM, Rajamony RK, et al. A review on ultrasonic alchemy of oil-based nanofluids for cutting-edge dielectric and heat transfer oils. J Mol Liq. 2024;408: 125312.
126. Bian T, Gardin A, Gemen J, Houben L, Perego C, Lee B, et al. Electrostatic co-assembly of nanoparticles with oppositely charged small molecules into static and dynamic superstructures. Nat Chem. 2021;13:940–9.
127. Kienle SM, Schneider T, Stuber K, Globisch C, Jansen J, Stengel F, et al. Electrostatic and steric effects underlie acetylation-induced changes in ubiquitin structure and function. Nat Commun. 2022;13: 5435.
128. Sultana S, Alzahrani N, Alzahrani R, Alshamrani W, Aloufi W, Ali A, et al. Stability issues and approaches to stabilised

nanoparticles based drug delivery system. J Drug Target. 2020;28:468–86.
129. Chakraborty S, Panigrahi PK. Stability of nanofluid: a review. Appl Therm Eng. 2020;174: 115259.
130. Brebels J, Manca JV, Lutsen L, Vanderzande D, Maes W. High dielectric constant conjugated materials for organic photovoltaics. J Mater Chem A. 2017;5:24037–50.
131. Lin Y, Ling X, Yu L, Huang S, Hsu AL, Lee YH, et al. Dielectric screening of excitons and trions in single-layer MoS2. Nano Lett. 2014;14:5569–76.
132. Cao T, Elimelech M. Colloidal stability of cellulose nanocrystals in aqueous solutions containing monovalent, divalent, and trivalent inorganic salts. J Colloid Interface Sci. 2021;584:456–63.
133. Yadav N, Jarial RK, Rao UM. Characterization of mineral oil based $Fe_3O_4$ nanofluid for application in oil filled transformers. Int J Electr Eng Inform. 2018;10:338–49.
134. Hwang JG, Zahn M, O'Sullivan FM, Pettersson LAA, Hjortstam O, Liu R. Effects of nanoparticle charging on streamer development in transformer oil-based nanofluids. J Appl Phys. 2010;107: 014310.
135. Zha J-W, Zheng M-S, Fan B-H, Dang Z-M. Polymer-based dielectrics with high permittivity for electric energy storage: a review. Nano Energy. 2021;89: 106438.
136. Kasap SO. Principles of electronic materials and devices. Fourth Edi. New York, NY: Tata McGraw-Hill; 2018.
137. Kaur M, Kumar V, Kaur P, Sharma R. Effect of synthesis methods on dielectric performance of ZnO nanoparticles. Mater Technol. 2022;37:1156–67.
138. Hoo DY, Low ZL, Low DYS, Tang SY, Manickam S, Tan KW, et al. Ultrasonic cavitation: an effective cleaner and greener intensification technology in the extraction and surface modification of nanocellulose. Ultrason Sonochem. 2022;90: 106176.
139. Vikash KV. Ultrasonic-assisted de-agglomeration and power draw characterization of silica nanoparticles. Ultrason Sonochem. 2020;65: 105061.
140. Kumar PG, Prabakaran R, Sakthivadivel D, Somasundaram P, Vigneswaran VS, Kim SC. Ultrasonication time optimization for multi-walled carbon nanotube based Therminol-55 nanofluid: an experimental investigation. J Therm Anal Calorim. 2022;147:10329–36.
141. Tiwari AK, Pandya NS, Said Z, Chhatbar SH, Al-Turki YA, Patel AR. 3S (sonication, surfactant, stability) impact on the viscosity of hybrid nanofluid with different base fluids: an experimental study. J Mol Liq. 2021;329: 115455.
142. Zheng Y, Shahsavar A, Afrand M. Sonication time efficacy on $Fe_3O_4$-liquid paraffin magnetic nanofluid thermal conductivity: an experimental evaluation. Ultrason Sonochem. 2020;64: 105004.
143. Sonawane SS, Khedkar RS, Wasewar KL. Effect of sonication time on enhancement of effective thermal conductivity of nano $TiO_2$–water, ethylene glycol, and paraffin oil nanofluids and models comparisons. J Exp Nanosci. 2015;10:310–22.
144. Chen Z, Shahsavar A, Al-Rashed AAAA, Afrand M. The impact of sonication and stirring durations on the thermal conductivity of alumina-liquid paraffin nanofluid: an experimental assessment. Powder Technol. 2020;360:1134–42.
145. Ahangaran F, Navarchian AH. Recent advances in chemical surface modification of metal oxide nanoparticles with silane coupling agents: a review. Adv Colloid Interface Sci. 2020;286: 102298.
146. Shrestha S, Wang B, Dutta P. Nanoparticle processing: understanding and controlling aggregation. Adv Colloid Interface Sci. 2020;279: 102162.
147. Zhao X, Soltani M, Golovin K. Residue-Free Droplet Transport Against Gravity via Wettability-Patterned Liquid-Like Surfaces. Adv Funct Mater. 2024;2403150:1–10.
148. Beroual A, Khaled U. Statistical investigation of lightning impulse breakdown voltage of natural and synthetic ester oils-based $Fe_3O_4$, $Al_2O_3$ and $SiO_2$ nanofluids. IEEE Access. 2020;8:112615–23.
149. Dessouky SS, Mansour DA, Shaban M, Abdelwahab SAM. Insulation performance enhancement of aged current transformers using nanofluids. Int J Electr Power Energy Syst. 2021;126: 106613.
150. Miao J, Dong M, Ren M, Wu X, Shen L, Wang H. Effect of nanoparticle polarization on relative permittivity of transformer oil-based nanofluids. J Appl Phys. 2013;113: 204103.
151. Farade RA, Abdul Wahab NI, Mansour D-EA, Azis NB, Jasni J, Soudagar MEM, et al. Development of graphene oxide-based nonedible cottonseed nanofluids for power transformers. Materials (Basel). 2020;13:2569.
152. Said Z, Sohail MA, Walvekar R, Liu C. Impact of sonication durations on thermophysical properties, contact angle and surface tension of f-MWCNTs nanofluid for heat transfer. J Mol Liq. 2022;358: 119164.
153. Farade RA, Wahab NIBA, Mansour D-EA, Azis NB, Jasni J, Banapurmath NR, et al. Investigation of the dielectric and thermal properties of non-edible cottonseed oil by infusing h-BN nanoparticles. IEEE Access. 2020;8:76204–17.
154. Baruah N, Maharana M, Nayak SK. Performance analysis of vegetable oil-based nanofluids used in transformers. IET Sci Meas Technol. 2019;13:995–1002.
155. Joshi AA, Majumdar A. Transient ballistic and diffusive phonon heat transport in thin films. J Appl Phys. 1993;74:31–9.
156. Nika DL, Balandin AA. Two-dimensional phonon transport in graphene. J Phys Condens Matter. 2012;24: 233203.
157. Jung J-Y, Yoo JY. Thermal conductivity enhancement of nanofluids in conjunction with electrical double layer (EDL). Int J Heat Mass Transfer. 2009;52:525–8.
158. Li Z, Kalbasi R, Nguyen Q, Afrand M. Effects of sonication duration and nanoparticles concentration on thermal conductivity of silica-ethylene glycol nanofluid under different temperatures: an experimental study. Powder Technol. 2020;367:464–73.
159. Cabaleiro D, Nimo J, Pastoriza-Gallego MJ, Piñeiro MM, Legido JL, Lugo L. Thermal conductivity of dry anatase and rutile nanopowders and ethylene and propylene glycol-based $TiO_2$ nanofluids. J Chem Thermodyn. 2015;83:67–76.
160. Momenzadeh L, Moghtaderi B, Belova IV, Murch GE. Determination of the lattice thermal conductivity of the $TiO_2$ polymorphs rutile and anatase by molecular dynamics simulation. Comput Condens Matter. 2018;17: e00342.
161. Mitra D, Howli P, Das BK, Das NS, Chattopadhyay P, Chattopadhyay KK. Size and phase dependent thermal conductivity of $TiO_2$-water nanofluid with theoretical insight. J Mol Liq. 2020;302: 112499.
162. Mahmood Katun M, Kadzutu-Sithole R, Moloto N, Nyamupangedengu C, Gomes C. Improving thermal stability and hydrophobicity of rutile-TiO2 nanoparticles for oil-impregnated paper application. Energies. 2021;14:7964.
163. Fal J, Sobczak J, Stagraczyński R, Estellé P, Żyła G. Electrical conductivity of titanium dioxide ethylene glycol-based nanofluids: Impact of nanoparticles phase and concentration. Powder Technol 2022;404.
164. Li M, Wang X, Li H, Di H, Wu X, Fang C, et al. Preparation of photoluminescent single crystalline MgO nanobelts by DC arc plasma jet CVD. Appl Surf Sci. 2013;274:188–94.
165. Zhou K, Li Y. Catalysis based on nanocrystals with well-defined facets. Angew Chem Int Ed Engl. 2012;51:602–13.
166. Lv Y, Ge Y, Sun Z, Sun Q, Huang M, Li C, et al. Effect of nanoparticle morphology on pre-breakdown and breakdown properties of insulating oil-based nanofluids. Nanomaterials. 2018;8: 476.

167. Tanaka T. Dielectric nanocomposites with insulating properties. IEEE Trans Dielectr Electr Insul. 2005;12:914–28.
168. Costi R, Saunders AE, Banin U. Colloidal hybrid nanostructures: a new type of functional materials. Angew Chem Int Ed. 2010;49:4878–97.
169. Remesal ER, Morales-García Á. Carbon-doped anatase titania nanoparticles: similarities and differences with respect to bulk and extended surface models. Phys Chem Chem Phys. 2022;24:21381–7.
170. Ibrahim ME, Abd-Elhady AM, Izzularab MA. Effect of nanoparticles on transformer oil breakdown strength: experiment and theory. IET Sci Meas Technol. 2016;10:839–45.
171. Khaled U, Beroual A. AC dielectric strength of mineral oil-based $Fe_3O_4$ and $Al_2O_3$ nanofluids. Energies. 2018;11:3505.
172. Khaled U, Beroual A. AC dielectric strength of synthetic ester-based $Fe_3O_4$, $Al_2O_3$ and $SiO_2$ nanofluids — conformity with normal and weibull distributions. IEEE Trans Dielectr Electr Insul. 2019;26(2):625–33.
173. Ise N, Sogami IS. Structure formation in solution: ionic polymers and colloidal particles. Berlin/Heidelberg: Springer-Verlag; 2005.
174. Mansour D-EA, Elsaeed AM, Izzularab MA. The role of interfacial zone in dielectric properties of transformer oil-based nanofluids. IEEE Trans Dielectr Electr Insul. 2016;23(6):3364–72.
175. Rajnak M, Timko M, Kopcansky P, Paulovicova K, Kuchta J, Franko M, et al. Transformer oil-based magnetic nanofluid with high dielectric losses tested for cooling of a model transformer. IEEE Trans Dielectr Electr Insul. 2019;26:1343–9.
176. Das AK. Exploring SiO2, TiO2, and ZnO nanoparticles in coconut oil and mineral oil under changing environmental conditions. J Mol Liq. 2024;397: 124168.
177. Jamshidi A, Hajilary N, Hajilari M. Insight into the investigation of applying MXene nanoparticles to enhance the properties of transformer oil. Nano-Structures & Nano-Objects. 2024;37: 101078.
178. Arun Ram Prasath RT, Mahato SN, Roy NK, Paramanandam T, Ansari MA, Biswas JC. Natural Ester Oil-Based High Permittivity CaCu3Ti4O12 (CCTO) Nanofluids an Eco-friendly Insulating Medium for Power Transformer. IEEE Trans Dielectr Electr Insul 2023.
179. Angayarkanni SA, Philip J. Review on thermal properties of nanofluids: Recent developments. Adv Colloid Interface Sci. 2015;225:146–76.
180. Babar H, Sajid M, Ali H. Viscosity of hybrid nanofluids: A critical review. Therm Sci. 2019;23:1713–54.
181. Ilyas SU, Pendyala R, Marneni N. Stability of nanofluids. Eng. Appl. Nanotechnol. from energy to drug Deliv., Springer Cham; 2017, pp. 1–31.
182. Amizhtan SK, Amalanathan AJ, Sarathi R, Srinivasan B, Gardas RL, Edin H, et al. Impact of surfactants on the electrical and rheological aspects of silica based synthetic ester nanofluids. IEEE Access. 2022;10:18192–200.
183. Amizhtan SK, Akash R, Gardas RL, Sarathi R, Aryanandiny B. Understanding the electro-rheological aspects of nano silica based ester fluid with surfactants and deep learning-based prediction of ECT. IEEE Access. 2023;11:1083–93.
184. Anju P, Aryanandiny B, Amizhtan SK, Gardas RL, Sarathi R. Investigation on the electrical and rheological properties of AlN-based synthetic ester nanofluids. IEEE Access. 2022;10:37495–505.
185. Maharana M, Baruah N, Nayak SK, Sahoo N, Wu K, Goswami L. Electrohydrodynamics analysis of dielectric 2D nanofluids. Nanomaterials. 2022;12: 1489.
186. Navlani-García M, Salinas-Torres D, Mori K, Kuwahara Y, Yamashita H. Tailoring the size and shape of colloidal noble metal nanocrystals as a valuable tool in catalysis. Catal Surv Asia. 2019;23:127–48.
187. Clendennen SK, Boaz NW. Betaine Amphoteric Surfactants—Synthesis, Properties, and Applications. Biobased Surfactants. Second Edi: Elsevier; 2019. p. 447–69.
188. Liu J, Zheng T, Wang J, Jia G. The inhibition performance of novel amino acid-based amphiprotic surfactants on aluminum alloys in sodium chloride solutions: experimental and theoretical studies. Mater Chem Phys. 2022;278: 125622.
189. Steiner K, Josef Schmolz J, Hoang F, Wolf H, Seiser S, Elbe-Bürger A, et al. Surfactants for stabilization of dermal emulsions and their skin compatibility under UVA irradiation: Diacyl phospholipids and polysorbate 80 result in high viability rates of primary human skin cells. Int J Pharm. 2024;653: 123903.
190. Yang X, Xiang L, Dong Y, Cao Y, Wang C. Effect of nonionic surfactant Brij 35 on morphology, cloud point, and pigment stability in *Monascus* extractive fermentation. J Sci Food Agric. 2020;100:4521–30.
191. Komesu D, Ichimura S, Morita H. Effects of nanoparticle concentration and surfactant on dielectric strength of nanofluids. 2019 IEEE Conf. Electr. Insul. Dielectr. Phenom., IEEE; 2019, pp. 38–41.
192. Li L, Zhou X, Wang R, Zhang X, Ma S, Su Y, et al. Microscopic experiment study on mechanisms of oil-gas interaction and CO2-surfactant flooding with different temperatures and pressures. J CO2 Util. 2023;69: 102389.
193. Koreh P, Lashkarbolooki M, Peyravi M, Jahanshahi M. Interfacial performance of cationic, anionic and non-ionic surfactants; effect of different characteristics of crude oil. J Pet Sci Eng. 2022;218: 110960.
194. Foo KS, Bavoh CB, Lal B, Mohd A. Rheology Impact of Various Non-Ionic Surfactants on Cyclopentane Hydrates. Molecules. 2020;25:3725.
195. Dhanola A, Garg HC. Influence of different surfactants on the stability and varying concentrations of TiO2 nanoparticles on the rheological properties of canola oil-based nanolubricants. Appl Nanosci. 2020;10:3617–37.
196. Fikri MA, Pandey AK, Rajamony RK, Sharma K, Kalidasan B, Samykano M, et al. Surfactant effects in functionalized multi-wall carbon nanotube-filled phase change materials. Mater Chem Phys. 2024;328: 129931.
197. Farade RA, Wahab NIA, Mansour D-EA, Azis NB, Jasni JB, Veerasamy V, et al. The effect of interfacial zone due to nanoparticle–surfactant interaction on dielectric properties of vegetable oil based nanofluids. IEEE Access. 2021;9:107033–45.
198. Protti M, Carotti A, Mercolini L, Sardella R. Co-solvents and mobile phase additives in HPLC. vol. 1. 3rd ed. Elsevier Inc.; 2023.
199. Ismail R, Phan TNQ, Laffleur F, Csóka I, Bernkop-Schnürch A. Hydrophobic ion pairing of a GLP-1 analogue for incorporating into lipid nanocarriers designed for oral delivery. Eur J Pharm Biopharm. 2020;152:10–7.
200. Tobias T, Rajnak M, Kopcansky P, Timko M, Agresti F, Barison S, et al. Dielectric breakdown study of a nanofluid based on goethite nanoparticles. IEEE Trans Dielectr Electr Insul. 2018;25:2206–11.
201. Mohamad NA, Azis N, Jasni J, Ab Kadir MZA, Yunus R, Yaakub Z. Impact of Fe3O4, CuO and Al2O3 on the AC breakdown voltage of palm oil and coconut oil in the presence of CTAB. Energies. 2019;12:1605.
202. Gayathri R, Deiva Sundari P, Thakur S, Sarathi R. Investigation on the dielectric performance of titania nanoparticles and surfactant added mixture of mineral and natural ester oil. Mater Res Express. 2019;6: 125020.
203. Kadim EJ, Noorden ZA, Adzis Z, Azis N, Mohamad NA. Surfactants effects on enhancing electrical performance of nanoparticle-based mineral transformer oil. IEEE Trans Dielectr Electr Insul 2023;pp.:1–1.

204. Rani N, Dehiya BS. Influence of anionic and non-ionic surfactants on the synthesis of core-shell Fe3O4@TiO2 nanocomposite synthesized by hydrothermal method. Ceram Int. 2020;46:23516–25.
205. Chakraborty B, Maur S, Pradhan AK, Chatterjee B, Dalai S. Study of nonlinearity, activation energy, and temperature effect on $Al_2O_3$ and $TiO_2$ nanoparticle-based mixed oil characteristics by dielectric spectroscopy. IEEE Trans Dielectr Electr Insul. 2023;30:997–1004.
206. Khan SA, Khan AA, Tariq M. Measurement of tan-delta and DC resistivity of synthetic ester based oil filled with $Fe_2O_3$, $TiO_2$ and $Al_2O_3$ nanoparticles. Smart Science. 2021;9:216–25.
207. Pillai SS, Aarathy AR, Gopinath D, Aryanandiny B, Sankar B. Effects of magnetite and titania nanoparticles on properties of transformer insulating oil. Nano Express. 2020;1: 020040.
208. Jacob J, S D, Tharamal L, Avinash Nelson A, Preetha P. Partial discharge characteristics of nanofilled mineral oil. 2019 IEEE Reg. 10 Symp., vol. 7, IEEE; 2019, p. 316–20.
209. Rafiq M, Chengrong L, Lv Y. Effect of $Al_2O_3$ nanorods on dielectric strength of aged transformer oil/paper insulation system. J Mol Liq. 2019;284:700–8.
210. Rafiq M, Lv Y, Li C, Sun Q. Effect of $Al_2O_3$ nanorods on the performance of oil-impregnated pressboard insulation. Electr Eng. 2020;102:715–24.
211. Havran P, Cimbala R, Kurimský J, Rajňák M, Dolník B, Medveď D, et al. Dielectric relaxation response of electrical insulating liquids under different natures of thermal stress. SSRN Electron J. 2023;11:826–35.
212. Khan SA, Tariq M, Khan AA, Alamri B, Mihet-Popa L. Influence of area and volume effect on dielectric behaviour of the mineral oil-based nanofluids. Energies. 2022;15: 3354.
213. Kurimský J, Rajňák M, Cimbala R, Rajnič J, Timko M, Kopčanský P. Effect of magnetic nanoparticles on partial discharges in transformer oil. J Magn Magn Mater. 2020;496: 165923.
214. Ravichandran V, Nguyen Cao TG, Choi DG, Kang HC, Shim MS. Non-ionic polysorbate-based nanoparticles for efficient combination chemo/photothermal/photodynamic therapy. J Ind Eng Chem. 2020;88:260–7.
215. Foster MJ, Carpenter AP, Richmond GL. Dynamic duo: vibrational sum frequency scattering investigation of pH-switchable carboxylic acid/carboxylate surfactants on nanodroplet surfaces. J Phys Chem B. 2021;125:9629–40.
216. Liu S, Zhang C, Du J, Huang H, Fang S, Li X, et al. Effect of dispersants on the stability of calcite in non-polar solutions. Colloids Surf A Physicochem Eng Asp. 2023;672: 131730.
217. Van TN, Ngoc NTH, Thuy DM, Van TL, Son HH, Long NP. Highly improved dielectric and thermal performance of polyalphaolefin oil-based fluids using MgO nanoparticles. Coatings. 2023;13:931.
218. Pyrgioti EC, Koutras KN, Charalampakos VP, Peppas GD, Bakandritsos AP, Naxakis IA. An experimental study on the influence of surface modification of TiO2 nanoparticles on breakdown voltage of natural ester nanofluid. Lect. Notes Electr. Eng.: Springer International Publishing; 2020. p. 279–88.
219. Cheng Y, Lan D, Jia Z, Gao Z, Liu X, Shi X, et al. MOF derivatives anchored to multichannel hollow carbon fibers with gradient structures for corrosion resistance and efficient electromagnetic wave absorption. J Mater Sci Technol. 2025;216:150–64.
220. Jin H, Morshuis PHF, Smit JJ, Andritsch T. The effect of surface treatment of silica nanoparticles on the breakdown strength of mineral oil. 2014 IEEE 18th Int. Conf. Dielectr. Liq., IEEE; 2014, pp. 1–4.
221. Kulkarni SV, Khaparde SA. Transformer Engineering. vol. 44. 1st ed. CRC Press; 2004.
222. Gherdaoui CE, Oumeddour H, Aldoori H, Alaoui C, Delbarre J-P, Bouberka Z, et al. Improving transformer oil decontamination: a synergistic approach integrating adsorption and radiative treatment for polychlorinated biphenyls. Sep Purif Technol. 2024;334: 126028.
223. Gherdaoui CE, Alaoui C, Oumeddour H, Bouchikhi N, Elaissaoui Elmeliani MEA, Aldoori H, et al. Advanced treatment of transformer mineral oils contaminated with aroclor mixtures using a combined UV–visible irradiation and adsorption method: effects of temperature and oil color according to ASTM D1500. Chem Eng J. 2024;497: 154614.
224. Koreh O, Torkos K, Bashir Mahara M, Boressay J, Izvekov V. Study of water clusters in insulating oils by Fourier transform infrared spectroscopy. IEEE Trans Dielectr Electr Insul. 1998;5:896–902.
225. Zhang C, Wang Y, Yan Z, He Z. Interplay between nanoparticles and water on dielectric properties of nanofluids. IEEE Trans Dielectr Electr Insul. 2019;26:1456–62.
226. Lyutikova MN, Korobeynikov SM, Ridel AV, Vagin DV, Konovalov AA. The Breakdown Voltage of Moistened Mineral Oil During Its Cooling. IEEE Trans Dielectr Electr Insul. 2022;29:2181–9.
227. Garcia B, Garcia T, Primo V, Burgos JC, Urquiza D. Studying the loss of life of natural-ester-filled transformer insulation: impact of moisture on the aging rate of paper. IEEE Electr Insul Mag. 2017;33:15–23.
228. Hadjadj Y, Fofana I, van de Voort FR, Bussieres D. Potential of determining moisture content in mineral insulating oil by fourier transform infrared spectroscopy. IEEE Electr Insul Mag. 2016;32:34–9.
229. Yu F, Chen Y, Liang X, Xu J, Lee C, Liang Q, et al. Dispersion stability of thermal nanofluids. Prog Nat Sci Mater Int. 2017;27:531–42.
230. Katiyar A, Dhar P, Nandi T, Das SK. Effects of nanostructure permittivity and dimensions on the increased dielectric strength of nano insulating oils. Colloids Surf A Physicochem Eng Asp. 2016;509:235–43.
231. Hamid MHA, Ishak MT, Din MFM, Suhaimi NS, Katim NIA. Dielectric properties of natural ester oils used for transformer application under temperature variation. 2016 IEEE Int. Conf. Power Energy, IEEE; 2016, p. 54–7.
232. Subramanian S, Devadasan Racheal PA, Sathianathan RV, Rajagopal A. Structural and dielectric properties of groundnut oil, mustard oil and ZnO nanofluid. Iranian J Sci Technol Trans A: Sci. 2019;43:1351–9.
233. Thabet A, Shaaban SA, Allam M. Enhancing dielectric constant of transformer oils using multi-nanoparticles technique under thermal conditions. 2016 18th Int Middle-East Power Syst Conf MEPCON 2016 - Proc 2017:220–5.
234. Koutras KN, Peppas GD, Fetsis TT, Tegopoulos SN, Charalampakos VP, Kyritsis A, et al. Dielectric and Thermal Response of TiO 2 and SiC Natural Ester Based Nanofluids for Use in Power Transformers. IEEE Access. 2022;10:79222–36.
235. Emara MM, Peppas GD, Pyrgioti EC, Chronopoulos DD, Bakandritsos A, Tegopoulos SN, et al. Thermal and dielectric performance of ester oil-based pentyl-graphene nanofluids. IEEE Trans Dielectr Electr Insul. 2022;29:1–1.
236. Liu R, Pettersson LAA, Auletta T, Hjortstam O. Fundamental research on the application of nano dielectrics to transformers. 2011 Annu. Rep. Conf. Electr. Insul. Dielectr. Phenom., Cancun, Mexico: IEEE; 2011, p. 423–7.
237. Taha-Tijerina J, Narayanan TN, Gao G, Rohde M, Tsentalovich DA, Pasquali M, et al. Electrically insulating thermal nano-oils using 2D fillers. ACS Nano. 2012;6:1214–20.

238. Du BX, Li XL. Dielectric and thermal characteristics of vegetable oil filled with BN nanoparticles. IEEE Trans Dielectr Electr Insul. 2017;24:956–63.
239. Michal O, Mentlik V, Trnka P, Hornak J, Totzauer P. Dielectric properties of biodegradable vegetable oil based nanofluid. 2018 19th Int. Sci. Conf. Electr. Power Eng., IEEE; 2018, pp. 1–4.
240. Mukherjee S, Mishra PC, Parashar SKS, Chaudhuri P. Role of temperature on thermal conductivity of nanofluids: a brief literature review. Heat Mass Transf. 2016;52:2575–85.
241. Du Y, Lv Y, Li C, Chen M, Zhou J, Li X, et al. Effect of electron shallow trap on breakdown performance of transformer oil-based nanofluids. J Appl Phys. 2011;110: 104104.
242. Nagashree AN, Champa V, Sumangala BV, Nagabhushana GR. Suitability of natural vegetable seed oil as liquid dielectric coolant in an insulation system. 2015 Int. Conf. Emerg. Res. Electron. Comput. Sci. Technol., Mandya, India: IEEE; 2015, pp. 429–34.
243. Prasath RTAR, Roy NK, Mahato SN, Thomas P. Mineral oil based high permittivity $CaCu_3Ti_4O_{12}$ (CCTO) nanofluids for power transformer application. IEEE Trans Dielectr Electr Insul. 2017;24:2344–53.
244. Maneerat N, Makmork K, Kittikhuntharadol Y, Suksai N, Chusang T, Pattanadech N. AC breakdown and resistivity of natural ester based nanofluids. In: 2020 8th Int. Conf. Cond. Monit. Diagnosis, IEEE; 2020, pp. 334–7.
245. Pastoriza-Gallego MJ, Lugo L, Legido JL, Piñeiro MM. Thermal conductivity and viscosity measurements of ethylene glycol-based $Al_2O_3$ nanofluids. Nanoscale Res Lett. 2011;6:221.
246. Apmann K, Fulmer R, Scherer B, Good S, Wohld J, Vafaei S. Nanofluid heat transfer: enhancement of the heat transfer coefficient inside microchannels. Nanomaterials. 2022;12:615.
247. Emara MM, Peppas GD, Tsovilis TE, Tegopoulos SN, Kyritsis A, Pyrgioti EC, et al. Thermal and Dielectric Analysis of an Ester-Based MgO Nanofluid. IEEE Trans Dielectr Electr Insul. 2023;30:2181–8.
248. Nayak B, Panda M, Mishra SR. Analysis of Brownian motion and thermophoresis effects with chemical reaction on Williamson nanofluid flow over permeable stretching sheet. Partial Differ Equations Appl Math. 2024;11: 100908.
249. Wang J, Yang X, Klemeš JJ, Tian K, Ma T, Sunden B. A review on nanofluid stability: preparation and application. Renew Sustain Energy Rev. 2023;188: 113854.
250. Liu D, Zhou Y, Yang Y, Zhang L, Jin F. Characterization of high performance AlN nanoparticle-based transformer oil nanofluids. IEEE Trans Dielectr Electr Insul. 2016;23:2757–67.
251. Dombek G, Nadolny Z, Przybylek P. The study of thermal properties of mineral oil and synthetic ester modified by nanoparticles TiO<inf>2</inf> and C<inf>60</inf>. 2014 ICHVE Int. Conf. High Volt. Eng. Appl., Poznan, Poland: IEEE; 2014, pp. 1–4.
252. Ilyas SU, Narahari M, Theng JTY, Pendyala R. Experimental evaluation of dispersion behavior, rheology and thermal analysis of functionalized zinc oxide-paraffin oil nanofluids. J Mol Liq. 2019;294: 111613.
253. Diego CF, Santisteban A, Fernandez FO, Delgado F, Ortiz A. Effect of TiO<inf>2</inf> nanoparticles on the performance of a natural ester dielectric fluid. In: 2017 IEEE Electr. Insul. Conf., IEEE; 2017, pp. 1–4.
254. Beheshti A, Shanbedi M, Heris SZ. Heat transfer and rheological properties of transformer oil-oxidized MWCNT nanofluid. J Therm Anal Calorim. 2014;118:1451–60.
255. Yepuri V. Cost-effective production of Titania nanoparticles for the modification of transformer insulating oil. J Indian Chem Soc. 2024;101: 101383.
256. Amalanathan AJ, Sarathi R, Prakash S, Mishra AK, Gautam R, Vinu R. Investigation on thermally aged natural ester oil for real-time monitoring and analysis of transformer insulation. High Volt. 2020;5:209–17.
257. Singha S, Asano R, Frimpong G, Claiborne CC, Cherry D. Comparative aging characteristics between a high oleic natural ester dielectric liquid and mineral oil. IEEE Trans Dielectr Electr Insul. 2014;21:149–58.
258. Maharana M, Bordeori MM, Nayak SK, Sahoo N. Nanofluid-based transformer oil: effect of ageing on thermal, electrical and physicochemical properties. IET Sci Meas Technol. 2018;12:878–85.
259. Koutras KN, Peppas GD, Tegopoulos SN, Kyritsis A, Yiotis AG, Tsovilis TE, et al. Aging Impact on Relative Permittivity, Thermal Properties, and Lightning Impulse Voltage Performance of Natural Ester Oil Filled With Semiconducting Nanoparticles. IEEE Trans Dielectr Electr Insul. 2023;30:1598–607.
260. Hussein AM, Lingenthiran KK, Noor MM, Aik LK. Palm oil based nanofluids for enhancing heat transfer and rheological properties. Heat Mass Transf. 2018;54:3163–9.
261. Ghasemi J, Jafarmadar S, Nazari M. Effect of magnetic nanoparticles on the lightning impulse breakdown voltage of transformer oil. J Magn Magn Mater. 2015;389:148–52.
262. Rajnak M, Timko M, Kurimsky J, Dolnik B, Cimbala R, Tobias T, et al. Electrical conduction in a transformer oil-based magnetic nanofluid under a DC electric field. J Magn Magn Mater. 2018;459:191–6.
263. Lv Y, Zhou Y, Li C, Wang Q, Qi B. Recent progress in nanofluids based on transformer oil: preparation and electrical insulation properties. IEEE Electr Insul Mag. 2014;30:23–32.
264. Lee J-C, Kim W-Y. Experimental study on the dielectric breakdown voltage of the insulating oil mixed with magnetic nanoparticles. Phys Procedia. 2012;32:327–34.
265. Lee J, Seo H, Kim Y. The increased dielectric breakdown voltage of transformer oil-based nanofluids by an external magnetic field. Int J Therm Sci. 2012;62:29–33.
266. Rajnak M, Wu Z, Dolnik B, Paulovicova K, Tothova J, Cimbala R, et al. Magnetic field effect on thermal, dielectric, and viscous properties of a transformer oil-based magnetic nanofluid. Energies. 2019;12:4532.
267. Chen Y, Luo P, He D, Ma R. Numerical simulation and analysis of natural convective flow and heat transfer of nanofluid under electric field. Int Commun Heat Mass Transf. 2021;120: 105053.
268. Farade RA, Abdul Wahab NI, Siddiqui VU, Sapuan SM. Bio-based liquid nanocomposites for electrical equipment. Phys Sci Rev. 2025;8943:1–24.
269. Badawi M, Ibrahim SA, Mansour D-EA, Ward SA, El-Faraskoury AA, Ghali M, et al. On Highlighting the Merits of Gas-to-Liquid Transformer Oil Under Accelerated Thermal Aging and Faults: Electrical and Physio- Chemical Properties. IEEE Access. 2024;12:93372–88.
270. Mansour D-EA, Taha IBM, Farade RA, Wahab NIBA. Partial discharge diagnosis in GIS based on pulse sequence features and optimized machine learning classification techniques. Electr Power Syst Res. 2022;211: 108162.
271. Rashed AK, Alshehawy AM, Mansour D-EA, Farade RA, Ghali M, Megahed TF. Optical Spectroscopy Techniques for Condition Assessment and Fault Diagnosis of Power Transformer Insulation: A critical Review on Technologies, Methods and Standards. IEEE Trans Dielectr Electr Insul 2025;pp.:1–1.